Review Article

Chemical Phase Diagrams for the $YBa_2Cu_3O_7$ Family

Pavel Karen, Orvar Braaten and Arne Kjekshus*

Department of Chemistry, University of Oslo, Blindern, N-0315 Oslo 3, Norway

Karen, P., Braaten, O. and Kjekshus, A., 1992. Chemical Phase Diagrams for the $YBa_2Cu_3O_7$ Family. – Acta Chem. Scand. 46: 805–840.

Phase diagrams for cuprates of alkaline earth and rare earth elements are reviewed, covering binary to quintenary oxides and including selected solid solution series with other elements. Basic crystal chemical data are included for most of the phases, whereas information on chemical properties is illustrated for $YBa_2Cu_3O_{6+w}$ as an example. Reactivity towards CO_2, leading in the first step to a formation of oxide carbonates, is consistently pointed out as one of the possible reasons for contradictory results in phase diagrams which comprise oxides with high basicity.

1. Introduction

Phase diagrams represent a condensed way of storing and conveying chemical information in solid-state chemistry. In, say, a three-component chemical phase diagram, the thermodynamics behind multitudes of chemical reactions is displayed and is made intelligible even when temperature and pressure changes agitate the complex chemical equilibria. Since relatively complete thermodynamic data are necessary to design a chemical phase diagram by calculation, the normal approach is to gather the chemical information experimentally. Particularly for subsolidus systems, this approach brings about problems concerning the chemical equilibria and even in defining the actual phase components. In the vastly expanded research on high-T_c superconductors, the flood of often conflicting results poses a concern in this sense. At the same time, chemical information is indeed needed for these systems where superconductivity often depends on a delicate balance on the edge of chemical stability, and the practical application often requires a step further.

Owing to the large volume of data, any comprehensive survey on chemical phase diagrams which includes high-T_c superconductors must be limited in scope. In the present review, systems related to the $YBa_2Cu_3O_7$ phase are treated, involving information about chemical and crystal structure properties complementary to the recent review on thermodynamics.[1] Some of the data included in this review have been obtained by the authors, and this first-hand knowledge has hopefully contributed to improved consistency.

1.1. Specification of scope. (1) All rare earths (REs) are treated except Sc. (2) Ba-rich phases are sometimes omitted owing to their tendency to form oxide carbonates. (3) High-temperature data for refractory oxides will be limited. (4) Illustrations are sometimes simplified in order to convey the overall message, and the readers should consult the original papers for details. Formulae on illustrations always specify the metal content, whereas only a principal oxygen content is often provided.

1.2. Specification of units and symbols. (1) Chemical inorganic nomenclature is used in accordance with the IUPAC recommendations (1990), and consistency for formulae of cuprates concerning the sequence of rare earth (RE) and alkaline earth (AE) elements is reached by following the said order. This conforms with the alphabetically incorrect but traditional way for the formula $YBa_2Cu_3O_7$, and the consequent Y→Ba→Cu anticlockwise orientation of the apices in ternary diagrams. Formulae for non-cuprate multicomponent oxides follow the electronegativity order, e.g. $SrDy_2O_4$. Owing to the main interest in oxide phases, the alphabetical order is ignored in the naming of the oxide carbonates etc. (2) Shorthand symbols of the type 123 (as for $YBa_2Cu_3O_7$) will be used when the relative cationic proportions of a phase rather than its complete formula are of importance. (3) When general compositional variables are used in chemical formulae, x relates to the RE host site in the structure, y to AE, z to Cu, w to oxygen and u to all other anions. (4) Symbols for physical variables are printed in italics, partial and relative values in lower case, absolute values in capitals. (5) Physical units follow the SI system. However, the absolute temperature unit (K) will be used only when the information is based or expressed in a thermodynamic connection. Melting points, reaction temperatures etc. are expressed in °C. (6) Crystal structure data are given when known, in a condensed form comprising *some or all* of the following information in square brackets: [formula; space group or crystal class (C, cubic; T, tetrago-

* To whom correspondence should be addressed.

nal; O, orthorhombic etc.); unit cell parameters (R in H setting) in the order: *a, b, c,* α, β, γ (always in units of pm or °, but not specified)]. References to overall structure data will be given at the word *structure,* or at the crystal class symbol, whereas a reference at the square bracket refers to unit cell data. (When more than one source of data are available, attempts have been made to select the best.) (7) Illustrations often include abbreviations for phase states, such as L, liquid; AF, antiferromagnetic; SC, superconducting etc. More special symbols are explained in captions. Solid solutions are marked by thick lines or dotted areas in illustrations. (8) Abbreviations for common solid-state chemistry techniques are used throughout the text: DTA, differential thermal analysis; TG, thermogravimetry, EDAX, energy dispersive analysis by X-rays; EMP, electron microprobe; HREM, high-resolution electron microscopy; NQR, nuclear quadrupole resonance; SEM, scanning electron microscopy; PND, powder neutron diffraction; PXD, powder X-ray diffraction; HIP, hot isostatic pressing.

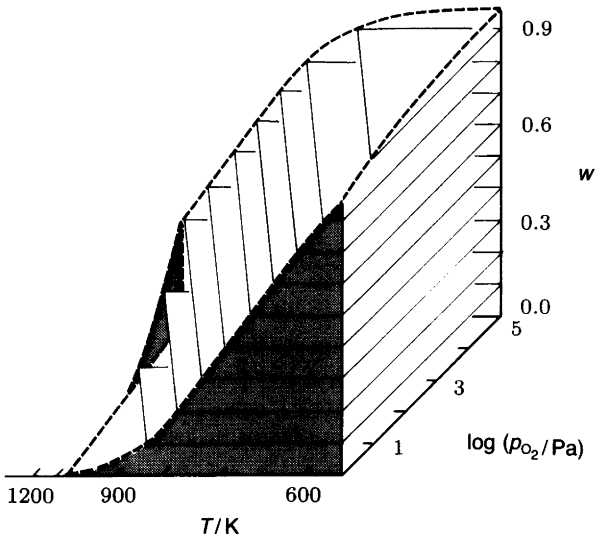

Fig. 1. Phenomenological illustration of the pseudochemical equilibrium between $YBa_2Cu_3O_{6+w}$ and oxygen.

2. Chemical properties

Some RE cuprates become superconducting when subjected to 'doping' by holes or electrons. To a large extent, this determines the chemical properties of these phases. As for hole 'doping', there are two usual ways of introducing holes: substitution by a lower-valent, more electropositive metal for RE, or addition of more non-metals. Both actions lead to an increased formal oxidation state for Cu, which requires participation of a metal with low polarizability, acting either indirectly through the substituent role (e.g. Sr in $La_{2-x}Sr_xCuO_4$) or directly as the stabilizer for the high oxidation state of copper (as Ba in $YBa_2Cu_3O_7$). These requirements specify the highly electropositive AE element, which in turn introduces an enhanced Lewis basicity to the oxygen atoms. As a result, the multicomponent oxide becomes reactive towards Lewis acids (e.g. Al_2O_3, SO_2, SiO_2, CO_2) and even H_2O.

Of the remaining components, Cu introduces its specific properties of variable valence and a tendency to form complexes, whereas RE brings less dominant properties.

2.1. Properties relevant to Cu. The variable valence states of Cu are manifested in the large variety of oxide compounds formed as a function of oxygen partial pressure. Whenever the structural features allow for the occurrence of mixed valences, this can be reached and varied either substitutionally or by a redox process. The latter is observed for $YBa_2Cu_3O_7$ and leads to a variable oxygen content in the solid state [reaction (1)], depending on p_{O_2} and

$$YBa_2Cu_3O_{(6+w)+\Delta w} \rightleftharpoons YBa_2Cu_3O_{6+w} + \frac{\Delta w}{2} O_2 \qquad (1)$$

T. An illustration of this relationship, based on equilibrium TG,[2] is shown in Fig. 1. Correspondingly, also structural,[3-7] chemical and thermodynamical,[8-12] and electrical transport[13-16] properties of $YBa_2Cu_3O_{6+w}$ vary as functions of the oxygen content *w*.

The oxygen vacant phase $YBa_2Cu_3O_{6+w}$ may also be oxidized by agents other than dioxygen. Oxidation by NF_3 at ~300 °C is described,[17] yielding $YBa_2Cu_3F_uO_{6+w}$ with $u \approx 0.4$ for $w \approx 1.0$, $u \approx 0.7$ for $w \approx 0.7$ and $u \approx 1.2$ for $w \approx 0.0$. Indication[18] that also hydrogen as such can partially be incorporated at vacant oxygen sites (at a temperature of, say, 100–200 °C) failed to give a definite structural proof upon PND of the deuterated version. In fact, the presence of traces of metallic Cu observed by PND,[18] as well as the occurrence of magnetic ordering very similar to that found upon oxygen removal,[19] and observation of highly mobile OH^- (comparable to that of oxygen in the original material)[20] suggest the need for a more detailed characterization before firmer conclusions can be drawn. Phases where the presence of halogen[21] or cyanide[22] incorporation has been suggested have apparently proved even more difficult to characterize.

Copper gives $YBa_2Cu_3O_{6+w}$ an oxidative power which strongly increases when *w* approaches 1.0. Thus H_2O, Cl^- and Br^- are oxidized in acid solutions to O_2, Cl_2 and Br_2 for $w > 0.5$, and I^- are oxidized to I_2 for $w > 0.0$. On the other hand, reduction properties occur only in relation to strong oxidants.

As a manifestation of properties reminiscent of the Cu affinity for formation of complexes, a reactive dissolution of the mixed valence cuprate in aqueous ammonia[23] [reaction (2)] may be mentioned. Such a reaction does not occur for the stoichiometric cuprate Y_2BaCuO_5.

$$2YBa_2Cu_3O_{6.5} \xrightarrow{11H_2O,24NH_3} 2YO(OH) + 4Ba^{2+} + 6[Cu(NH_3)_4]^{2+} + 20OH^- . \qquad (2)$$

Table 1. An acidity scale for selected oxides (χ denotes electronegativity of the metal, *a* the acid/base parameter).

Oxide	χ	*a*
BaO	0.9	−10.8
Y_2O_3	1.3	−6.5
CuO	1.9	−2.5
H_2O	2.1	±0.00
CO_2	2.5	5.5
SO_2	2.5	7.1

2.2. Properties relevant to AE. The low electronegativies of Ca, Sr and Ba enhance the reactivity of their multicomponent oxides towards hydrogen acids and their precursors. The relative acidity/basicity scale,[24,25] based on electronegativity or neutralization enthalpy data, is given for the oxides concerned in Table 1. Possible reactions with the surrounding chemical environment are of the greatest concern. Solid-state reactions of, say, $YBa_2Cu_3O_{6+w}$ with acidic transition metal oxides and analogous materials are found[26,27] to proceed readily upon formation of unwanted Ba containing oxides. Complex equilibria in liquid systems of various molten salts were investigated,[28] and NaCl–KCl melts proved to be the least reactive towards $YBa_2Cu_3O_{6+w}$. The reaction with NO_2 at 200 °C is found[29] to comply with both the acidic and oxidative properties of the gas, forming barium nitrite and simultaneously oxidizing the residuary cuprate when oxygen-deficient $YBa_2Cu_3O_{6+w}$ is involved.

Reactions with H_2O and with CO_2 are of particular importance, since H_2O and CO_2 commonly occur in the chemical environment and some preparation routes involve carbon-containing compounds. Ideally, the hydrolysis by H_2O at $100 < t < 300$ °C should follow reaction (3), but in

$$2YBa_2Cu_3O_{6.5} \xrightarrow{5H_2O} 2YO(OH) + 4Ba(OH)_2 + 6CuO \quad (3)$$

practice the omnipresence of CO_2 gives rise to complex mixtures.[30] There is an indication[20] that OH^- might be incorporated in $YBa_2Cu_3O_{6+w}$ at relatively low partial pressures of H_2O vapour (270 Pa, at 100–200 °C), before the cuprate is subject to the complete degradation.

Analogous behaviour is found for the reaction with CO_2. At low partial CO_2 pressures, an oxide carbonate with composition $YBa_2Cu_3(CO_3)_uO_{6+w}$ is formed before the complete carbonatization.[31,32]

If the degradation in a dry O_2–CO_2 mixture is allowed to be completed, reactions (4)–(6) are observed,[2,33] in which *w*

$$400 < t < 730\,°C: \quad 2YBa_2Cu_3O_{6+w} \xrightarrow{4CO_2}$$

$$Y_2O_3 + 4BaCO_3 + 6CuO + (w - \tfrac{1}{2})O_2 \quad (4)$$

$$730 < t < 950\,°C: \quad 2YBa_2Cu_3O_{6+w} \xrightarrow{4CO_2}$$

$$Y_2Cu_2O_5 + 4BaCO_3 + 4CuO + (w - \tfrac{1}{2})O_2 \quad (5)$$

$$950\,°C < t: \quad 2YBa_2Cu_3O_{6+w} \xrightarrow{3CO_2}$$

$$Y_2BaCuO_5 + 3BaCO_3 + 5CuO + (w - \tfrac{1}{2})O_2 \quad (6)$$

and the question of CuO or Cu_2O depend on p_{O_2} and temperature. The observed onset of the carbonatization of $YBa_2Cu_3O_{6+w}$ is shown in Fig. 2 in comparison with the CO_2 dissociation pressures of $CaCO_3$, $SrCO_3$ and $BaCO_3$ according to thermodynamic data.[34,35] The high temperature necessary to reverse the carbonatization (or to synthesize a carbon-free oxide from carbonaceous starting materials) reflects the high thermal stability of $BaCO_3$. The tendency to stabilize carbonate ions in the crystal structure of multicomponent barium oxide phases (notably cuprates) has not been recognized in many phase diagram studies, even when carbonates were used as starting materials. Precautions are normally not taken to remove CO_2 from the oxygen gas flushed through the reaction space.

3. Oxide carbonates in the Y(O/CO$_3$)–Ba(O/CO$_3$)–Cu(O/CO$_3$) system

Formation of yttrium barium oxide carbonates was recognized by de Leeuw *et al.*,[36] and almost simultaneously the existence of oxide carbonates among yttrium barium cuprates was also indicated.[37,38] One of the yttrium barium oxide carbonates was specified[32] as $Y_2Ba_3(CO_3)_uO_{6-u}$, [$u \approx 1$; T; 438.63(4), 1185.9(2)]. Related phases with higher barium content apparently also occur, depending on the CO_2 partial pressure and the temperature.

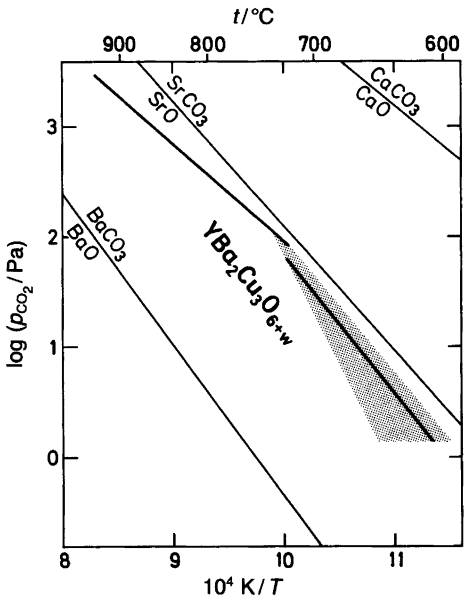

Fig. 2. $YBa_2Cu_3O_{6+w}$ stability with respect to carbonatization in O_2–CO_2 atmospheres at ambient pressure; after Ref. 2. Equilibrium according to reaction (4) is indicated by shaded area, equilibrium according to reaction (5) by solid line. Data for AEs are given for comparison.

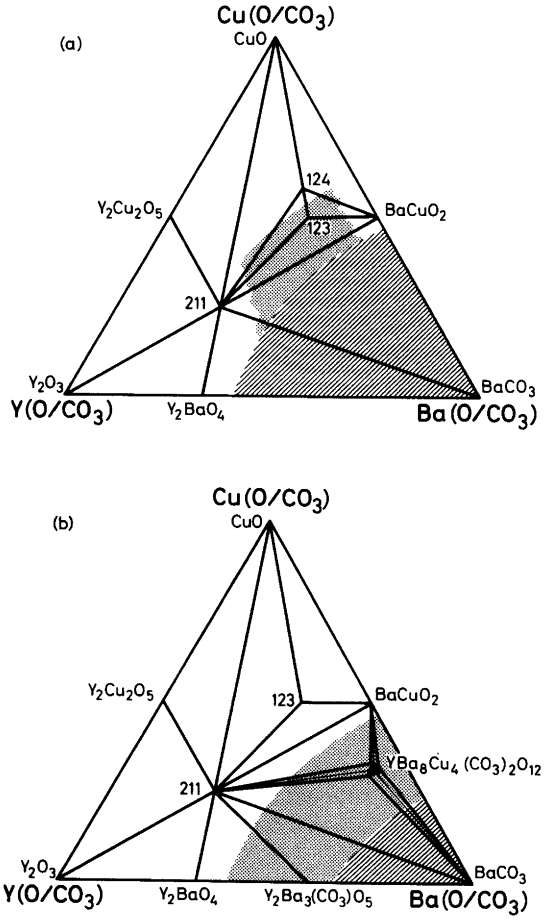

Fig. 3. Phase compatibilities in the $Y(O/CO_3)$–$Ba(O/CO_3)$–$Cu(O/CO_3)$ system, from Ref. 32, as seen by PXD after repeated firings of citrate precursors at (a) 800 and (b) 900 °C in oxygen of ambient pressure containing ~40 ppm CO_2. Phenomenological frontiers of oxide carbonate stability are shown by dotted shading, of carbonate stability by line shading. Only indicative formulae are given.

The barium-rich, yttrium barium cuprate phase, which was commonly referred to as 'the other perovskite', owing to its ambiguous location in the phase diagram, is shown[31] to be an oxide carbonate with composition[32,38] $Y_{1+x}Ba_8Cu_{4+z}(CO_3)_uO_{11+w}$, where $u \approx 2$, $x \in (0, 0.3)$, $z \in (0, 0.4)$ and $w \in (0.05(2), 1.08(2))$ for $x = z = 0$. Its structure, which accommodates vacancies on both cationic and anionic sites, is closely related to (the hypothetic perovskite) $BaCuO_3$.

An oxide carbonate phase at the '123' composition was indicated[31,39,40] and characterized[32] as $YBa_2Cu_3(CO_3)_uO_{6+w}$. The product formed at 800 °C in oxygen with ~40 ppm CO_2 and oxygenated at 320 °C has an extended *a* and contracted *c*, as compared with the parent oxide, [$u = 0.2$, $w = 0.7$; *P4/mmm*; 387.38(3), 1161.2(4)], and does not exhibit superconductivity.[32]

The thermal stability of the oxide carbonates of the $Y(O/CO_3)$–$Ba(O/CO_3)$–$Cu(O/CO_3)$ system decreases with increasing Cu and decreasing Ba content. In oxygen with $p_{CO_2} \approx 4$ Pa, an upper limit of 960 °C is observed[32] for $Y_2Ba_3(CO_3)O_5$, 940 °C for $Y_{1+x}Ba_8Cu_{4+z}(CO_3)_2O_{11+w}$ and 830 °C for $YBa_2Cu_3(CO_3)_{0.2}O_{6+w}$. Subsolidus phase diagrams of the $Y(O/CO_3)$–$Ba(O/CO_3)$–$Cu(O/CO_3)$ system at 800 and 900 °C, as obtained for a large number of samples,[31,32,38] are shown in Fig. 3.

Generally, each of the oxide carbonates in question is stable in a narrow shell defined by the degree of basicity for the constituents (notably the BaO content), and delimited by the concentration of CO_2 in the surrounding atmosphere and the temperature. At lower BaO contents and CO_2 concentrations, as well as at higher temperatures, pure oxide phases become stable. At larger BaO contents, higher CO_2 concentrations or lower temperatures, $BaCO_3$ is stabilized next to the other oxides. The crystal structures of the oxide carbonates are closely related to those of their parent oxide phases. This is particularly intriguing in the case of $YBa_2Cu_3O_7$, since the conversion into a non-superconducting, but yet structurally very similar oxide carbonate, is induced even when comparatively minute amounts of carbonate have exchanged oxygen. For the phase diagrams (particularly in the Ba-rich regions) this means that an oxide carbonate phase may easily have been overlooked, and structural data consequently misinterpreted as belonging to an oxide. Hence, in some of the phase diagrams in this review, the Ba-rich corner is simply omitted.

Oxide carbonates are not specific to AE-rich oxides but also occur in relation to other electropositive metals. Thus, e.g., RE oxide carbonates are recorded, but the thermal stability of these does not exceed some 500 °C at ambient pressure.[41] Extending the analogy further, say, oxide nitrates (or oxide nitrites) may be formed in multicomponent Ba-rich systems at relatively high temperatures, in view of the thermal stability of the RE (~500 °C)[42] and Cu (~250 °C)[43] oxide nitrates.

4. Binary and pseudobinary systems

4.1. Oxides of AE metals. The melting point of the AE oxides decrease from CaO, 2576 °C through SrO, 2430 °C to BaO, 1923 °C.[44] An analogous trend is observed for the vaporization temperature at a given pressure.[45] As an example, a partial pressure of 1 Pa of CaO, SrO and BaO in 20 kPa O_2 is reached at ~2350, ~2100 and 1450 °C, respectively. The crystal structures are of the NaCl type; CaO [481],[46] SrO [514][47] and BaO [552].[47]

4.2. Peroxides of AE metals. At relatively low temperatures, peroxides of the AEs are stable. The equilibrium oxygen pressure for CaO_2 is estimated[48] to reach 100 kPa at around ambient temperature, at ~350 °C for SrO_2,[49] and at ~820 °C for BaO_2.[50] A significant miscibility is expected in the AE oxide–peroxide systems, as indicated in Fig. 4 for the Ba case.[50] This should be taken into consideration in the evaluation of the oxygen dissociation pressure, which will vary with the content of peroxide in the solid-solution phase.[50] To illustrate rough trends, equilibrium oxygen

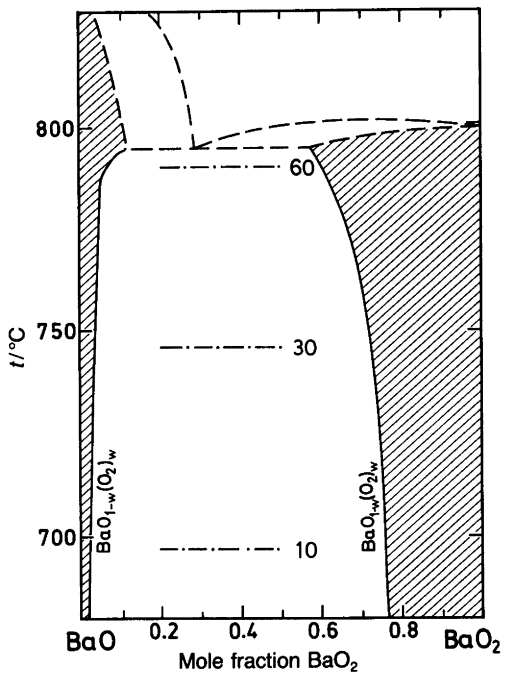

Fig. 4. An *x–t* diagram for the $BaO–BaO_2$ system in pure dry oxygen, with some equilibrium O_2 pressures (in kPa) indicated by chain lines; after Ref. 50. The two separated regions of the $BaO_{1-w}(O_2)_w$ phase are emphasized by the line shading.

pressures for $SrO_{1.97}$[49] and the oxide-saturated barium peroxide are expressed in eqns. (7) and (8) (p in Pa, T in K),[49,50] where w for the oxide-saturated peroxide is specified by eqn. (9). The peroxides crystallize in the CaC_2-type structures: CaO_2 [*P4/mmm*; 356, 596][51] SrO_2 [355, 655][52] and BaO_2 [380.7(7), 684.1(5)].[53]

$$SrO_{1.97}\,(s) \rightleftharpoons SrO(s) + \frac{0.97}{2}\,O_2(g):$$

$$\log_{10} p_{O_2} = 11.4 - 4050/T \qquad (7)$$

$$BaO_{1-w}(O_2)_w(s) \rightleftharpoons BaO(s) + \frac{w}{2}\,O_2(g):$$

$$\log_{10} p_{O_2} = 11.83 - 7500/T. \qquad (8)$$

$$\log_{10}(1 - w) = 0.975 - 1552/T. \qquad (9)$$

4.3. Carbonates of AE metals. As intermediate precursors in many preparation routes, AE carbonates must be considered. The temperature at which the CO_2 pressure of the carbonate dissociation reaches 100 kPa increases from 879 (1) °C for $CaCO_3$[2,54] to 1250 °C for $SrCO_3$.[55] The corresponding temperature for $BaCO_3$ (expectedly, some 1600 °C) is not directly measured, since strong sintering hampers the kinetics. For the temperature dependence of the equilibrium CO_2 pressures of the AE carbonates see Fig. 2.

The thermodynamically stable modification of calcium carbonate is calcite[56] [$CaCO_3$; $R\bar{3}c$; 499.00(2), 1700.2(1)], whereas the structures[57] of strontium and barium carbonate are of the argonite-type: $SrCO_3$ [(7 % Ca, 4 % Ba); *Pmcn*; 509.0(2), 835.8(2), 599.7(4)]; $BaCO_3$ [531.26(5), 889.58(5), 642.84(5)].

4.4. Oxides of RE elements. The oxides of the trivalent REs are typical refractory materials with melting points above 2300 °C. They form polymorphic modifications depending on temperature, pressure and atom size.[58] At ambient pressure, the sesquioxides of the larger (lighter) lanthanoids, La–Nd, form hexagonal structures[59] when subject to free cooling from any temperature up to the melting point, e.g. La_2O_3 [$P6_3/mmc$; 393.7, 613.0]. The sesquioxides of the small (heavier) lanthanoids Dy–Lu have the cubic[60] bixbyite-type structure [Lu_2O_3; $Ia\bar{3}$; 1039.07] and this also applies[61] to Y_2O_3 [1060.3]. In the intermediate size region, a monoclinic structure is preferred for Sm, Eu and Gd [Sm_2O_3; *C2/m*; 1418, 363.3, 884.7, 99.96].[62]

Ce, Pr, and Tb also take a tetravalent state in the oxides. In line with the close structural relationship between the bixbyite (for the sesquioxides) and the fluorite (for the dioxides) structure types,[63] a sequence of intermediate phases occurs, with a formula $2RE_2O_3 \cdot nRE'O_2$. Symbols have been assigned to the occurring phases: $n = 0$, θ-phase (hexagonal RE_2O_3); $n = 0$, σ-phase (cubic RE_2O_3); $n = 3$, ι-phase (RE_7O_{12}); $n = 4$, (RE_8O_{14}); $n = 5$, ζ-phase (RE_9O_{16}); $n = 6$, ε-phase ($RE_{10}O_{18}$); $n = 7$, δ-phase ($RE_{11}O_{20}$); $n = 8$, β-phase ($RE_{12}O_{22}$); $n = \infty$, α-phase (REO_2). The pseudocell parameter a generally increases with increasing oxygen content.[63]

The most oxygen-rich CeO_2 [$Fm\bar{3}m$; 541.1][64] is formed virtually stoichiometric up to some ~1300 °C in 100 kPa O_2.[65] At room temperature, CeO_2 is a well defined stoichiometric compound, whereas above some 600 °C it broadens into an appreciable range of homogeneity with oxygen vacancies (e.g. to a composition of $CeO_{1.72}$ at 1000 °C). However, the equilibrium oxygen pressures of these solid solutions are very low (at 1000 °C, $\sim 10^{-15}$ Pa for $CeO_{1.72}$ and $\sim 10^{-5}$ Pa for $CeO_{1.99}$).[65] At ambient temperature, three phases (δ, ζ and ι)[65,66] occur between CeO_2 and Ce_2O_3. Similar compositional features are found among the praseodymium oxides, but here the dissociation pressures are much higher.[63,67] The most oxygen-rich praseodymium dioxide [$Fm\bar{3}m$; 539.3(1)][68] is formed when $p_{O_2} > 100$ kPa and it decomposes above 310 °C in 100 kPa oxygen[68] into the β-phase, with a subsequent decomposition into lower oxides above some 480 °C. At ambient temperature, four phases (β, ε, ζ and ι)[63,67] are considered stable between PrO_2 and Pr_2O_3, the fifth, δ-phase, emerging only in a limited temperature region. Oxygen dissociation pressures of 1–100 kPa between 800 and 1300 °C are reported for the range between Pr_2O_3 and Pr_7O_{12}.[69]

Similar dissociation pressures are measured for the

largely analogous terbium oxides. TbO_2 [$Fm\bar{3}m$; 521.9(1)][70] is formed only on disproportionation in acidic solutions[70] (similarly to PbO_2) and decomposes above 340 °C in 100 kPa O_2 into the δ-phase.[71] The δ-phase is the most oxygen-rich terbium oxide which can be obtained by oxidation with O_2 (TbO_2 forms in atomic oxygen)[72] and decomposes into ι-phase at ~450 °C (p_{O_2} = 1.3 kPa) and subsequently into Tb_2O_{3+w} (σ) at ~800 °C for p_{O_2} = 1.3 kPa.[73] However, the most common preparation route for RE oxides, which involves thermal decomposition of oxalate in air at 600–1000 °C, gives reproducibly Tb_4O_7. This composition is, moreover, invariably obtained during various synthesis reactions in O_2 at ambient and reduced pressures.[42,72,74] Correspondingly, distinct plateaus at the Tb_4O_7 composition are observed[75,76] by TG. However, diffraction methods failed to reveal any specific superstructure for the Tb_4O_7 composition, which accordingly is suggested to be a consequence of the sluggish kinetics.[73,77] Oxygen dissociation pressures for the terbium oxides up to 100 kPa between 500 and 1000 °C are reported.[78]

4.5. Copper oxides. Apart from the exotic conditions[79] under which CuO_2 may be formed, only two copper oxides CuO and Cu_2O are normally encountered (for the mineral paramelaconite, Cu_4O_3, see Ref. 80), both with very narrow homogeneity ranges.[81–83] In line with the noble nature of copper, the Cu oxides have rather limited thermal stability and the Cu–O system depends strongly on the partial pressure of oxygen in the surrounding atmosphere. The situation for p_{O_2} = 100 kPa is shown in Fig. 5, where also additional O_2 isobars are indicated. At p_{O_2} = 100 kPa, both oxides melt incongruently, Cu_2O at 1229 °C, and CuO at some 1100 °C.[81,85] In air, however, dissociation of CuO into Cu_2O and O_2 at 1030 °C precedes the melting of the monoxide. The temperature dependence of the dissociation pressure for CuO is found[81] to follow eqn. (10) (in Pa, K; $T <$ 1374 K). Values of 14.50 and 13 290 are obtained for the

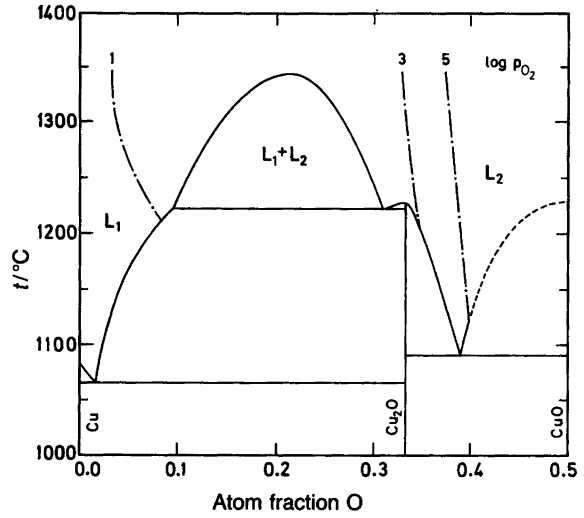

Fig. 5. An *x–t* diagram for the Cu–O system with some equilibrium O_2 pressures (in Pa) indicated by chain lines; after Ref. 84.

$2CuO(s) \rightleftharpoons Cu_2O(s) + \frac{1}{2}O_2(g)$:

$$\log_{10} p_{O_2} = 14.53 - 13260/T. \quad (10)$$

constants from thermodynamic data.[34] The analogous expression for Cu_2O, eqn. (11), can only be established from thermodynamics[34] (T < 1339 K). CuO is monoclinic[86]

$Cu_2O(s) \rightleftharpoons 2Cu(s) + \frac{1}{2}O_2(g)$:

$$\log_{10} p_{O_2} = 12.258 - 17290/T. \quad (11)$$

[$C2/c$; 468.37(5), 342.26(5), 512.88(6), 99.54(1)] and Cu_2O is cubic[87] [$Pn\bar{3}m$; 425.7].[88] Of near precursors to the copper oxides, the metallic $Cu_7O_{8-w}NO_3$ [$Fm\bar{3}m$; 948] is worth mentioning as the last intermediate product of the thermal decomposition of copper nitrate.[43]

5. Ternary oxides

5.1. AE(O)–AE′(O) systems. SrO and BaO have unlimited solid solubility above ca. 1100 °C.[47,89] At lower temperatures, segregation of the solid solutions should occur according to thermodynamics, but it is kinetically hindered,[90] and the solid solution is readily maintained on cooling. A similar situation occurs in the Ca(O)–Sr(O) system.[91]

5.2. AE(O)–RE(O) systems. The refractory character of the components suggests low rates of diffusion and problems with the establishment of equilibrium. Experimental data are frequently accompanied by a note that 'phase-pure samples could not be obtained' or 'a variety of other phases seem to appear if other conditions are applied'. The AE(O)–RE(O) systems are also very sensitive to moisture,[92] and complications due to oxide carbonate formation are certainly expected when the AE content becomes high.

5.2.1. Ba(O)–RE(O) systems. The tendency toward oxide carbonate formation is particularly pronounced for AE = Ba, where only RE-rich phases such as $BaRE_2O_4$ can safely be considered as true oxides. The $BaRE_2O_4$ phases are formed by the larger trivalent REs from La to Er and Y,[93] and have the $CaFe_2O_4$-type structure [BaY_2O_4; *Pnam*; 1039.85(8), 1211.94(9), 345.06(2)].[94] For RE = Nd and Sm, this phase melts congruently, whereas for the larger and smaller REs decomposition occurs before melting: between 1850 °C[93] for RE = La and 1400 °C[93] for RE = Y (a markedly different value of ~1030 °C also being reported[95]). The phase diagram for RE = Sm is illustrated in Fig. 6; for further diagrams, see Refs. 93, 96 and 97.

For Sm and smaller REs, $Ba_3RE_4O_9$ is formed from RE oxides and $BaCO_3$. The syntheses require a high temperature that increases with the electropositive character of the involved RE from 1000 °C for RE = Lu to 1550 °C for RE = Sm.[93] The crystal structures[98] of the $Ba_3RE_4O_9$

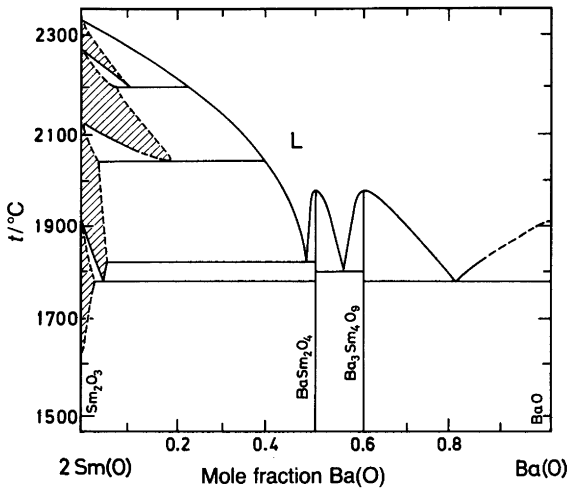

Fig. 6. An *x–t* diagram for the Sm(O)–Ba(O) system in air; after Ref. 93.

phases are rhombohedral [e.g. $Ba_3Tm_4O_9$; *R*3; 605.56(4), 2495.7(2)].

Data for the Ba-rich phases should be accepted with caution. For example, $Y_2Ba_2O_5$ claimed in Refs. 92, 99 and 100 was proved to be an oxide carbonate,[36] and later even the metal ratio turned out to be wrong; $Y_2Ba_3(CO_3)O_5$.[32] The latter phase decomposes at 960 °C (in O_2 with ~ 5 ppm CO_2) into $Ba_3Y_4O_9$ and $Ba_4Y_2O_7$ or another oxide carbonate.[36,100,101]

In an O_2 atmosphere the tetravalent Ce, Pr and Tb form only one ternary oxide with BaO, viz. $BaREO_3$,[102] the crystal structures of which are slightly distorted variants of perovskite (orthorhombic for RE = Ce and Pr, and rhombohedral for RE = Tb).[103,104] Under reducing conditions, $BaRE_2O_4$ are also obtained for RE = Ce, Pr and Tb.[93,105]

5.2.2. Sr(O)–RE(O) systems. Compared to $BaRE_2O_4$, the presence of the smaller Sr makes the structure more attractive for the smaller trivalent REs and less favourable for the largest RE = La.[93] Except for RE = Nd, where decomposition occurs before melting, all these phases [SrY_2O_4; *Pnam*; 1008, 1191, 340][106] melt congruently at temperatures around 2100 °C.[93]

Analogous phases to (rhombohedral) $Ba_3RE_4O_9$ are not observed, but an equicompositional series of phases forms for La, Pr and Nd which are also metastable at ambient temperatures.[93,107] The crystal structure[108–110] is monoclinic, [e.g. $Sr_3La_4O_9$; *Cc*; 1165.7, 734.8, 1347.1, 115.6].[108]

The tetravalent REs Ce, Pr and Tb form two ternary oxides with SrO, $SrREO_3$ and Sr_2REO_4, the latter being known only for Ce (stable up to ~ 1400 °C, where it decomposes into $SrCeO_3$ and SrO).[111] The crystal structure[112] of the former is derived from perovskite [e.g. $SrCeO_3$; $P2_12_12_1$; 601.1, 858.8, 615.6]. Sr_2CeO_4 is reported[113] to be triclinic [607.0, 897.6, 1059.8, 94.7, 90.4, 95.8], but the present authors have indexed 32 of the first 36 PXD reflections orthorhombically [1034.9(5), 612.4(2), 360.0(2)].

Under reducing conditions, phases which can accommodate trivalent Ce, Pr and Tb can be formed. This is the case for $SrTb_2O_4$, which adopts the calcium ferrite-type structure.[114]

5.2.3. Ca(O)–RE(O) systems. No stable ternary compounds are reported[93] at ambient temperature for the largest REs, but some solid solubility in (hexagonal) RE_2O_3 is found,[93,115] e.g. $x = 0.08$ for RE = La.[115] Starting from Sm, the smaller REs form a high-temperature stable phase $CaRE_4O_7$. For the even smaller RE = Dy, the calcium ferrite-type phase is formed, and its analogue is still found in the $CaO–Sc_2O_3$ system,[116] [$CaSc_2O_4$; *Pnma*; 946.1, 1112.2, 314.3].[117] No ternary oxide has been found for RE = Ce^{IV}.[111]

5.3. RE(O)–RE'(O) systems. With the exception of the most different pairs of REs by size, which form a 1:1 ternary oxide, no further ternary compounds are found, but wide ranges of solid solubility occur for the RE sesquioxides. The structure of these solid solutions follows the behaviour of the binary oxides as a function of temperature and ionic size.[58]

As may be expected for these refractory oxides, the solid-state diffusion rate is rather low, and the formation of the 1:1 ternary oxides requires temperatures above 1600 °C, long sintering times and the use of pressure.[118] It has therefore been suggested[119] that they in fact are metastable under ambient conditions. Structurally, these oxides are perovskite-related [e.g. $LaYO_3$; *Pnam*; 587.7, 849.3, 608.7].[120–122] When based on La, they occur for Ho (or Y) and smaller REs,[118,122] but they are only found for Lu and Sc when based on Pr.[122] Scandium, on the other hand, forms $ScREO_3$ with all larger REs than Y.[123]

The fluorite-type CeO_2 phase forms (at say 1600 °C) an almost continuous series of solid solutions with trivalent REs, maximum extension being found between Sm and Ho (or Y).[124–126] These elements of similar size are able (or nearly able) to form the cubic sesquioxide, the structure of which is closely related to fluorite. A nearly continuous conversion occurs from the fluorite-type CeO_2 phase through a (related vacant) *bcc* solid-solution oxide, followed by a narrow ($\Delta x \approx 0.1$) miscibility gap into the regime of either the *fcc* or monoclinic sesquioxide.[126] These trends are subject to alterations when equilibrium is established at lower temperature than 1600 °C[58] or low O_2 pressures are used. The latter specification is particularly important for the otherwise analogous systems with RE^{IV} = Pr[127,128] and Tb.[129]

5.4. Cu(O)–AE(O) systems. These systems have proved rather difficult to investigate. The variability of the Cu valence, combined with the strong basicity of the AE oxides, results in a tendency to adopt more and more oxidized cuprates when the AE content increases. Simultaneously, however, this gives a correspondingly more and more limited thermal stability for the phases formed. At the same time, increasing temperatures for the syntheses are re-

Table 2. Structurally characterized AE cuprates.

Phase	Space group	*a*/pm	*b*/pm	*c*/pm	Ref.
Ba_3CuO_4	...	788.3		1555	130
Ba_2CuO_{3+w}	*Immm*	1296.6	410.1	390.7	131
$BaCuO_{2+w}$	*Im*$\bar{3}$*m*	1828			132
$BaCu_2O_2$	*I*4$_1$/*amd*	572		1006	133
Sr_2CuO_3	*Immm*	1269	391	348	134
$SrCuO_{2+w}$	*Cmcm*	356	1633	392	135
$SrCuO_2$[a]	*P*4/*mmm*	392.6		343.2	136
$Sr_{14}Cu_{24}O_{41}$[b]	*Fmmm*	1147	1337	395	137
$SrCu_2O_2$	*I*4$_1$/*amd*	548		982	138
Ca_2CuO_3	*Immm*	1224	378	326	135
$Ca_4Cu_5O_{10}$[b]	*Fmmm*	280.7	635.1	1059.7	139
$CaCu_2O_3$	*Pmmn*	985	411	347	140

[a]High pressure. [b]Superstructure(s).

quired if CO_2 is present in the environment. In addition, vacancies are often encountered either in the AE or oxygen sub-lattices, and this leads to a variety of order–disorder phenomena. Phases which have so far been structurally characterized are listed in Table 2.

5.4.1. The Cu(O)–Ba(O) system. 5.4.1.1. Ambient oxygen pressure. At 800 °C and ambient oxygen partial pressure, the Ba(O)–Cu(O) subsolidus system contains two phases: $BaCuO_{2+w}$ and Ba_2CuO_{3+w}. The *x*–*t* phase diagram, as seen[141,142] by microscopy, DTA and TG at p_{O_2} = 21 kPa in Ar, is shown in Fig. 7.

The $BaCuO_{2+w}$ phase is cubic,[143] and, despite the high symmetry, one oxygen site and one Cu site are only partially occupied in the currently accepted structural model.[132,144] The sites which have variable occupation would lead to compositions $BaCu_{0.955}O_{1.91}$ and $BaCu_{1.091}O_{2.45}$, if the sites concerned are empty and filled, respectively. However, a more limited oxygen content of $BaCuO_{2.09}$ [*Im*$\bar{3}$*m*; 1830.3(6)][31] is obtained after treatment in

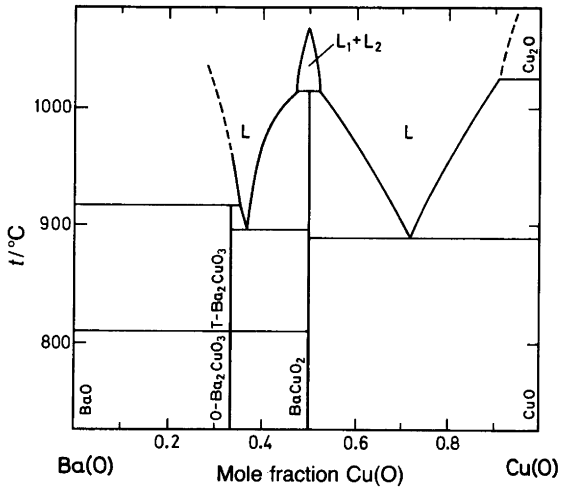

Fig. 7. An *x*–*t* diagram for the Ba(O)–Cu(O) system in an Ar–O_2 mixture with p_{O_2} = 21 kPa; after Refs. 141 and 142.

O_2 at 320 °C, and sparse data[144] are available for the homogeneity range with respect to the Cu content.

The Ba_2CuO_{3+w} phase takes a K_2NiF_4-related structure,[131] which is orthorhombically deformed at ambient temperature. At 810 °C, an orthorhombic-to-tetragonal transition is observed and the high-temperature phase can be quenched to room temperature [$Ba_2CuO_{3.3}$; *I*4/*mmm*; 399.2, 1297.5].[142,145] In accordance with the high Ba content, the oxidation state of Cu is maintained high, even for the tetragonal high-temperature modification.[146] Although no decisive data are available, it may be inferred that the low-temperature orthorhombic modification takes even higher Cu valence and oxygen content. The Ba_2CuO_3 phase is not formed on firing of carbonaceous starting materials or in air at temperatures below the melting point for the carbonate-containing system (the pure oxide system has a higher melting point), but is readily obtained[142] from the oxides (or BaO_2). Therefore, this phase is not an oxide carbonate, and it is unlikely that its structure can accommodate carbonate under various conditions.

It has been suggested that additional, Cu- and O-rich phases exist in this system ($BaCuO_{2.5}$,[147] $Ba_2Cu_3O_{5+w}$,[148,149] $Ba_3Cu_5O_{8+w}$,[36] $BaCu_3O_{4+w}$[150]) at low temperatures. These proposals are not included in the phase-diagram data in Refs. 142 and 151, obtained at temperatures between 500 and ~850 °C.

5.4.1.2. High oxygen pressures. There is a considerable discrepancy concerning the stability and formation of the copper barium oxides at high oxygen pressures. The Ba_2CuO_{3+w} phase is reported[152] to be stable at p_{O_2} = 20 MPa and *t* = 980 °C, differing only in an increased oxygen content from the situation at ambient pressure. In another study,[153] Ba_2CuO_{3+w} was not observed at p_{O_2} = 9 MPa and *t* = 1000 °C. In fact, both the stated temperatures are above the reported[142] limit of thermal stability at ambient pressure (920 °C for p_{O_2} = 21 kPa).

The $BaCuO_{2.5}$ phase[147] is reported[154] at elevated temperatures and high oxygen pressures, tentatively described[152] as perovskite-related [$BaCuO_{2.5}$; T; 569, 1420]. However, an identical PXD diagram has been obtained[153] for a slightly more Cu-rich composition $Ba_2Cu_3O_{5+w}$, and this composition is confirmed[155] by EDAX. The latter phase is therefore considered[153] to be the only ternary phase in the Ba(O)–Cu(O) system at p_{O_2} = 9 MPa and *t* = 1000 °C. Some clues to the nature of $Ba_2Cu_3O_{5+w}$ can be deduced from the fact that it is succeded by cubic $BaCuO_{2+w}$ at higher temperatures, depending on the partial pressure of oxygen (700 °C, ambient pressure).[147,149,153] This speaks for an entropy driven dissociation reaction, as if $Ba_2Cu_3O_{5+w}$ were a high Cu-valence compound, or contained peroxide or carbonate anions. All these possibilities are feasible in a closed system, where CO_2 can enter as an impurity of the reactants or originate from the oxygen atmosphere.

5.4.1.3. Low oxygen pressures. Oxygen-rich, mixed-valent barium cuprates loose oxygen at low pressures. For example, deoxidation of $BaCuO_{2+w}$ gives formally 'stoichiometric' $BaCuO_{2.00}$ [*Im*$\bar{3}$*m*; 1829.3(4)] at 800 °C and p_{O_2}

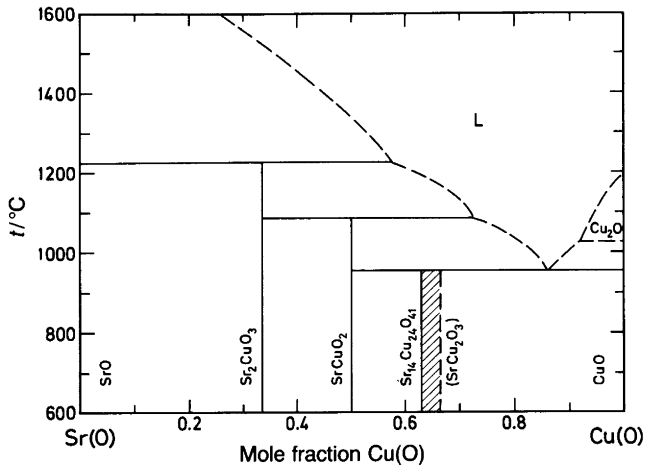

Fig. 8. An *x–t* diagram for the Sr(O)–Cu(O) system in air; after Ref. 156.

= 150 Pa (in a closed system with CuO/Cu_2O).[31] Ba_2CuO_{3+w} obtains 'stoichiometry' above 950 °C and at a very low O_2 pressure of 0.1 Pa.[130] This illustrates nicely how Ba increases the stability of the high valence state of Cu. It is therefore not surprising that Ba_3CuO_4, with a structurally fixed oxygen content and divalent copper, can only be prepared under virtually reducing conditions of high temperature and low oxygen pressure (950 °C and p_{O_2} = 0.1 Pa).[130] For even lower oxygen pressures, $BaCu_2O_2$ (and BaO) is favoured, with a typical linear coordination around Cu^I.[133]

5.4.2. The Cu(O)–Sr(O) system. In equilibrium with oxygen at ambient pressures, three ternary oxides are found,[156] as shown in the *x–t* diagram in Fig. 8. Their existence ranges with respect to pressure and temperature are determined by solid-state cell EMF measurements and TG.[157] In addition to these phases, $SrCu_2O_2$ can be obtained under low partial oxygen pressures, and there occurs a high-pressure modification of $SrCuO_2$ (Table 2).

The most copper-rich phase in Fig. 8 was originally specified as $Sr_{14}Cu_{24}O_{41}$. Its crystal structure is described as incommensurate,[137] although it is approximately compatible with a rather indistinct superstructure with $c' = 7c$.[156] Owing to the complex structural features, diffraction methods have failed to establish unequivocally the composition limits, and various proportions have been proposed for the Sr:Cu ratio: 8:13,[158] 3:5,[157] 4:7,[159] 14:24,[137] and most recently, (1+*y*):2.[160] Structure examinations in terms of observed and simulated HREM patterns (a rather powerful approach for large supercells), indicate[160] that the atomic arrangement may be derived from an hypothetical $SrCu_2O_3$ structure and that a series of solid solutions, described by $Sr_{1+y}Cu_2O_3$, may exist up to the Sr:Cu ratio 14:24 (y = 1/6). However, surprisingly small differences in unit cell parameters are observed between the Sr:Cu ratios 14:24 and 4:7,[160] and the latter is found to have a commensurate $c' = 9c$ superstructure. The weakness of the structural model based on $Sr_{1+y}Cu_2O_3$ is that the formula presumes $\nu_{Cu} \leq 2$, and this is not consistent with the experimentally established fact[157] that this phase is stable only for $\nu_{Cu}(\approx 2.24) > 2$. The oxygen content is almost independent of temperature ($\Delta w < 0.002$ per Cu between 670 and 970 °C) and is also preserved when the oxygen partial pressure is decreased. For example, at 920 °C and $p_{O_2} < 6$ kPa, a sudden decomposition is observed[157] and $SrCuO_{2+w}$ plus CuO are formed.

The structure of the ambient-pressure phase $SrCuO_{2+w}$ contains edge-sharing, double-square cuprate anions, connected into zig-zag chains.[135] Despite this rather rigid arrangement, the oxygen content may be slightly varied, $1.975 < w < 2.035$ being observed for $0.01 < p_{O_2} < 100$ kPa at 900 °C.[157]

The crystal structure of the high-pressure $SrCuO_2$ phase (6 GPa at 1050 °C) contains sheets of corner sharing, copper–oxygen coordination squares.[136] Substituted variants, containing up to 1/3 Ba or up to 2/3 Ca at the Sr site, can also be obtained under similar conditions.

Virtually no variation in oxygen content is noted[157] for Sr_2CuO_3, despite the presence of chains of copper–oxygen coordination squares in the crystal structure. The phase is fairly stable and it still exists at conditions when the ambient-pressure phase $SrCuO_2$ decomposes upon formation of $SrCu_2O_2$ (e.g. at 820 °C for p_{O_2} = 10 Pa).[157]

5.4.3. The Cu(O)–Ca(O) system. The *x–t* phase diagram of the Cu(O)–Ca(O) system, as obtained[161,162] in air, is shown in Fig. 9. Apart from Ca_2CuO_3, which has Sr and Ba analogues, two phases specific to the Cu(O)–Ca(O) system are encountered (Table 2):

(i) $Ca_{1-y}CuO_2$ is stable in oxygen only up to 835 °C (in air up to 755 °C), the homogeneity range varying presumably slightly with the temperature and oxygen pressure (e.g. y = 0.172 at 700 °C in oxygen).[162] Provided that the oxygen content is structurally fixed, the Ca deficiency corresponds to a high Cu valence of +2.34, which in turn could account for the thermal instability of this phase. The crystal structure (Table 2), related to $NaCuO_2$,[163] appears to support

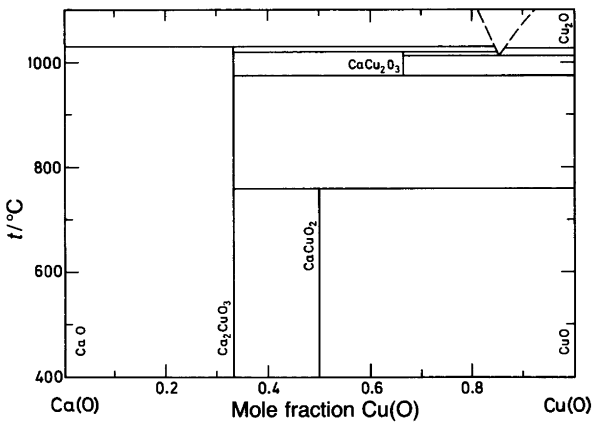

Fig. 9. An *x–t* diagram for the Ca(O)–Cu(O) system in air; after Refs. 161 and 162.

this feature, since it contains linear edge-sharing chains of cuprate squares which stabilize the oxygen content. Unlike the structure prototype, the Ca site is defect and the variable vacancy content results in various possibilities for superstructure[139] ordering [e.g. $Ca_4Cu_5O_{10}$; *Pnca*; $a' = 5a$]. Remarkably, $Ca_{1-y}CuO_2$ is reported to be an insulator, and the presence of the two chemically non-equivalent Cu atoms apparently also contributes to the order–disorder characteristics.[139]

(ii) $CaCu_2O_3$, has square-planar coordination at Cu. Double edge-sharing squares are 'aligned' into zig-zag chains, which in turn are connected into what can be described as 'corrugated sheets'.[140] As a result of this arrangement, the oxygen content is fixed, and this apparently contributes to the narrow range of thermal stability for $CaCu_2O_3$. This Cu^{II} phase becomes unstable towards more oxidized phases (in oxygen) at lower temperatures and against Cu^{I} phases at higher temperatures.

5.5. Cu(O)–RE(O) systems. Various phases in the Cu(O)–RE(O) systems are formed depending on oxygen partial pressure and the RE element. Generally, Cu^{II} compounds are formed at ambient oxygen pressures, below 1000–1100 °C. Formation of ternary oxides with formally Cu^{III} is easier for the more electronegative, larger REs, but still requires high oxygen overpressures, and temperatures that are too high must be avoided. Compounds of Cu^{I} are obtained under reducing conditions or at very high temperatures.

5.5.1. Ambient oxygen pressures. Two compounds are observed, depending on the RE. For trivalent REs smaller than Ho (including Y and Sc) a $RE_2Cu_2O_5$ phase is formed,[164,165] for larger REs (Gd to La) the composition[166] RE_2CuO_4 is adopted.

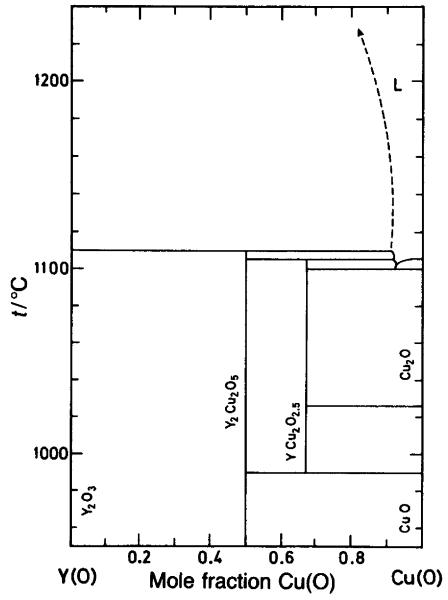

Fig. 10. An *x–t* diagram for the Y(O)–Cu(O) system in air; after Ref. 170.

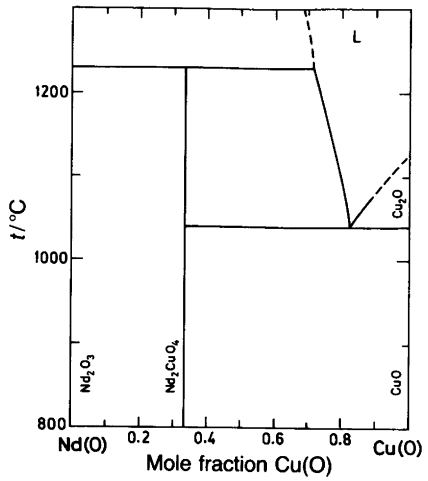

Fig. 11. An *x–t* diagram for the Nd(O)–Cu(O) system in air; after Ref. 176.

The $RE_2Cu_2O_5$ phase has an orthorhombic structure[164] [e.g. $Y_2Cu_2O_5$; $Pna2_1$; 1080.03(8), 349.53(2), 1245.88(8)].[167] For $T < 13$ K, AF magnetic ordering is observed.[168] The *x–t* phase diagram for the Y(O)–Cu(O) system in air, as obtained[169,170] by DTA and PXD, is shown in Fig. 10. The existence of an additional high-temperature phase with tentative composition $YCu_2O_{2.5}$ is indicated at 1000–1100 °C.[170]

For RE_2CuO_4, there occur two structure types, depending on the RE size:

(i) For RE = Gd, Sm, Nd and Pr a tetragonal structure[171] is formed: Gd_2CuO_4 [*I4/mmm*; 380, 1180],[172] Nd_2CuO_4 [394.5, 1217.1],[171] and Pr_2CuO_4 [396.01(3), 1223.0(1)],[173] also designated as the T′-phase. This structure contains sheets of square-planar, corner-sharing cuprate anions, interchanging with layers of isolated oxide anions, and both layers are interleaved by RE. Therefore RE_2CuO_4 is really a cuprate oxide, and the formula should rather be $RE_2CuO_2(O)_2$. This series of phases is remarkable in the sense that its members become superconducting upon electron doping, which may be achieved either by partial F for O[174] or Ce for Nd(=RE)[175] substitution, but not by deoxidation, since the oxygen content is structurally fixed. The *x–t* phase diagram for the Nd(O)–Cu(O) system in air, as obtained[176] by DTA, TG, SEM, EMP and PXD, is shown in Fig. 11. An analogous diagram is obtained[177] for RE = Eu.

(ii) For RE = La, an orthorhombically distorted, K_2NiF_4-type structure[172,178] is adopted [La_2CuO_4; *Bmab*; 536.3(5), 540.9(5), 1317(1)],[178] usually designated as T-phase. This structure contains layers of octahedral, corner-sharing cuprate anions. The layers are slightly buckled, owing to a tilt of the octahedral building units. At ~480 K the tilt disappears, and a transformation into the tetragonal K_2NiF_4-type structure is observed.[179] The T-phase, as hole-doped by Ba for La substitution, is the responsible[180] for the discovery[181] of the high-T_c cuprate superconductors.

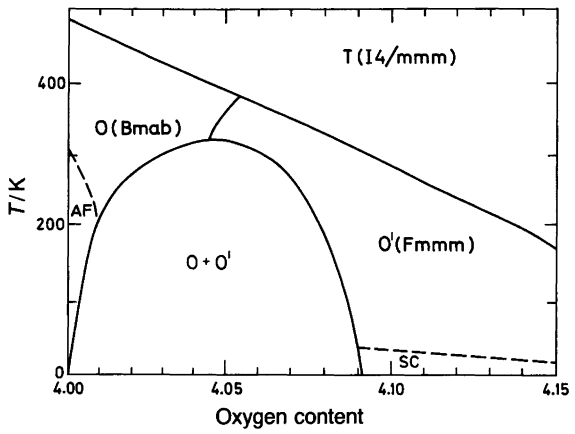

Fig. 12. Low-temperature *x–t* diagram for La_2CuO_{4+w}; after Ref. 179.

No ternary oxides of tetravalent Ce, Pr and Tb with CuO have hitherto been reported.[176,182] However, there is no reason why these REs should not be accommodated in structures appropriate to RE^{III} if reducing conditions are adopted. Pr_2CuO_4 even shows high-temperature stability in air.[105]

As a consequence of the structural features, the boundary conditions with respect to formation of oxygen vacancies or oxygen interstitials are markedly different for these compounds. This is clearly reflected in their equilibrium towards high or low oxygen pressures.

5.5.2. High oxygen pressures. $RE_2Cu_2O_5$ is reported to be stable at p_{O_2} = 20 MPa.[152] At even higher pressures, a phase based on Cu^{III} is expected to take over, but this prediction has so far only been confirmed for RE = La [$LaCuO_3$; R; 549.9, 1338].[183]

No data are available for the behaviour of the Nd_2CuO_4-type phases at high oxygen pressures, almost certainly owing to the occurrence of superconductivity upon reduction (electron doping). For the same reason, there is an abundancy of data for the high oxygen pressure behaviour of La_2CuO_4, since weak indications of superconductivity were rather surprisingly recorded for this insulating oxide. Later it was realized that additional oxygen can be inserted into this K_2NiF_4-type structure and that, below a certain temperature, this results in separation into two phases: an insulating La_2CuO_4 and a conducting La_2CuO_{4+w}, the latter being responsible for the superconductivity.[180,184–187] The distinction in oxygen content, which may amount up to 0.09 per formula, depends on temperature.[180] The relations are illustrated in the phase diagram in Fig. 12.

5.5.3. Low oxygen pressures. At low (partial) pressures of oxygen, only the La_2CuO_4 phase becomes slightly oxygen deficient. Judging from the behaviour of the $(La,Sr)_2CuO_{4+w}$ solid solution, the deficiency goes no further than to an oxygen content of 3.95 per formula, at 900 °C and $p_{O_2} = 10^{-1}$ Pa.[188] Also the Nd_2CuO_4- and $Y_2Cu_2O_5$-type phases decompose at high temperatures and low oxygen pressures (1120 °C and p_{O_2} = 400 Pa for Nd_2CuO_4).[169,172] A Cu^I-containing ternary oxide $RECuO_2$ is formed in these cases, with a structure[189,190] of the delafossite-type [$YCuO_2$; $R\bar{3}m$; 353.3, 1713.6].

6. Quaternary oxides

6.1. The Ba(O)–Sr(O)–Cu(O) system. Owing to the chemical similarity of the AEs, no true quaternary oxides occur, but there are ranges of solid solubility between the corresponding cuprates. Of these mixed systems, the mutual solid solubility of Ba_2CuO_{3+w} and Sr_2CuO_3 is investigated in particular.[145] Since the oxygen content of the former phase is variable, whereas it is constant in the latter, the homogeneity range varies with the partial pressure of oxygen. For samples quenched from 1000 °C, there is almost complete solid solubility between tetragonal $Ba_2CuO_{3.3}$ and orthorhombic $Sr_2CuO_{3.0}$, with continuous variation in the unit cell parameters and oxygen content across the composition range. Observed anomalies in the unit cell parameters can be explained away as due to fluctuation in oxygen content imposed by the quenching, which is consistent with the idea of a correlation between high oxygen content and low orthorhombic distortion.

6.2. The Ba(O)–Ca(O)–Cu(O) system. The size difference between Ba and Ca is appreciable in the Ba(O)–Ca(O)–Cu(O) subsolidus system (Fig. 13), and a true quaternary oxide $CaBa_4Cu_3O_w$ is reported[191] with a cubic, perovskite-related, $YBa_4Cu_3O_{8.5+w}$-type structure [$CaBa_4Cu_3O_w$; $Pm\bar{3}$; 817(10)].[191]

6.3. The Sr(O)–Ca(O)–Cu(O) system. Wide ranges of solid solubility exist between pairs of corresponding cuprates in the phase diagram for the Ca(O)–Sr(O)–Cu(O) subsolidus system[192] (Fig. 14). A complete solid solubility occurs between Sr_2CuO_3 and Ca_2CuO_3.[161] Roughly half of the stron-

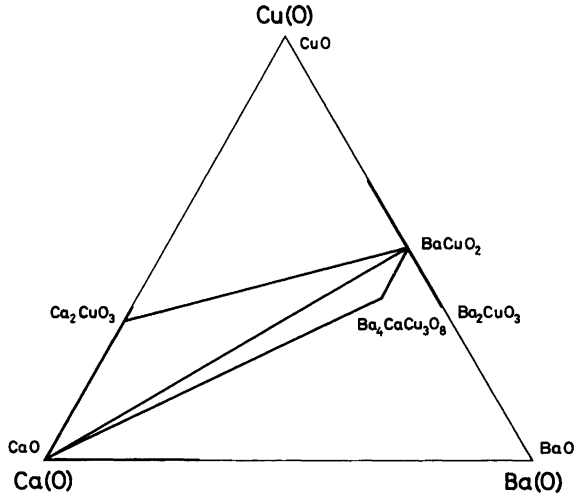

Fig. 13. A portion (indicated by the thick frame) of the subsolidus Ca(O)–Ba(O)–Cu(O) phase diagram as observed for syntheses from $BaCuO_2$ and Ca_2CuO_3 precursors in oxygen at 920–950 °C; after Ref. 191.

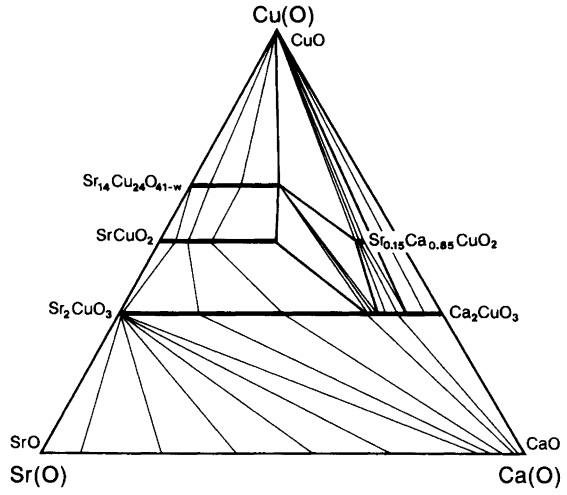

Fig. 14. Subsolidus Sr(O)–Ca(O)–Cu(O) phase diagram at 850 °C as observed for syntheses from oxides in air; after Ref. 192.

tium may be replaced by Ca in $Sr_{14}Cu_{24}O_{41}$, and about 3/4 of Sr in the ambient-pressure phase $SrCuO_2$ can be exchanged with Ca.[161]

In addition to that, a very specific partial Sr/Ca replacement may also stabilize high-pressure structures of the $SrCuO_2$-type (Table 2) at ambient conditions. Single-phase specimens with composition $Ca_{1-y}Sr_yCuO_2$ are obtained for $0.13 < y < 0.17$, specifically for $y = 0.14$ [*P4/mmm*; 386.11 (2), 319.95(2)][193] and for $y = 0.16$ [*P4/mmm*; 386.7(2), 321.95(2)].[161] The discovery of this phase was given considerable attention, since its crystal structure contained only the parallel, corner-shared CuO_2-square sheets, and was quickly dubbed 'the parent structure of the high-T_c superconductors'. However, this phase long resisted actually becoming superconducting, and only recently was superconductivity obtained for a high-pressure synthesized, electron-doped cuprate $(Sr_{1-y}Nd_y)CuO_2$, with $0.14 < y < 0.16$.[194]

6.4. The Y(O)–Ba(O)–Cu(O) system. Being the most widely studied within the scope of this review, the Y(O)–Ba(O)–Cu(O) system deserves a separate chapter. Moreover, the principal chemical and crystallographic features of the Y-based system are preserved for REs between Yb and Dy for all phases involved. Since oxide carbonates may occur in the barium-rich parts of the diagrams and may have passed undistinguished from the oxides, both phase locations and compatibility are less certain in this region (see also section 3).

6.4.1. Subsolidus pseudoternary phase diagrams. 6.4.1.1. Ambient oxygen pressures at 900 °C. As a starting point for the description of changes related to temperature and oxygen pressure, the situation at $p_{O_2} = 100$ kPa and 900 °C is presented in Fig. 15, based on selected data collected with particular attention to carbonatization problems.[23,31,195] Four quaternary oxides are included in Fig. 15:

(i) Y_2BaCuO_5 is a typical stoichiometric compound and an insulator. This oxide has an orthorhombic structure[23,196,197] with isolated square-pyramidal cuprate anions [Y_2BaCuO_5; *Pbnm*; 713.3, 1218, 565.9]. The structure is also adopted for Sm and smaller REs.[198] For a Cu^{II} compound, Y_2BaCuO_5 is extremely stable. It melts incongruently at 1270 °C,[199] and the proclaimed[200] phase transition at 1265 °C is just the decomposition into solid Y_2O_3 and a melt. The suggested[201] Cu for Y substitution in Y_2BaCuO_5 (based on samples from carbonate starting materials) may at best represent an intermediate oxide carbonate formation, since the expected polyphase mixture of 123, 211 and CuO was obtained at higher temperatures.

(ii) $YBa_4Cu_3O_{8.5+w}$ is a typical mixed-valence compound, semiconducting, with a low energy of oxygen vacancy formation, which is manifested in the variable oxygen content, depending on the partial pressure of oxygen. After oxidation at 320 °C, $w = 0.7$ is reached,[31] whereas quenching from 1000 °C results in $w = 0$.[202] The $YBa_4Cu_3O_{8.5+w}$ phase is formed readily from nitrate precursors, while unsuccessful synthesis is reported[202] from carbonates. However, above 960 °C in pure O_2, the carbonate route is possible, but the system is close to melting.[94] These facts give confidence that this phase is not an oxide carbonate. In the crystal structure[202] of $YBa_4Cu_3O_{9.2}$ [$Pm\bar{3}$; 810.2][31] all Y can be replaced by Ca.[203]

(iii) $YBa_6Cu_3O_{10+w}$ is a mixed-valence oxide, obtained only recently[204] under CO_2-free conditions. Its crystal structure is proposed[204] to be of the $Sr_3Ti_2O_7$ type (a double K_2NiF_4 variant), allowing a considerable variation in oxygen content; e.g. $w = 0.2$ [*I4/mmm*; 398.1(8), 406.5(8), 2211(1)] or $w = 1.0$ [400.4(4), 411.1(4), 2158.5(8)]. However, there is a disturbing feature in this model, in that the RE and Cu are presumed to share one crystallographic site,

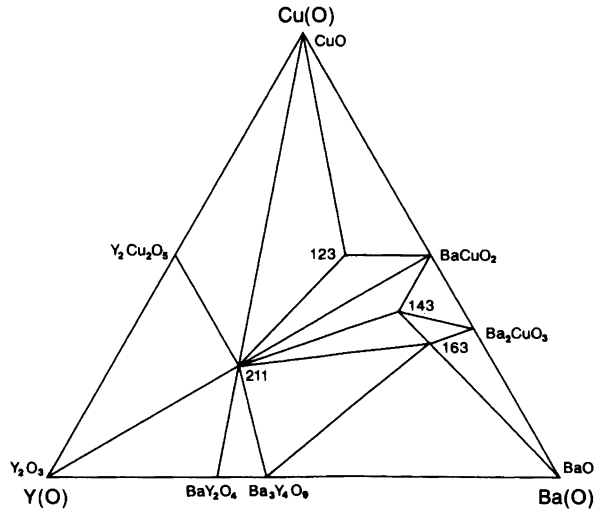

Fig. 15. Subsolidus Y(O)–Ba(O)–Cu(O) phase diagram at 900 °C in oxygen at ambient pressure, involving phase-stability data (not necessarily representing requirements for phase formation), compiled from Refs. 23, 31, 93 and 195, with special attention paid to avoidance of oxide carbonates.

a feature which is not attained above a 2 % level even for the smallest RE = Sc in $YBa_2Cu_3O_7$[205] and not found for the RE cuprates of the single K_2NiF_4 type.

(iv) $YBa_2Cu_3O_7$ is a mixed-valence oxide and the first superconductor with T_c above the boiling temperature of liquid nitrogen. Its crystal structure contains slightly deformed square-planar and square-pyramidal copper coordination in the infinite cuprate polyanion. The crystal structure[5,206] is orthorhombic [$YBa_2Cu_3O_{6.95(2)}$; *Pmmm*; 381.87 (3), 388.59(3), 1167.95(11)].[31] For the variation in the unit cell parameters close to oxygen saturation see Ref. 207. There are indications[208,209] of slight displacements of the oxygens linking the square chains, which would not be compatible with the space group *Pmmm*.

In pure oxygen at ambient pressure, $YBa_2Cu_3O_{6+w}$ reaches its maximum oxygen content of $w = 0.96(2)$ at some 310 °C, after a still fairly rapid oxygen uptake.[2] At higher temperatures the oxygen content decreases and the equilibrium oxygen pressures vary both with oxygen content and temperature. When the composition is maintained constant, the equilibrium is described by a straight line in a van't Hoff plot, e.g. eqn. (12), valid for $800 < T < 1050$ K.[2]

$$YBa_2Cu_3O_{6.5}: \log_{10} p_{O_2} = 12.99 - 8350/T \quad (12)$$

A further increase in temperature leads to the decomposition of the phase, and the oxygen pressure at the stability limit follows eqn. (13)[210] (in Pa; $800 < T_{decomp} < 1050$ K).

$$\log_{10} p_{O_2} = 9.57 - 8500/T_{decomp} \quad (13)$$

Upon deoxidation, the orthorhombic crystal structure becomes tetragonal,[211–213] and the lowest oxygen content corresponds to a complete depletion of the Cu–O square chains, leaving a linear coordination [$YBa_2Cu_3O_{6.00(5)}$; *P4/mmm*; 385.83(1), 1182.53(8)].[31] Since the deoxidation can be induced thermally, an orthorhombic to tetragonal structure transition is observed upon heating,[23,214] depending on the O_2 pressure.[6,213] Since the transformation into the tetragonal structure is a combined result of the thermally induced deoxidation and a thermally increased tendency for disorder, the oxygen content $6 + w$ *at the transition* increases with temperature[10] [eqn. (14), valid for $823 <$

$$(6 + w)_{O,T} = 6.152 + 0.483 \times 10^{-3} T_{O,T} \quad (14)$$

$T_{O,T} < 973$ K]. For the same reason, various degrees of order–disorder characteristics can be obtained for any given oxygen content $6 + w$. In the interval $0.25 < w < 0.4$, this may result in either orthorhombic or tetragonal samples for the same w, depending on the manner of cooling.[5,213] Particularly below some 300 °C, ordering of the oxygen atoms and vacancies occurs[4,6,7,215–217] in oxygen-deficient samples, observed by electron diffraction and recently also by neutron diffraction on single crystals.[218] Although a distinct ordering requires hundreds of hours of annealing at a temperature of, say, 200 °C,[217] rapidly quenched oxygen-deficient samples undergo subtle changes even at room temperature.[219] Formation of an ordered orthorhombic phase, denoted OII,[220,221] is proposed from physical properties and theoretical calculations. The combined phase properties are illustrated in Fig. 16. However, the available crystallographic evidence for insisting on a single type of ordering across the OII region is inconclusive, although the theoretical predictions are in accordance with other properties deduced from the ordering model.[224]

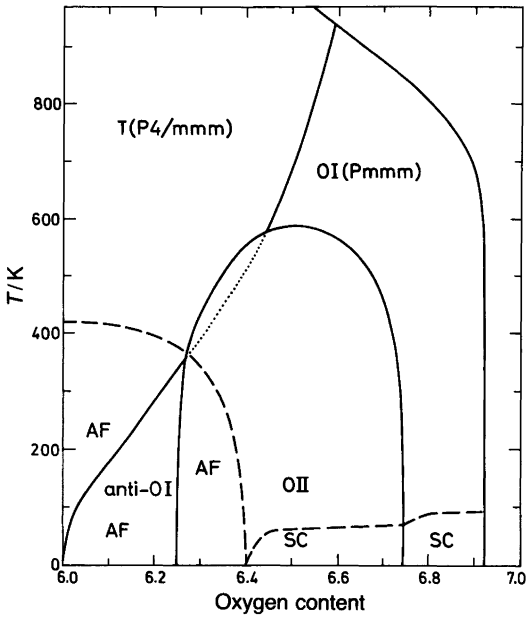

Fig. 16. Low-temperature x–T diagram for $YBa_2Cu_3O_{6+w}$, constructed from data for OII/OI,[222] AF,[223] SC,[5] and O/T[6] transitions.

The copper- and yttrium-rich portion of the Y(O)–Ba(O)–Cu(O) subsolidus system[195] in Fig. 15 agrees with the numerous diagrams published for similar conditions.[23,36,37,141,225–231] Discrepancies occur in the Ba-rich region, but these are attributed to the oxide carbonate formation (section 3). This complication is considerably veiled by the fact that all phases in this region have perovskite- or K_2NiF_4-type related structures, and thus similar d-spacings occur. The 184 oxide carbonate, which has a distinct range of homogeneity towards both Y and Cu,[32,38] was originally confused with $YBa_4Cu_3O_{8.5+w}$ and misinterpreted as a 132 oxide,[141,226–229] despite the ~6 wt % content of CO_2. Also, an 163 oxide[23,230] (a composition within the homogeneity range of the oxide carbonate[38]) and a 153 oxide[231] have been proposed. Some of these phases have also been associated[37,38] with a certain carbonate content. The situation for compositions like 152 and 385[36] is less clear, but these are certainly not carbonate-free, single-phase compounds.[32,195]

6.4.1.2. Ambient oxygen pressures at 800 °C. Lowering of the temperature to 800 °C brings an even larger part of the system into the risk zone of oxide carbonate formation (cf. Fig. 3), which now also includes the 123 phase. An in-

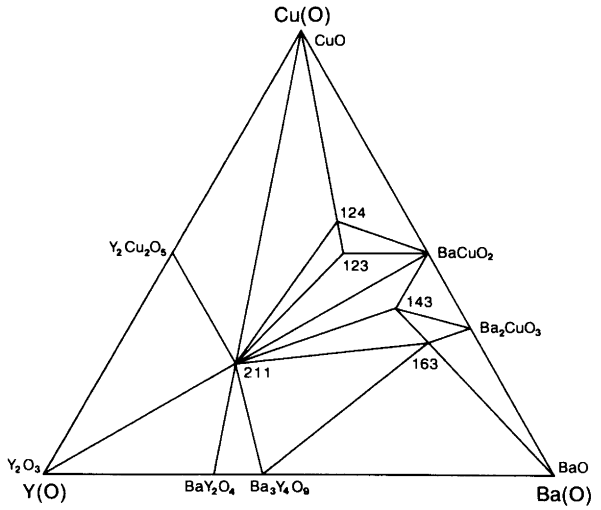

Fig. 17. Subsolidus Y(O)–Ba(O)–Cu(O) phase diagram at 800 °C in oxygen at ambient pressure, involving phase-stability data (not necessarily representing requirements for phase formation), compiled from Refs. 23, 31, 93 and 195, with special attention paid to avoidance of oxide carbonates.

teresting compositional feature of the carbonatized 123 phase is that the accommodation of rather small 'sized' cations at the Ba site is promoted, compared with the parent oxide phase. Thus even Y can now partially replace Ba, and an extended solid solution $Y(Ba_{1-y}Y_y)_2Cu_3(CO_3)_{0.2}O_{6.7+y}$, $y \in (0, 0.2)$, is obtained.[32] A substantial contraction of c occurs owing to the exchange of the large Ba with the smaller Y [$y = 0.2$; *P4/mmm*; 387.7(2), 1157.3 (13)]. Such solid solutions have variously been reported in the literature[232,233] without the authors realizing that the products are in fact oxide carbonates. It should be noted that at, say, 780 °C segregation into other phases, particularly Y_2BaCuO_5, starts after a few repeated firings of this solid solution in oxygen with ~40 ppm CO_2.

In pure oxygen, $YBa_2Cu_3O_{6+w}$ is stable[31,153] at 800 °C (duration of up to 1000 h investigated), see Fig. 17. $YBa_2Cu_4O_8$ is the only additional phase that emerges, since its thermal stability does not exceed some 850 °C at ambient oxygen pressure. Despite this low temperature, $YBa_2Cu_4O_8$ can readily be prepared[234] from carbonate starting materials in purified oxygen, and also nitrate[235] and (123 + CuO)[236] routes are described. The crystal structure[237,238] of $YBa_2Cu_4O_{7.995}$ [*Ammm*; 384.3(1), 387.0(1), 2725.0(5)][31] is related to that of $YBa_2Cu_3O_7$ by doubling the Cu–O square chains through a zig-zag edge-sharing of the squares (see also Ref. 239 for generalization to 125, 126 etc.). The resulting structural rigidity ascertains a virtually constant oxygen content up to the decomposition temperature.[240] Since gas is formed by the decomposition, the Le Chatellier principle determines that the thermal stability of this phase can be extended at higher (oxygen) pressures. In fact, this was the approach that led to the discovery of $YBa_2Cu_4O_8$.[241]

6.4.1.3. High oxygen pressures at 900–1000 °C. As an example of the effect of high oxygen pressures, a phase diagram at some 950 °C for p_{O_2} = 9 MPa is shown in Fig. 18. As can be seen, yet another new phase emerges between 123 and 124, viz. $Y_2Ba_4Cu_7O_{14+w}$. The crystal structure[242] of $Y_2Ba_4Cu_7O_{15}$ [*Ammm*; 385, 387, 5030] indeed represents a combination of the $YBa_2Cu_3O_7$ and $YBa_2Cu_4O_8$ structures. In accordance with this, there occurs a homogeneity range of some $0.0 < w < 1.0$[243-245] with respect to the oxygen content.

The 247 phase can be formed by deoxidation of 124 at elevated oxygen pressures for temperatures above some 900 °C.[246] The stability range of 247 is also narrow with respect to oxygen pressure and diminishes with both decreasing temperature and pressure. Below ~900 °C, the deoxidation of 124 leads directly to the 123 phase. The three reactions involved may be expressed as reactions (15)–(17).

$$2YBa_2Cu_4O_8(s) \rightarrow$$

$$Y_2Ba_4Cu_7O_{14+w}(s) + CuO(s) + \frac{1-w}{2}O_2(g) \quad (15)$$

$$Y_2Ba_4Cu_7O_{14+w}(s) \rightarrow$$

$$2YBa_2Cu_3O_{6+w'}(s) + CuO(s) + \frac{1+w-2w'}{2}O_2(g) \quad (16)$$

$$YBa_2Cu_4O_8(s) \rightarrow$$

$$YBa_2Cu_3O_{6+w'}(s) + CuO(s) + \frac{1-w'}{2}O_2(g) \quad (17)$$

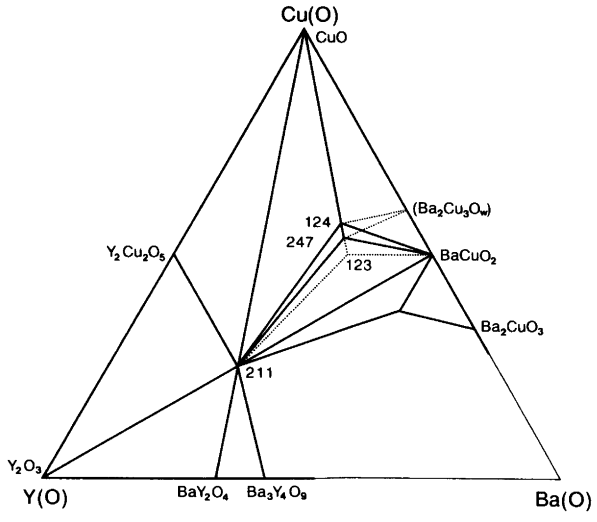

Fig. 18. Subsolidus Y(O)–Ba(O)–Cu(O) phase diagram at 950 °C in oxygen of p_{O_2} = 9 MPa, corresponding to phase stability data (not necessarily representing requirements for phase formation). The Ba-rich region is omitted, and the controversial instability of 123 is expressed by dotting. For references, see text.

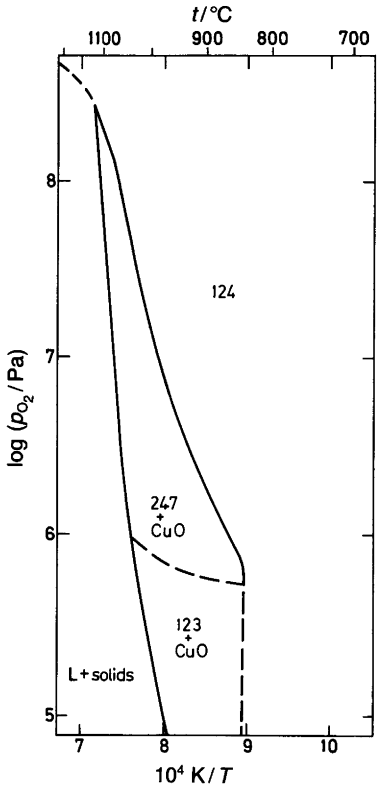

Fig. 19. A *p–T* diagram for the 124 ($YBa_2Cu_4O_8$) composition; after Refs. 244 and 246.

Comparisons[247] of various experimental results obtained for these equilibria by EMF measurements, DTA and TG with thermodynamic modelling give approximately eqn. (18) (in Pa, K) for the temperature dependence of the

$$\log_{10} p_{O_2} = 16 - 12\,500/T \qquad (18)$$

oxygen pressure of the 124 phase [eqn. (17)] over the interval $900 < T < 1250$ K, neglecting the influence of the variable oxygen content. An equilibrium *p–T* diagram is proposed[244,246] for the nominal 124 composition and oxygen pressures up to 300 MPa, showing regions of stability for the phases involved, 123, 247 and 124 (Fig. 19).

Notably, at these high pressures, the 123 composition is also reported[244] to be unstable against the formation of 124, 211 and 011, but, unfortunately, insufficient data are provided for $BaCuO_w$ for us to judge this proposal. The oxygen pressure for the decomposition of 123 over the range 900–950 °C varies surprisingly much in the literature: 20 MPa,[244] > 2 MPa[246] and < 8 MPa.[155] A decomposition of 123 under HIP-conditions is also observed.[248] The 124 and 211 phases are found among the decomposition products, but no third phase is mentioned. Adopting a cautious approach, the question of the stability of 123 at high oxygen pressures should be considered open.

Since $YBa_2Cu_4O_8$ has a structurally fixed oxygen content, whereas $YBa_2Cu_3O_7$ always contains and easily forms oxygen vacancies, the formation of 124 from 123 and CuO will always consume more oxygen than expected according to the trivial equation for its formation, and the reaction is promoted by increased gas pressures. (Note, however, that the molar volume of 124 is larger than the sum of molar volumes of CuO and $YBa_2Cu_3O_{6+w}$ for any w.) A somewhat different situation occurs when $YBa_2Cu_3O_{6+w}$ is presumed to decompose into 124 under oxygen pressure, because now a different reaction situation is encountered, where CuO is lacking for the formation of 124 according to the reverse of reaction (17). Hence 211 and a barium cuprate must also be formed, but an ambiguity occurs concerning the latter component (section 5.4.1). If $BaCuO_{2+w}$ is the product, reaction (19) should apply, or reaction (20)

$$4YBa_2Cu_3O_{6+w} \rightleftharpoons 2YBa_2Cu_4O_8 + 3BaCuO_{2+w'} + Y_2BaCuO_5 + \frac{4w - 3w' - 3}{2} O_2 \qquad (19)$$

$$5YBa_2Cu_3O_{6+w} \rightleftharpoons YBa_2Cu_4O_8 + 3Ba_2Cu_3O_{5+w''} + 2Y_2BaCuO_5 + \frac{5w - 3w'' - 3}{2} O_2 \qquad (20)$$

if $Ba_2Cu_3O_{5+w''}$ is one of the products. The 124 phase would be absent (as found in Ref. 155) if 035 were the composition of the barium cuprate. Whether oxygen is formed or consumed, viz. whether the 123 decomposition will be promoted by pressure or not, depends on the last term in reaction (19) or (20). Thus, if a Cu valence state of $\nu_{Cu} > 2.66$ for $w' = 0.33$ according to reaction (19) or $\nu_{Cu} > 2.44$ for $w'' > 0.66$ according to reaction (20) is involved next to $YBa_2Cu_3O_{7.00}$ in a certain *p–T* region, the forward reaction should be promoted by an increase of the pressure. Both situations are feasible (section 5.4.1) at high oxygen pressures.

At ambient oxygen pressure, pure 123 and 124 are simultaneously stable[31] at, say, 800 °C for at least 1000 h in pure (CO_2-free) oxygen of atmospheric pressure. When oxygen with carbonaceous impurities is used under the same conditions, oxide carbonate is formed for 123 while the pure oxide emerges for the 124 composition.[31] The difference in basicity between 123 and 124 thus makes a difference to their stability towards CO_2.

There is accordingly a serious potential source of error for experiments in closed pressurized systems, because any CO_2 inadvertently brought into the reaction chamber, either as a surface, atmosphere or carbonate-phase impurity, will not leave the system during the experiment. Moreover, elevated pressures increase the thermal stability of the oxide carbonates, which have an ample opportunity to be formed within the long-term bakings which are introduced to obtain equilibrium. For example, the typical non-superconducting, tetragonal $YBa_2Cu_3(CO_3)_uO_{6+w}$ with shortened *c* axis (section 3) is formed when a carbonate impurity from BaO_2 is introduced into closed-ampoule experiments at

910 °C.[23] This phase is also observed in high-pressure studies.[152,249] This underlines the necessity for a critical attitude towards high-pressure results, particularly when the Ba-rich region is involved.

There is virtual consent concerning the Cu-rich region [for the Ba(O)–Cu(O) subsystem at high pressures see section 5.4.1], but considerable disagreement about the Ba-rich corner. Ref. 152 claims $YBa_2Cu_2O_6$ (122) and $YBa_5Cu_2O_{10}$ (152) as new phases at p_{O_2} = 20 MPa and 980 °C, but simultaneously the occasional occurrence of tetragonal 123 immediately implies that some CO_2 has been introduced into the reaction system. Another corresponding study[153] identified only $Y_2Ba_9Cu_6O_w$ (296), and, by analysis of the data thereby presented, $YBa_4Cu_3O_{8.5+w}$ (143) must also be declared stable at p_{O_2} = 9 MPa and 1000 °C. Of these four phases, only 143 (with a known structure at ambient pressure which is unable to accommodate carbonate ions) may safely be considered as indisputable. Unsuccessful attempts to prepare 143 at high O_2 pressures and the seemingly conflicting finding that it persisted for 100 h at p_{O_2} = 9 MPa and 1000 °C, when first synthesized at ambient pressure, illustrates another problem of the high-pressure studies. Most of the experimental points in the recorded phase diagrams are obtained starting from oxides and actually performing the syntheses under high-pressure conditions (a procedure requiring long reaction times and tedious repetitions even at ambient pressures). Only occasionally is a pure phase synthesized at ambient pressure subjected to equilibrium at high oxygen pressures. In fact, enhanced credibility is often given to the former procedure, instead of crosschecking both the formation and stability of the products at ambient as well as high pressures. As discussed in section 6.4.1.1, the failure to obtain 143 is obviously due to an exposure to too much CO_2, which favours a 184 oxide carbonate during the synthesis. In fact, the reported high-pressure phases 152 and 296 may well have been mistaken for the 184 oxide carbonate,[37,38] whose homogeneity range[32] is close to 152 on the Ba–Y side and to 296 on the Y–Cu side. A necessity for oxygen atmosphere purification, and subsequent CO_2 analyses in both the atmosphere and the samples, cannot be overemphasized.

6.4.1.4. Low oxygen pressures at 800 °C. Various experimental methods exist for establishing a low partial oxygen pressure inside an oxide-containing system. One of the most exact ways to accomplish a stable oxygen pressure in a closed reaction system is to place a mixture of a metal and its oxide into the system containing the experimental specimen separately, but under a common atmosphere. Above a certain temperature, this arrangement acts as a buffer for the oxygen pressure, the exact value of which is determined by the temperature of the metal/metal-oxide mixture. The isobaric phase diagrams for the Cu- and Y-rich region of the Y(O)–Ba(O)–Cu(O) system, shown in Fig. 20, have been established this way.[31] Using a Cu_2O/CuO buffer at 800 °C, with p_{O_2} = 150 Pa in a low pressure of Ar, for 100 h of annealing time, the following compositions were ob-

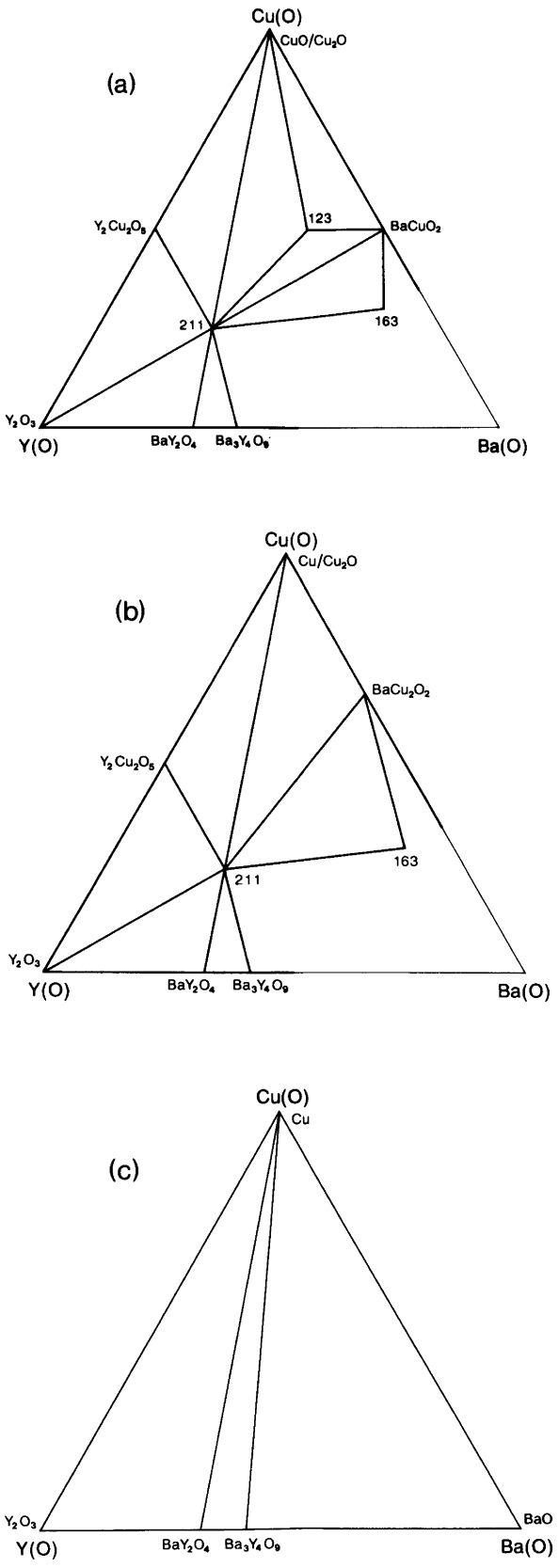

Fig. 20. Subsolidus Y(O)–Ba(O)–Cu(O) phase diagrams at 800 °C for low oxygen pressures: (a) maintained by a Cu_2O/CuO buffer, (b) defined by $YBa_2Cu_3O_6$ decomposition, (c) maintained by an Ni/NiO buffer; after Refs. 31 and 250.

Table 3. Phases involved and oxygen partial pressures (in Pa) for invariant reactions near 123 at 850 °C.

Plateau	p_{O_2}	Reaction components[a]
I	560	$YBa_2Cu_3O_{6+w} + BaCuO_2 + CuO \rightleftharpoons L + O_2$
II	410	$CuO \rightleftharpoons Cu_2O + O_2$
III	300	$BaCuO_2 + L \rightleftharpoons BaCu_2O_2 + O_2$
IV	300	$BaCuO_2 + L \rightleftharpoons YBa_2Cu_3O_{6+w} + BaCu_2O_2 + O_2$
V	270	$Y_2BaCuO_5 + BaCuO_2 \rightleftharpoons YBa_2Cu_3O_{6+w} + QB + O_2$
VI	150	$L \rightleftharpoons BaCu_2O_2 + Cu_2O + YBa_2Cu_3O_{6+w} + O_2$
VII	100	$YBa_2Cu_3O_{6+w} + Cu_2O \rightleftharpoons Y_2BaCuO_5 + BaCu_2O_2 + O_2$
VIII	70	$YBa_2Cu_3O_{6+w} + BaCuO_2 \rightleftharpoons QB + BaCu_2O_2 + O_2$
IX	40	$YBa_2Cu_3O_{6+w} \rightleftharpoons QB + Y_2BaCuO_5 + BaCu_2O_2 + O_2$

[a]QB denotes the quaternary, Ba-rich phase, indicated to occur somewhere between 132, 184, 385 and 152.

tained for the phases which have variable oxygen content: $YBa_2Cu_3O_{6.18(3)}$ [*P4/mmm*; 385.99(2), 1180.61(9)] and $BaCuO_{2.0}$ [$Pm\bar{3}m$; 1829.3(4)].[31] The 143 phase was not found stable, and the 163 phase was not examined, but according to the data in Ref. 204, the latter should be stable under these conditions. Of the phases with fixed oxygen content, the 124 phase with high Cu valence is already unstable, whereas Y_2BaCuO_5 is stable (Fig. 20a). Lower oxygen pressures (obtained with a Cu/Cu_2O buffer, $p_{O_2} = 1.4\times10^{-4}$ Pa) lead to a complete reduction of the 123 phase [$YBa_2Cu_3O_{6.00(5)}$; *P4/mmm*; 385.83(1), 1182.53(8)].[31]

Since the presented isobaric and isothermal sections of the pseudoternary system are invariant with respect to the oxygen content, and a complete description of the system would require large amounts of such sections, additional isothermal information on the subsolidus redox reactions is desirable to complete the picture. One of the most convenient methods for investigation of such univariant reaction paths is coulometric titration, which represents a stepwise, high-temperature electrolytical reduction, performed in a solid-state cell. Chemically, the reduction follows the univariant deoxidation of the phases with variable oxygen content and after each electrolysis step the cell EMF gives the oxygen equilibrium pressure for the acquired composition. A pressure plateau emerges whenever a solid polyphase region is reached by decomposition. Ahn *et al.*[1,250] investigated the Cu-rich portion of the phase diagram at 850 °C and found nine subsequent invariant reactions around the 123 point, four of them involving an intermediate formation of a liquid phase (Table 3).

Two of the equations in Table 3 represent a decomposition of a single phase, viz. CuO (II) and $YBa_2Cu_3O_{6+w}$ (IX), and the situation which emerges after the last step is shown in Fig. 20b. The equilibrium oxygen pressure for reaction II agrees well with earlier results [eqn. (9)], but a significantly higher oxygen dissociation pressure results for 123 (reaction IX) than that obtained through equilibrium experiments with Cu/Cu_2O mixtures. This may be caused by a generally low rate for the establishment of equilibrium via buffer systems at very low oxygen partial pressures and/or by the fact that the most Ba-rich phase formed by the decomposition is not well defined (subject to oxide carbonate formation). In any case, rather low O_2 pressures may be required for the removal of the last oxygen from the defect site in 123, in much the same way as it is difficult to fill the last vacancies in the opposite end of the homogeneity range (cf. Fig. 1).

A further lowering of the O_2 partial pressure reduces $Y_2Cu_2O_5$ into $YCuO_2$.[169] In a closed system with a Ni/NiO oxygen pressure buffer ($p_{O_2} = 10^{-9}$ Pa at 800 °C) nothing but copper and barium yttrium oxides is left, as seen from Fig. 20c.

6.4.2. Solidus–liquidus pseudoternary phase diagrams. As a necessary prerequisite for a successful growing of single crystals of superconducting cuprate materials, the solidus–liquidus equilibria have been much studied in the Cu-rich region of the Y(O)–Ba(O)–Cu(O) system. It was soon found that $YBa_2Cu_3O_{6+w}$ decomposes upon melting, but nevertheless plate-like single crystals can be isolated after solidification of a partially melted polyphase material.[23] The incongruent melting temperature of $YBa_2Cu_3O_{6+w}$ varies with w and in turn depends on the O_2 pressure in the surrounding atmosphere (~1000 °C in O_2),[251] according to a linear approximation[252] to a van't Hoff plot [eqn. (22), $10^2 < p_{O_2} < 10^5$ Pa]. However, a

$$\log_{10} p_{O_2} = 36.8(26) - 41\,200(3000)/T_m \qquad (22)$$

liquidus is often observed at lower temperatures than indicated above. Perhaps minor, undetected, CuO-rich phases could cause such an effect. A recent study[253] of phase-pure $YBa_2Cu_3O_{6+w}$ has indicated that, already below the melting point, Cu may have a tendency to migrate to the surface of the bulk particles. This excess of Cu on the grain boundaries causes the formation of a peritectic liquid, which in turn results in a partial phase separation upon cooling.[253] Vaporization of $YBa_2Cu_3O_{6+w}$ has been investigated[254] in a Knudsen cell (sensitivity ~ 10^{-6} Pa), and demonstrated a loss of CuO above 950 °C and a loss of BaO above 1140 °C.

The solidus–liquidus (s–l) equilibria in the Y(O)–Ba(O)–Cu(O) system are very complex, and investigations have therefore usually been limited to various pseudo-(pseudo) binary sections, a few such cuts being edited together in Fig. 21. When interpreting these data, it should be born in mind that the crucial problem concerning any phase diagram, i.e. whether a real equilibrium state is achieved or not, is considerably reinforced for s–l boundaries. In fact, each examination (microscopy, diffraction, thermal analyses, quenching, physical phase separation etc.) provides a slightly different viewpoint. Refs. 256 and 258 give instructive examples of quenching versus DTA. Different primary crystallization fields were found in a section of the pseudoternary system very close to Cu(O), resulting from the lack of equilibrium conditions during a DTA experiment. Hence, crystallizations of either $Y_2Cu_2O_5$ (DTA) or Cu_2O (quenching) were observed for one and the same composition in a certain composition interval.[256]

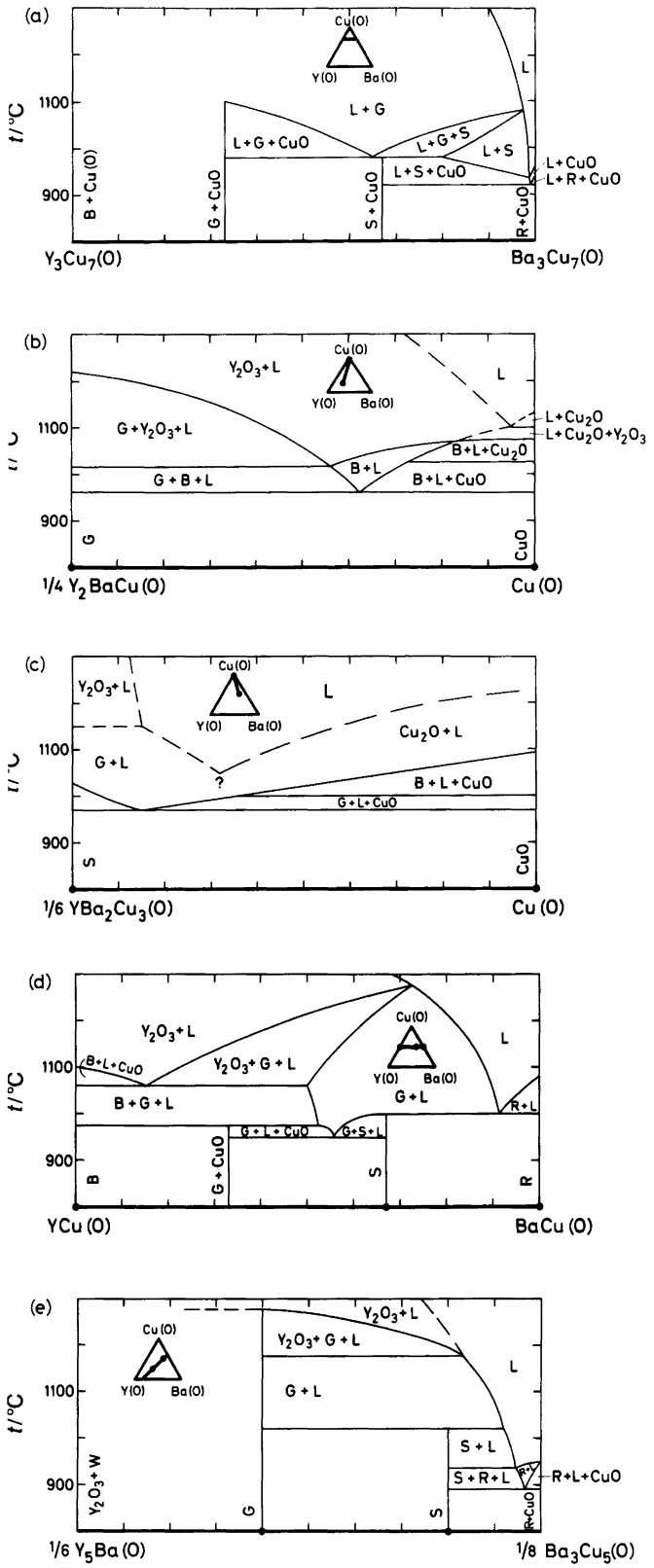

Fig. 21. Pseudobinary *x–t* diagrams for certain cuts (shown in the thick-line insets) of the Y(O)–Ba(O)–Cu(O) system: (a) from Ref. 255; in air, (b) from Ref. 256; in air, (c) from Ref. 258; in oxygen, (d) from Ref. 37; in air and (e) from Ref. 257; in air. Ternary and quaternary phases are marked as follows: (B) $Y_2Cu_2O_5$, (G) Y_2BaCuO_5, (R) $BaCuO_{2+w}$, (S) $YBa_2Cu_3O_{6+w}$ and (W) BaY_2O_4.

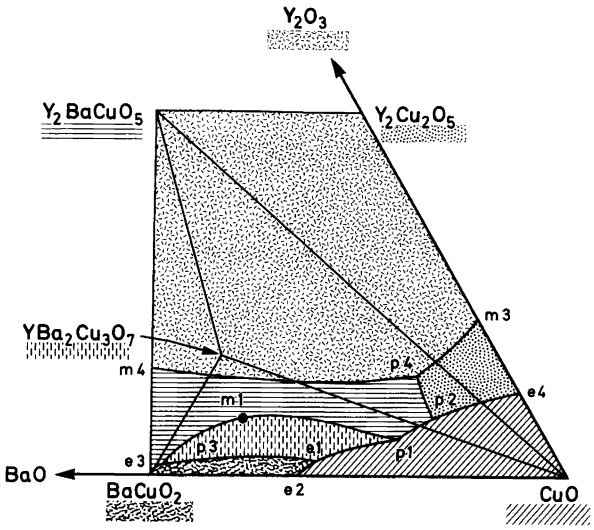

Fig. 22. Liquidus surface of Cu-rich portion of the Y(O)–Ba(O)–Cu(O) phase diagram in air; after Refs. 1, 199 and 259. Primary crystallization fields for individual phases are distinguished by shading; labelling of the points corresponds to Table 4.

A combination of all available information into a spatial *x–t* pseudoternary diagram was also attempted,[259] but here attention will only be focused on the liquidus surface for the Cu-rich portion of the system (Fig. 22). Eleven invariant reactions were observed[199] in this system, and are listed in Table 4. These reactions explain why the degree of sintering varies depending on whether or not a small excess of CuO is present, since a liquid phase is involved above 940 °C, and acts as a transport medium. An analogous explanation applies for the strong densification often observed upon the first firing, since the intimate mixtures of the particles of the individual components may produce sufficient amounts of the lowest melting eutectic (890 °C) to promote sintering.

Table 4. Phases involved and temperatures (in °C) for invariant reactions at the liquidus surface in air.

t	Invariant point[a]	Reaction components
890	e1	$YBa_2Cu_3O_{6+w} + BaCuO_2 + CuO \rightleftharpoons L(e1)$
920	e2	$BaCuO_2 + CuO \rightleftharpoons L(e2)$
940	p1	$YBa_2Cu_3O_{6+w} + CuO \rightleftharpoons Y_2BaCuO_5 + BaCuO_2 + L(p1)$
975	p2	$Y_2BaCuO_5 + CuO \rightleftharpoons Y_2Cu_2O_5 + L(p2)$
1000	e3	$Y_2BaCuO_5 + BaCuO_2 \rightleftharpoons L(e3)$
1000	p3	$YBa_2Cu_3O_{6+w} + BaCuO_2 \rightleftharpoons Y_2BaCuO_5 + L(p3)$
1015	m1	$YBa_2Cu_3O_{6+w} \rightleftharpoons Y_2BaCuO_5 + L(m1)$
1015	m2	$BaCuO_2 \rightleftharpoons L$
1026		$CuO \rightleftharpoons Cu_2O$
1110	e4	$Y_2Cu_2O_5 + Cu_2O \rightleftharpoons L(e4)$
1122	m3	$Y_2Cu_2O_5 \rightleftharpoons Y_2O_3 + L(m3)$
1270	m4	$Y_2BaCuO_5 \rightleftharpoons Y_2O_3 + L(m4)$

[a] Labelling of invariant points corresponds to Fig. 18; e is used for eutectic, p for pseudoperitectic, and m for melting point.

6.5. RE(O)–Ba)O)–Cu(O) systems. 6.5.1. Trivalent REs. In the subsolidus region, RE = Dy, Ho, Er, Tm and Yb behave similarly to yttrium.[260] However, RE = Lu is found not to be fully compatible with the $YBa_2Cu_3O_{6+w}$ structure, and a limited miscibility of some 1/3 of Lu at the Y site is found.[205] On the other hand, if the size of RE is increased, Gd is already incompatible with the $Y_2Cu_2O_5$-type structure.

An example of such a diagram at 950 °C for RE = Eu is shown in Fig. 23. In this system, Eu_2CuO_4 [*I4/mmm*; 390.1 (1), 1190.2(2)][261] appears instead of the $Y_2Cu_2O_5$-type cuprate and has none or negligible solid solubility of Ba at the Eu site. An intermediate formation of another new phase, $Eu_3Ba_3Cu_6O_{13.5+w}$, was observed upon the first firing of the carbonate precursors, with decomposition upon further annealings in pure oxygen. The tetragonal structure of the latter phase with its shortened *c*-axis, the use of carbonate starting materials and the annealing instability strongly suggest that this phase is in fact an oxide carbonate. The 336 point is accordingly omitted in Fig. 23, where also the more conservative solid-solubility limit for the $Eu(Ba_{1-y}Eu_y)_2Cu_3O_{6+w+y}$ phase according to Ref. 263 is adopted. A similar oxide carbonate problem also concerns another study[264] of the Eu(O)–Ba(O)–Cu(O) system where $BaCO_3$ was used as a starting material for investigation of the Ba-rich region around the 184 composition at temperatures which certainly would have been insufficient[32,38] to decompose the analogous $Y_{1+x}Ba_8Cu_{4+z}(CO_3)_2O_{11+w}$. At lower temperatures or higher oxygen pressures, the 247 and 124 phases appear in the Eu(O)–Ba(O)–Cu(O) system.[265] Generally, when the size of RE increases, the stability regions of the 124 and 247 phases become narrower. The region for 247,

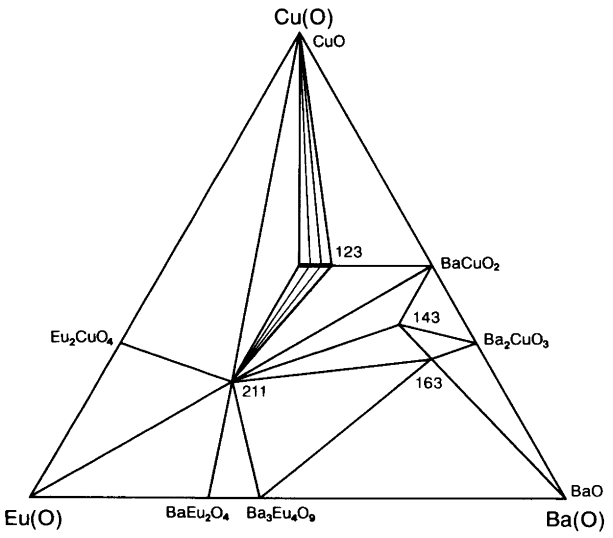

Fig. 23. Subsolidus Eu(O)–Ba(O)–Cu(O) phase diagram at some 950 °C as expected in oxygen at ambient pressure, involving phase-stability data (not necessarily representing requirements for phase formation), compiled from Refs. 93, 204, 261 and 262 with special attention paid to the avoidance of oxide carbonates.

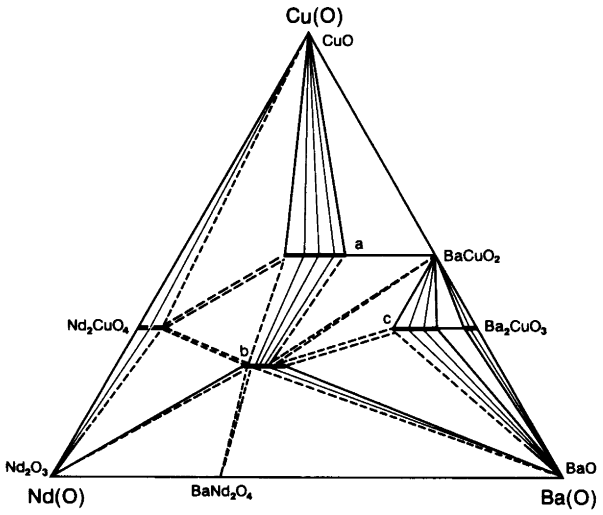

Fig. 24. Subsolidus Nd(O)–Ba(O)–Cu(O) phase diagram at some 950 °C as presumed to be seen in oxygen at ambient pressure, involving phase-stability data (not necessarily representing requirements for phase A formation), compiled from Refs. 31, 105, 262 and 266 with special attention paid to the avoidance of oxide carbonates. Phase designations:
(a) $Nd(Ba_{1-y}Nd_y)_2Cu_3O_{6+w+y}$ $(0.03 < y < 0.38)$,[105,205]
(b) $(Nd_{1-x}Ba_x)_2BaCuO_5$ $(0.00 < x < 0.15)$[266,267] and
(c) $(Ba_{1-y}Nd_y)_2CuO_{3+w+y}$ $(0.06 < y < 0.25)$.[262]

which is wedge-shaped between the 123 and 124 regions, shifts to higher pressures.[265]

Upon a further increase in the size of RE, Sm is the last to form the 143 and 163 phases.[262] In the system with RE = Nd[31,105,262,266] (Fig. 24), two principal differences occur compared with the Eu case: (i) when the RE size is large enough, there will occur some RE for Ba substitution in the true oxides, and (ii) a phase with the Y_2BaCuO_5-type structure no longer is stable.

A $Nd(Ba_{1-y}Nd_y)_2Cu_3O_{6+w+y}$ solid solution (up to y = 0.38) is observed,[105] and, for example, $Nd(Ba_{0.75}Nd_{0.25})_2Cu_3O_{\sim 7}$ [*P4/mmm*; 388.2(1), 1168.0(2)] is found stable upon repeated firings in oxygen ($BaCO_3$ was used). However, a $y > 0$ lower composition limit has been established in Ref. 205. When the $REBa_2Cu_3O_{6+w}$ nominal compositions for RE = Nd, Pr and La are annealed at 910 °C in pure oxygen until no further change in the products occurs, $RE(Ba_{1-y}RE_y)_2Cu_3O_{6.96+y}$ is formed with y = 0.030(5), 0.05 (1), and 0.09(2) for RE = Nd, Pr and La, respectively. The inferrence is that the RE site in the $YBa_2Cu_3O_7$-type structure is becoming too small to accommodate the atom concerned unless some RE is simultaneously present at the Ba site. Note that the replacement of the trivalent RE for divalent Ba results in an increase in the oxygen content, whereas the formal Cu valence is preserved.[205]

A phase with the composition RE_2BaCuO_5 and a brown colour (cf. the green Y_2BaCuO_5) is formed for Nd and the larger REs.[31] This phase has a distinct Ba for RE solid-state miscibility which may be expressed by a $(RE_{1-x}Ba_x)_2BaCuO_5$ formula with $\sim 0.0 < x < 0.15$ for RE = Nd and $0.04 < x < 0.4$ for RE = La.[266,267] Here we observe an analogous

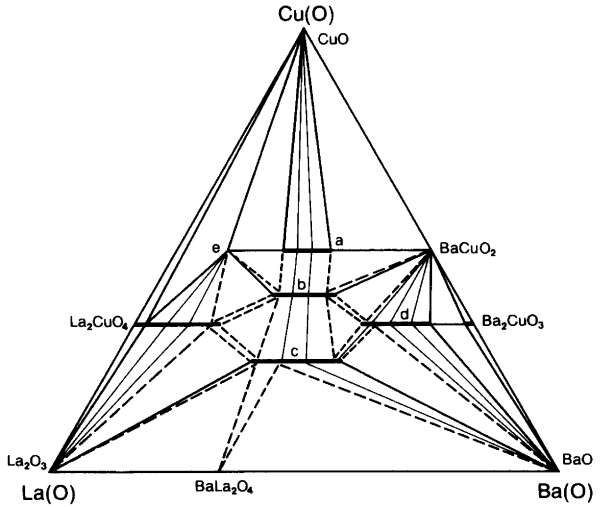

Fig. 25. Subsolidus La(O)–Ba(O)–Cu(O) phase diagram at ca. 950 °C as presumed to be seen in oxygen at ambient pressure, involving phase-stability data (not necessarily representing requirements for phase formation), compiled from Refs. 205, 262, 266, 267 and 271–273 with special attention paid to the avoidance of oxide carbonates. Phase designations:
(a) $La(Ba_{1-y}La_y)_2Cu_3O_{6+w+y}$ $(0.09 < y < 0.38)$,[105,205]
(b) $(La_{1-x}Ba_x)_2BaCu_2O_{6+w}$ $(0.10 < x < 0.40)$,[271]
(c) $(La_{1-x}Ba_x)_2BaCuO_5$ $(0.04 < x < 0.40)$,[266,267]
(d) $(Ba_{1-y}La_y)_2CuO_{3+w+y}$ $(0.12 < y < 0.33)$[262] and
(e) $BaLa_4Cu_5O_{13}$.[274]

(converse) size effect to the Ba–RE occupation discussed above, in that the phase exists with a full occupation at the Ba site only when Ba is partially present at the La site. The range of homogeneity then does not include $x = 0$, and this has apparently confused the structural description[268] and led to the rather complicated formula $La_{4-2x}Ba_{2+2x}Cu_{2-x}O_{10-2x}$. Also a 311 formula, proposed[105] for this 211 phase, is originating from a misjudgement of these solid-solution features. The crystal structure[268,269] of $(RE_{1-x}Ba_x)_2BaCuO_5$ contains isolated CuO_4 square-planar anions and belongs to the Nd_2BaPtO_5-type,[270] for example, Nd_2BaCuO_5 [*P4/mbm*; 669.80(2), 582.10(2)], $(Nd_{0.85}Ba_{0.15})_2BaCuO_5$ [670.36(5), 582.19(4)] and $(La_{0.96}Ba_{0.04})_2BaCuO_5$ [685.64 (5), 587.37(6)].[266]

In the system with RE = La[267,271,272] (Fig. 25) two additional La-specific phases emerge:

(i) An ordered, oxygen-deficient perovskite ($a = a_p\sqrt{5}$) $BaLa_4Cu_5O_{13+w}$, containing octahedral and square-pyramidal coordinations of Cu.[273] The oxygen-saturated phase is tetragonal[273] [$BaLa_4Cu_5O_{13.16}$; *P4/m*; 864.75(1), 385.94(1)] and the oxygen content decreases only slightly up to 1015 °C at ambient oxygen pressure.[274] At low oxygen partial pressures, the oxygen content can be varied between $-2.6 < w < 0.16$ without a bulk decomposition into Cu and La,Ba oxides. However, for $w \leq -0.2$, different superstructures are observed.[274]

(ii) A $Sr_3Ti_2O_7$-type, $(La_{1-x}Ba_x)_2BaCu_2O_{6+w}$ with $0.1 < x < 0.4$.[271] The structural and compositional trends which are promoted by an increase of the RE size are most pronounced for RE = La: wide solid-solubility limits extending towards Ba and La, frequently an inability to adhere to a single RE site without a simultaneous participation of RE at the Ba site and a possible parallel Ba for RE and RE for Ba substitution maintaining the 'stoichiometric' composition.

6.5.2. Tetravalent REs. The Pr(O)–Ba(O)–Cu(O) system[105] has very similar features to the RE = Nd analogue and Pr behaves virtually as a trivalent RE at ambient oxygen pressures.[205] Of the quaternary phases, only the 211 phase is not formed. Although Pr does not prevent the formation of the 123 phase, the tendency of Pr to acquire a higher oxidation state apparently interferes with hole doping and superconductivity.

6.6. RE(O)–Sr(O)–Cu(O) systems. In the Y(O)–Sr(O)–Cu (O) system,[158,159] no true quaternary phase occurs at ambient pressure. However, a possible structural analogue of $YBa_2Cu_3O_7$ is reported[275] at $p_{O_2} = 7$ GPa, created by $KClO_3$ in gold capsules encased inside the anvils of a high-pressure apparatus, [$YSr_2Cu_3O_w$; *P4/mmm*; 379.5, 1141].[275] Owing to this procedure, the stabilization of the phase by Cl or K cannot be excluded. On the other hand, attempts to obtain a 124 phase under analogous conditions failed. Another way to stabilize the Sr variant of 123 is suggested to be a substitution of a portion of Cu by Al, according to the formula $YSr_2(Cu_{1-z}Al_z)_3O_{6+w}$, $z \in (0.13, 0.3)$.[276] However, there is a significant difference in unit cell dimensions for $YSr_2(Cu_{0.78}Al_{0.22})_3O_w$ [*P4/mmm*; 381.4, 1130] compared with the high-pressure approach. Of the ternary oxides, a noticeable solid solubility of Y at the Sr site(s) is found only for $(Sr_{1-y}Y_y)_{14}Cu_{24}O_{41}$, $0.0 < y < 0.3$.[158,159]

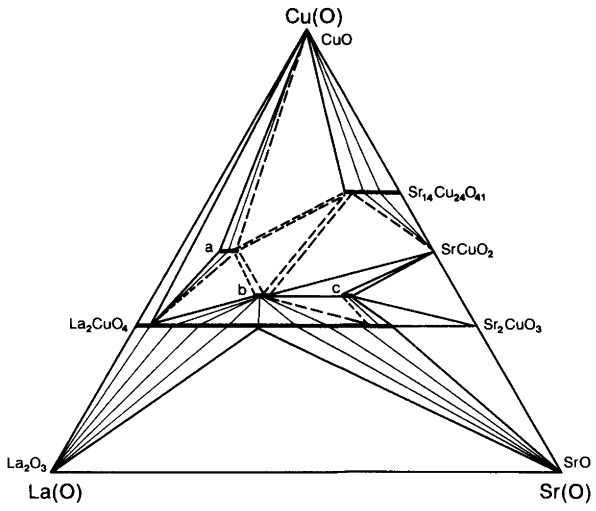

Fig. 26. Subsolidus La(O)–Sr(O)–Cu(O) phase diagram at 950 °C as presumed to be seen in oxygen at ambient pressure, involving phase-stability data (not necessarily representing requirements for phase formation), compiled from Refs. 158, 159, 271, 277, 284 and 287. Phase designations:
(a) $(Ba_{1-y}La_y)CuO_{3-w}$ $(0.16 < y < 0.24)$,[284]
(b) $(La_{1-x}Sr_x)_2SrCu_2O_{6+w}$ $(0.00 < x < 0.07)$[287] and
(c) $La(Sr_{1-y}La_y)Cu_2O_{5+w}$ $(0.025 < y < 0.075)$.[277]

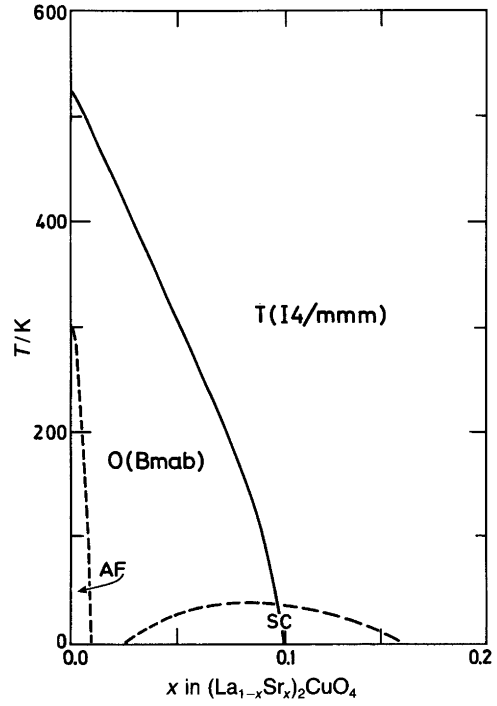

Fig. 27. Low-temperature x–T diagram for $(La_{1-x}Sr_x)_2CuO_4$; after Refs. 279 and 282.

The pseudoternary phase diagram of the La(O)–Sr(O)–Cu(O) system is shown in Fig. 26. Of the strontium cuprates, only $Sr_{14}Cu_{24}O_{41}$ exhibits a significant La for Sr solid solubility (up to 36%).[277] The K_2NiF_4-related structure of lanthanum cuprate has a broad homogeneity range with respect to Sr, [up to $x = 0.75$ according to $(La_{1-x}Sr_x)_2CuO_4$],[277] however, a transformation into a disordered tetragonal K_2NiF_4-type structure occurs as a consequence of the Sr for La substitution, with a critical concentration of $x = 0.04$[278–280] at room temperature [$(La_{0.925}Sr_{0.075})_2CuO_4$; *I4/mmm*; 377.17(8), 1322.6(3)].[281] The oxygen content remains constant on increasing substitution up to some $x = 0.14$ in an oxygen atmosphere at ambient pressure. This implies that up to a certain limiting x, defined by the actual oxygen pressure, the substitution of La by Sr increases the formal Cu valence. If this concentration is exceeded, vacancies are formed, also manifested by a drop in the unit cell parameter c and an increase in a.[278] $(La_{1-x}Sr_x)_2CuO_4$ melts incongruently, and thus single crystals cannot be grown directly from the melt, but instead a CuO solvent technique can be used.[283] A portion of the x–t phase diagram, according to Refs. 279 and 282, is shown in Fig. 27.

Apart from the phases just considered, the La(O)–Sr(O)–Cu(O) pseudoternary diagram contains three new quaternary phases:

(i) $(La_{1-x}Sr_x)CuO_{3-w}$ with $0.16 < x < 0.24$[284] (0.20 instead of 0.16 is found for the lower limit in Ref. 277) is obtained at ambient oxygen pressure. This is an ordered, oxygen-deficient perovskite ($a = a_p2\sqrt{2}$)[284] [$(La_{0.8}Sr_{0.2})CuO_{2.48}$; *P4/mbm*; 1084.0(4), 386.1(2)], with corner-sharing Cu-coordination octahedra, pyramids and squares and a variable oxygen content.[284,285] The possible formation of Cu vacancies in the copper–oxygen octahedra was indicated recently.[286] The mixed Cu valence is manifested in the metallic nature of the phase, but does not lead to superconductivity.[285]

(ii) $(La_{1-x}Sr_x)_2SrCu_2O_{6+w}$ with $0.00 < x < 0.07$[287] (0.025 instead of 0.00 is given for the lower limit in Ref. 277) has an air-quenched oxygen content of $w \approx 0.0$ which can be increased to some $w = 0.25$ upon heating at $p_{O_2} = 100$ kPa between 200 and 400 °C.[288] The latter treatment converts the original semiconductor into a metal.[289] The tetragonal crystal structure[288,290] can be derived from the doubled-K_2NiF_4, $Sr_3Ti_2O_7$-type structure and contains oxygen vacancies in corner-shared Cu-coordination octahedra, thus forming virtual Cu-coordination square-pyramids. The La atoms are located predominantly on the sheet side of the pyramids and Sr predominantly on the apex side, e.g. $La_2SrCu_2O_{6.08}$ [*I4/mmm*; 386.7(2), 1991(1)],[291] and $(La_{0.925}Sr_{0.075})_2SrCu_2O_{6.25}$ [385.30(1), 2008.33(3)].[288] Formation of analogous structures is also observed for RE = Pr, Nd, Sm, Eu and Gd.[292,293] Except for RE = Pr, a specific ordering with a tripling of b is observed by PXD[293,294] and HREM.[295] The presence of infinite square-pyramidal cuprate sheets in this structure suggested that this phase should become superconducting upon hole doping. However, superconductivity was not observed before an adjustment of the bond distances was accomplished by a simultaneous substitution by Ca (see sections 6.7 and 7.5).

(iii) $La(Sr_{1-y}La_y)_2Cu_2O_{5+w}$ with $0.025 < x < 0.075$ is obtained with an oxygen content $5 + w = 5.8$ when oxidized in oxygen at ambient pressure.[154] The crystal structure[154] is orthorhombic, perovskite-related [$La(Sr_{0.95}La_{0.05})_2Cu_2O_{5.8}$; *Immm*; 380.6, 1148.4, 2023.4].

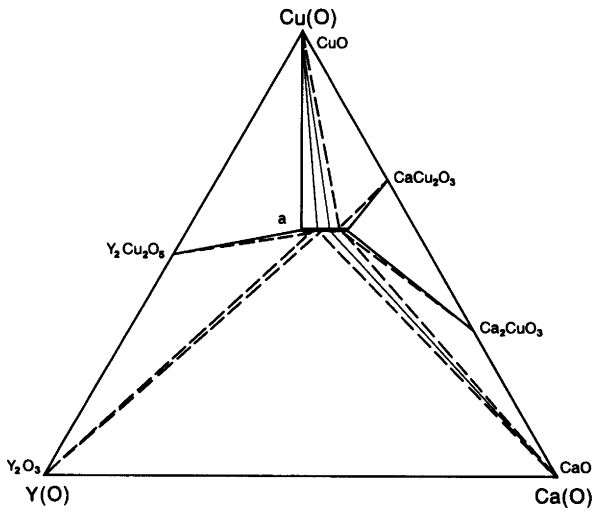

Fig. 28. Subsolidus Y(O)–Ca(O)–Cu(O) phase diagram at 1000 °C in air, including phases formed and seen under these conditions.[296] Phase designation: (a) $(Y_{1-x}Ca_x)_4Cu_5O_{10}$ $(0.5 < x < 0.7)$.

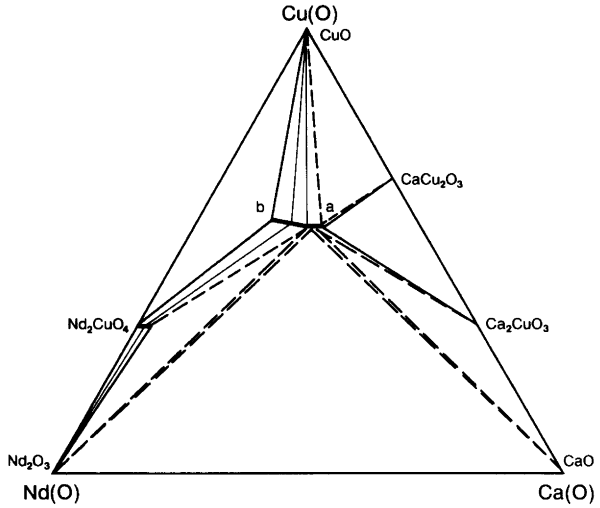

Fig. 29. Subsolidus Nd(O)–Ca(O)–Cu(O) phase diagram at 1000 °C in air, including phases formed and seen under these conditions.[296] Phase designations: (a) $(Nd_{1-x}Ca_x)_4Cu_5O_{10}$ $(0.50 < x < 0.57)$ and (b) $Nd_2Ca_{2-y}Cu_{5-y}O_{10-2y}$ $(0 < y < 1)$.

6.7. RE(O)–Ca(O)–Cu(O) systems. In the Y(O)–Ca(O)–Cu(O) system (Fig. 28), practically no regions of solid solubility are observed for the ternary oxides. However, a true quaternary phase is formed in the Cu-rich region, and has a considerable range of homogeneity with respect to the Ca,Y content. This phase is compositionally and structurally[296] linked to $Ca_{0.8}CuO_2$,[162] as expressed by the formula $(Y_{1-x}Ca_x)_4Cu_5O_{10}$ with $0.5 < x < 0.7$. Its PXD diagram is analogous to that of $Ca_{0.8}CuO_2$, including the presence of the superstructure reflections.[296] The main portion of the diagram could be indexed orthorhombically [$Y_2Ca_2Cu_5O_{10}$; *Fmmm*; 281.7, 618.5, 1059.4]. While the main reflections shift little with the variable composition, large changes occur in the rather strong superstructure lines. An incommensurate model is proposed, with $a' = 5a$ and $c' = 4.11c$ (for $x = 0.5$), based on electron diffraction.

The Nd(O)–Ca(O)–Cu(O) system (Fig. 29) contains an analogous quaternary phase. In fact, the solid solubility of Ca in $(RE_{1-x}Ca_x)_4Cu_5O_{10}$ decreases with increasing size of RE; for RE = Nd $0.50 < x < 0.57$. However, analogies in the PXD diagrams are also observed for higher Nd contents ($x < 0.5$), but the extension of the homogeneity range is not a simple continuation of that for $x > 0.5$. A single phase is observed between $Nd_2Ca_2Cu_5O_{10}$ and $Nd_2CaCu_4O_8$ (direction towards 203). At the Nd-rich limit, the superstructure peaks merge into a simple pattern corresponding to $a' = 4a$.

The entire La(O)–Ca(O)–Cu(O) system has not been reported, but from the available information[291,297] it is possible to infer that the La variant of $(RE_{1-x}Ca_x)_4Cu_5O_{10}$ is not formed. In analogy to the corresponding system with Sr, there occurs instead a $(La_{1-x}Ca_x)_2CaCu_2O_{6+w}$ phase with $0.0 < x < 0.1$.[291,297] The range of homogeneity is tentative for both ends. For example, the $x = 0$ variant is reported only when La_2CuO_4 is used as a starting material.[297] For $x = 0.055$, only oxygen contents up to some $6 + w = 6.0$ could be obtained upon oxidation in oxygen, leaving the phase semiconducting,[291] whereas the Sr variant could readily be oxidized to some $6 + w = 6.2$. The crystal structure[297] of $La_2CaCu_2O_{6.04}$ [*I4/mmm*; 383.35(1), 1951.7 (1)] or $(La_{0.95}Sr_{0.05})_2SrCu_2O_{5.97}$ [382.5, 1940][291] contains square-pyramidal cuprate sheets, which has drawn considerable attention, since this presents itself as another parent structure for the high-T_c superconductors. There is, however, an important distinction in that the copper–oxygen square-chains, which are considered to be the 'charge reservoirs' in the $YBa_2Cu_3O_7$ superconductor, are absent in $La_2CaCu_2O_6$. In line with this, (and parallel to La_2CuO_{4+w}) only weak indications of superconductivity were observed when the oxygen content exceeded the stoichiometric composition. Although $La_2CaCu_2O_6$ resists becoming fully superconducting on an attempted hole doping by a Ba for La substitution,[298] bulk superconductivity was obtained upon substitution of La by Sr.[299]

6.8. RE(O)–RE'(O)–Cu(O) systems. The similarity of REs is reflected in the formation of solid solutions with wide ranges of homogeneity in the RE(O)–RE'(O)–Cu(O) systems. Individual quaternary oxides are formed exceptionally and are then structurally related to the ternary phases. These systems have attracted considerable attention owing to the fact that they comprise both the Nd_2CuO_4- (T'-)type structures with square-planar cuprate anions in sheets, which become superconducting upon electron doping, and the La_2CuO_4- (T-)type structures with octahedral cuprate anions in layers which become superconducting upon hole doping.

The $(La_{1-x}RE'_x)_2CuO_{4+w}$ mixed crystals adopt one of these two structure types when a trivalent RE' larger than Gd is introduced, depending on the amount of RE'.[300] Partially for RE' = Gd and fully for the smaller Dy (or Tb) a hybrid structure[301] emerges (designated as T*-type) within the interval $0.4 < x < 0.5$. This structure contains square-pyramidal cuprate anions $[CuO_3^{(4+\delta)-}]_n$ in sheets together with isolated oxide anions $[(La_{0.625}RE'_{0.375})_2CuO_3O$; *P4/nmm*; 386.61(1), 1244.75(2)]. The phase is apparently stabilized by the presence of La in the T-like part of the structure (between the apices of the pyramids), whereas the smaller RE' prevail at the T'-like part (separating the square-planar bases of the pyramids). For Ho and smaller REs (also Y), tri-phase compositions of a La_2CuO_4-type phase, the $RE_2Cu_2O_5$-type phase and CuO are obtained when syntheses of the T*-phase are attempted.[300] The T*-type phase is also encountered for other combinations of larger and smaller REs; however, only upon the condition that the site of the larger RE is shared with another relatively large atom, e.g. Sr. Otherwise, the T'-structure emerges.

Considering the square-pyramidal, corner-sharing cuprate anion layers, it is not surprising that the hybrid T*-type phases become superconducting on hole doping, either by oxidation under high pressure of oxygen[302] or by a

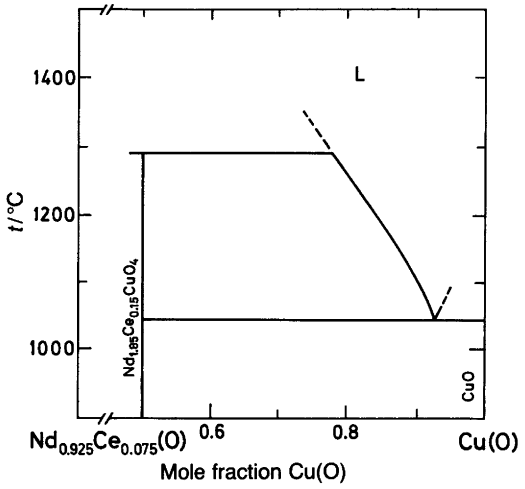

Fig. 30. An *x–t* diagram of the $Nd_{0.925}Ce_{0.075}(O)$–Cu(O) system in air; after Ref. 310.

Sr substitution for the larger REs,[303] but not by electron[301,304] doping.

The T′-type phases with square-planar cuprate anions in sheets become superconducting upon electron doping by a partial substitution of Nd by Ce,[305] but not by hole doping upon Nd substitution by Ca.[306] In the latter case, oxygen vacancies are formed instead, even when high oxygen overpressures are utilized. Superconductivity is observed for the slightly oxygen-deficient $(RE_{1-x}Ce_x)_2CuO_{4-w}$, with RE = Nd when $0.075 < x < 0.085$,[307] but the homogeneity range ($0.0 < x < 0.12$?)[307] is appreciably broader than the superconductivity region. The oxygen deficiency is very small ($w = 0.01$), but appears to be indispensable[308] for the occurrence of superconductivity. Remarkably, the same effect may also be achieved by electron doping at the Cu site (by In).[309] By analogy with $(La_{1-x}Sr_x)_2CuO_4$, $(RE_{1-x}Ce_x)_2CuO_{4-w}$ also melts incongruently, as illustrated in the *x–t* phase diagram for the $(Nd_{0.925}Ce_{0.075})_2CuO_4$–CuO[310] system in Fig. 30.

7. Quintenary oxides

7.1. RE(O)–RE′(O)–Ba(O)–Cu(O) systems. The presence of two REs does not usually bring enough difference in size and bond peculiarity to promote a new structure type. Instead, wide solid-solution ranges emerge within the structure types of the quaternary oxides.

At conditions defined by a firing temperature of 910 °C and subsequent oxygen saturation at 340 °C, full mutual miscibility occurs at the RE site of $REBa_2Cu_3O_7$ for RE = Y in combination with RE′ = Yb–Dy, Gd, Eu and Sm.[205,311–316] Less compatibility is found for the potentially tetravalent Ce and Tb, whose solid solubility at the Y site does not exceed a few per cent for Ce and some 25 % for Tb.[205,266] Substitution of Y by the smallest lanthanide Lu occurs up to some 30 %.[205] For the large Nd, Pr and La atoms, an equilibrium distribution between the Y and Ba sites exists. This implies that Nd and larger REs will not enter solely the Y site unless some RE also finds its way to the Ba site.[263] When a partial or complete replacement of only Y is attempted by Nd and larger REs, the $BaCuO_{2+w}$ phase is formed to tie up the amount of Ba which has

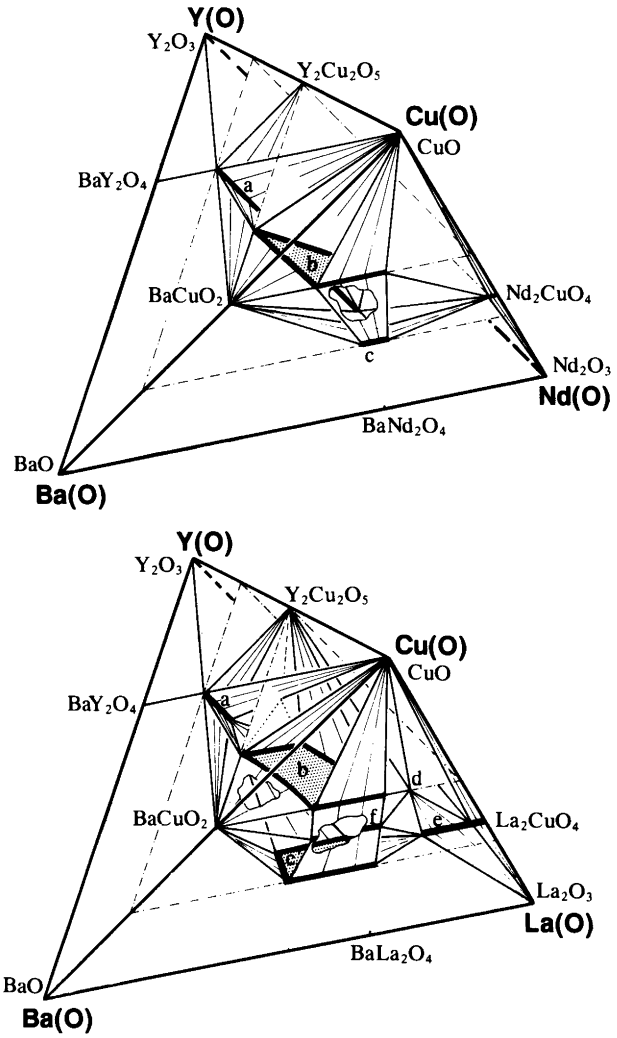

Fig. 31. Subsolidus (pseudoquaternary) tetrahedral phase diagrams of the Y(O)–Nd(O)–Ba(O)–Cu(O) and Y(O)–La(O)–Ba(O)–Cu(O) systems at 900 °C in oxygen, covering the neighbourhood of the $YBa_2Cu_3O_{6+w}$-type phase and the Cu-rich corner; after Refs. 31 and 317. Planes at Cu atomic fractions 1/4 and 1/2 are drawn (broken lines) as if they were non-transparent, and intersections of these planes with three-phase walls are drawn as dashed lines. Phase designations: (a) $(Y_{1-x}RE_x)_2BaCuO_5$ (RE = Nd: $0.00 < x < 0.85$;[31] RE = La: $0.00 < x < 0.30$[317]), (b) $(Y_{1-x}RE_x)(Ba_{1-y}RE_y)_2Cu_3O_{6+w+y}$ (RE = Nd:[105,205] $y = 0.0$ for $x = 0$ and $0.03 < y < 0.38$ for $x = 1$; RE = La:[205,317] $0.0 < y < 0.36$ for $x = 0$ and $0.09 < y < 0.38$? for $x = 1$), (c) $[(RE_{1-x}Ba_x)_{1-x'}Y_{x'}]_2BaCuO_5$ (RE = Nd: $0.00 < x < 0.15$ for $x' = 0$ and $0.0 < x' < 0.05$ for $x = 0$; RE = La: $0.04 < x < 0.40$ for $x' = 0$ and $0.0 < x' < 0.15$ for $x = 0$),[31,266,267] (d) $BaLa_4Cu_5O_{13}$,[273] (e) $(RE_{1-x}Ba_x)_2CuO_4$ (RE = Nd: $0.0 < x < 0.05$?; RE = La: $0.0 < x < 0.15$?) and (f) $(La_{1-x}Ba_x)_2BaCu_2O_{6+w}$ ($0.10 < x < 0.40$).[271]

been replaced by RE.[205] On the other hand, only La is large enough to participate at the Ba site alone (up to $y = 0.36(2)$).[205,317] If the just-mentioned critical concentration is exceeded, a substitution of Y by La also occurs and $Y_2Cu_2O_5$ appears as a second phase. This situation and the relative difference between the size effect of Nd and La is illustrated in the selected parts of the tetrahedral diagrams for the Y(O)–Nd(O)–Ba(O)–Cu(O) and Y(O)–La(O)–Ba(O)–Cu(O) systems (Fig. 31). The insertion of trivalent RE at the Ba site has a remarkable effect on the oxygen content, since the Cu valence of the oxygen-saturated (p_{O_2} = 100 kPa at 340 °C) samples is virtually preserved upon such substitutions, as expressed by the general formula $(Y_{1-x}RE_x)(Ba_{1-y}RE_y)_2Cu_3O_{6.95(2)+y}$.[317] The additional oxygens are accommodated at the vacant sites adjacent to the copper–oxygen squares. This also turns the originally orthorhombic structure into tetragonal when y exceeds a certain value, as a combined effect of the oxygen insertion and a structural deformation due to the partial replacement of (large) Ba by (smaller) RE.[263,317–320] For example, oxygen-saturated $Y(Ba_{1-y}La_y)_2Cu_3O_{6.95(2)+y}$ is tetragonal at ambient temperatures for $y > 0.140(5)$ [$Y(Ba_{0.8}La_{0.2})_2Cu_3O_{7.15}$; *P4/mmm*; 385.46(2), 1156.6(1)].[317] When the oxygen content is varied, T_c of the $Y(Ba_{1-y}La_y)_2Cu_3O_{6+y+w}$ solid solution is neither coupled to the orthorhombicity nor to whether the oxygen content exceeds 7 per formula. A correlation occurs between T_c and the Cu valence in the square-pyramidal sheets. The valence is influenced by the substitution-induced deformation of the bond lengths and by introduction of additional Cu–O bonds in the square-planar chains. Therefore, despite the constant overall Cu valence in $Y(Ba_{1-y}La_y)_2Cu_3O_{6.95(2)+y}$, T_c decreases with y. In addition, it also decreases with any reduction in the oxygen content (viz. compared with the oxygen saturated samples).[321]

Extended regions of solid solubility are found also between the Y_2BaCuO_5 and Nd_2BaCuO_5 phases; 85 % Nd on the Y side and 5 % Y on the Nd side (the corresponding figures for La as solute being 30 and 10 %, respectively). The Nd_2BaCuO_5-type structure may moreover accommodate some Ba at the RE sites, viz., up to 15 % in the RE = Nd case and 4–40 % for RE = La.[31,267]

A possibility for a minute substitution of Ba by the larger REs (Nd–La) in the $BaCuO_{2+w}$ phase follows from observations of unit cell volume changes for this phase in polyphase equilibrium samples.[266]

When the $REBa_2Cu_4O_8$ phase is considered, the span in size tolerance for the RE site is apparently slightly shifted in favour of smaller atoms as compared to $YBa_2Cu_3O_7$.[265] This means that the larger REs tend to favour the combination of 123 and CuO against 124. However, also in the 124 phase, La can partially substitute for Ba[322,323] and $Y(Ba_{1-y}La_y)_2Cu_4O_8$ is formed for $0.0 < y < 0.1$.[323] Above this limit, the reported observation of CuO could indicate that La simultaneously enters the Y site. The La substitution does not bring about any change in the oxygen content, and a rapid decrease in T_c is observed[323] with increasing y. This is in line with the structural feature of the rigid, double-square chains of the cuprate anions.

New phases appear in the RE(O)–RE′(O)–Ba(O)–Cu(O) systems when tetravalent Ce is introduced, the structures being best described as a combination of simpler structure types supplemented with degrees of solid-state miscibility. One of the structures[324,325] contains infinite slabs of corner-sharing cuprate units (with vacancies) assembled in a square-pyramid-to-octahedra-to-square-pyramid sequence, reminiscent of $YBa_2Cu_3O_7$. However, these $[Cu_3O_{8-w}]_n$ slabs contain a Ba,RE mixed occupied site and are separated by fluorite arranged layers of a RE,Ce mixed occupied site and oxygen, reminiscent of CeO_2. The chemically and crystallographically rational formula for this cuprate oxide would be: $(RE_{1-x}Ce_x)_2(Ba_{1-y}RE_y)_2Cu_3O_8(O)_2$, [e.g. $(Eu_{0.67}Ce_{0.33})_2(Ba_{0.67}RE_{0.33})_2Cu_3O_{8-w}(O)_2$; *I4/mmm*; 385.04(1), 2846.0(1)].[324] The oxygen content corresponds to $w \approx 1.1$ even after a high-pressure oxygen saturation, and the formal copper valence is relatively low, but still exceeds 2.[326] This structure is formed only for a narrow span in size of RE = Nd, Sm and Eu and the phases in question are superconducting with $T_c \approx 43$ K.[324] A large number of substituted variants has appeared.[327–329]

Another exception to the lack of new structures as a consequence of the introduction of the second RE element comes about when there is large size difference between the (otherwise trivalent) RE elements. Thus, La and Lu, the largest and smallest lanthanoid, give rise to a new structural arrangement, derived from the $YBa_2Cu_3O_7$-type structure by cation ordering, but preserving the cuprate sheets.[330] The structure is tetragonal [$La_2LuBa_3Cu_6O_{14.3}$; *P4/mmm*; 546.6, 1161.5] and by oxidation at p_{O_2} = 5 MPa it becomes orthorhombic (superconducting with $T_c = 40$ K).[330]

7.2. RE(O)–RE′(O)–Sr(O)–Cu(O) systems. No new structures are discovered in the RE(O)–RE′(O)–Sr(O)–Cu(O) systems, but solid solutions of Sr in the T*-phases are widely studied as a means of hole doping and for fine tuning of the structural size-tolerance range for the T*-phases. The Sr-substituted T*-phases (see section 6.8) of the $(La_{1-x}RE_x)_2CuO_{4+w}$ type cover a wide variety of RE combinations (RE = Sm, Eu, Gd, Tb, Dy and Y as compared to only Tb and Dy without Sr substitution).[331] Other REs than La are also stabilized by the Sr substitution at the RE site, and $(Nd,Sr,Ce)_2CuO_4$ was actually the first T*-phase observed and found to be superconducting.[332] No oxygen excess is detected (3.99 per formula)[331] in the Sr-substituted samples, and the attainable oxygen deficiency is also very low, corresponding to some 0.03 per formula unit between 1000 °C and ambient temperature.[331] An ordered distribution of the metal atoms between the non-equivalent sites is observed,[333,334] with the larger REs and Sr preferring the site between the pyramid apices (resembling the T-phase), and the smaller REs preferring the site between the pyramid squares (resembling the T′-phase).

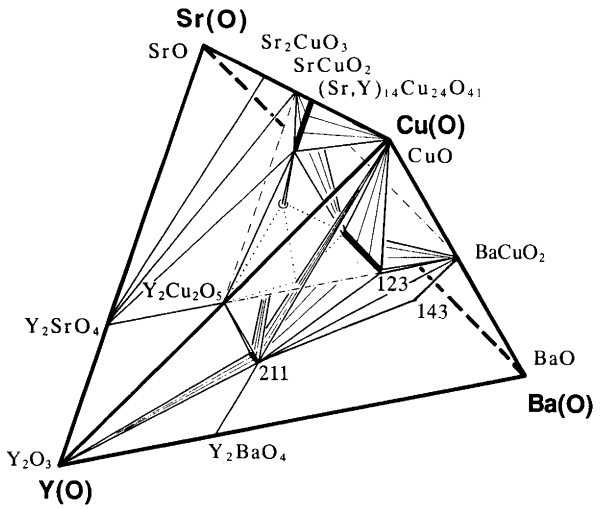

Fig. 32. Subsolidus (pseudoquaternary) tetrahedral phase diagram of the Y(O)–Sr(O)–Ba(O)–Cu(O) system at 900 °C in oxygen, covering the neighbourhood of the $YBa_2Cu_3O_{6+w}$-type phase and the Cu-rich corner; after Refs. 159 and 335. Plane at Cu atomic fraction 1/2 is drawn (broken lines) as if it was non-transparent, and intersections of this plane with three-phase walls are drawn in dashed lines.

7.3. RE(O)–Sr(O)–Ba(O)–Cu(O) systems. In the Y(O)–Sr(O)–Ba(O)–Cu(O) system, limited regions of solid miscibility are observed (Fig. 32). A Sr for Ba solid solubility is observed up to $y \approx 0.10$ in $Y_2(Ba_{1-y}Sr_y)CuO_5$ and up to $y \approx 0.4$ in $Y(Ba_{1-y}Sr_y)_2Cu_3O_{6.95}$ at 910 °C.[335] When a higher substitution is attempted for the latter phase, $Y_2(Ba_{0.9}Sr_{0.1})CuO_5$ and $(Sr_{2/3}Ba_{1/3})_{14}Cu_{24}O_{41}$ emerge and some Sr apparently enters the Y site, thus enabling even higher concentrations of Sr at the Ba site. However, the Sr for Y substitution limit in $(Y_{1-x}Sr_x)Ba_2Cu_3O_{6.95-x/2}$ is close to $x = 0$. A rather low solid solubility for Sr at the Ba site is found for $Y(Ba_{1-y}Sr_y)_2Cu_4O_8$, and $y = 0.10$ is observed[234] as the upper limit at 800 °C.

7.4. RE(O)–Ca(O)–Ba(O)–Cu(O) systems. In these systems, Ca shows solid solubility with smaller REs, whereas new structures are formed in combination with larger REs.

Most of the available information stems from RE = Y, where Ca substitutes Y up to $x \approx 0.25$ in $(Y_{1-x}Ca_x)Ba_2Cu_3O_{6.95-x/2}$ at 910 °C and $p_{O_2} = 100$ kPa.[266,336,337] Substitutions up to $x = 0.5$ were reported when the pressure was enhanced to as little as $p_{O_2} = 400$ kPa.[338] However, the observation of a $BaCuO_2$-type impurity indicates a simultaneous Ca for Ba substitution, but this possibility has not been checked.[338] Neither has the alternative that the product was an oxide carbonate been explored. The oxide carbonate hypothesis (section 6.4.1.2) would indeed explain the unusual structural features above $x = 0.25$ in $(Y_{1-x}Ca_x)Ba_2Cu_3O_{6.95-x/2}$, where a transition to tetragonal symmetry accompanied by a shortened *c*-axis is observed.

In accordance with the fairly low formation energy for vacancies in the 123 phase, the substitution of divalent Ca for trivalent Y does not increase the Cu valence, but rather decreases the oxygen content. Consequently, T_c also decreases.[266,336] Remarkably, for appreciably deoxygenated $YBa_2Cu_3O_{6+w}$ which is already non-superconducting and also tetragonal ($w \approx 0.1$), the energy of formation for oxygen vacancies becomes higher, and the Ca substitution does cause a localized hole doping at the pyramidal sheets of the cuprate anion. Hence, superconductivity reappears with low T_c.[339,340] The structure remains tetragonal, but changes in bond distances confirm the hole doping.[341]

Such a hole doping and an increase in T_c is also observed for the 124 phase, which has a structurally fixed oxygen content. Because formation of oxygen vacancies is not possible, all the extra charge brought about by the aliovalent substitution is accummulated within the cuprate network, thus increasing the formal Cu valence (and in turn T_c).[342] This acts against a high solid solubility of Ca at the Y site. From section 6.5 we know that the Y site in 124 is smaller than that in 123, and this manifests itself in a decreased relative stability of 124 when the size of RE increases. The same effect is caused by the relatively large Ca, i.e. the stability region of the Ca-substituted 124 phase is shifted towards higher oxygen pressures and Ca-substitution vanishes entirely for the 247-type structure.[343] In fact, attempted substitution of Ca (solely) for Y in 124 always produces some $BaCuO_{2+w}$, which suggests that a portion of Ba is also substituted by Ca.[266]

When the substitution of Ba by Ca in 124 was attempted, the admixture of Y_2BaCuO_5 and CuO (also $BaCuO_{2+w}$), together with the main phase, indicates possible simultaneous partial substitution of Y by Ca. The presence of Ca at the Ba site in these samples was evidenced by NQR.[344,345] The real situation apparently involves an equilibrium distribution of Ca between the Y and Ba sites. The situation is accordingly parallel to that encountered for substitutions by Nd in 123.[205]

The variation in solid solubility serves to emphasize how the size compatibility is constrained by the cuprate network in the anisotropic 123 and 124 type structures. In the more isotropic structure of $YBa_4Cu_3O_9$, a complete solid-solubility region apparently occurs, extending towards the isostructural Ca variant.[191] Naturally, no Ca–Y homogeneity region would be expected in the stoichiometric Y_2BaCuO_5 phase.

In the presence of large REs, various ordering schemes may arise when Ca is included (instead of the formation of solid solutions). Thus, a tetragonal $LaBaCaCu_3O_{6+w}$ phase is reported[346–348] virtually of the 123-type, with weak superstructure reflections in the diffraction pattern (next to some impurities). Various models for ordering are proposed[349,350] based on doubled unit cell dimensions, but these could not be confirmed in recent structure refinements using high-resolution PND data.[351] The possibility of the simultaneous presence of two variants, $La(BaCa)Cu_3O_{6+w}$ and $Ca(BaLa)Cu_3O_{6+w}$, is suggested[351] from the superconducting behaviour and the roughly halved oxygen homogeneity range ($0.55 < w < 0.93$; 400–925 °C), compared with

$YBa_2Cu_3O_{6+w}$. A detailed study[352] of similar solid solutions of the $(Y_{1-x}Ca_x)(Ba_{1-x/2}La_{x/2})_2Cu_3O_7$ type has shown that there is a solid-solution range, limited by $x \approx 0.5$, whereafter La starts to substitute at the Y,Ca site. By analogy with the La(O)–Y(O)–Ba(O)–Cu(O) system (section 7.2), such an explanation seems likely. It is therefore fairly credible that for $x = 1$ ($LaBaCaCu_3O_7$) demixing into $(La_{0.5}Ca_{0.5})(Ba_{0.625}La_{0.375})_2Cu_3O_{7.125}$, Ca_2CuO_3 and CuO occurs, in contradiction with the suggestions in Ref. 351.

7.5. RE(O)–Ca(O)–Sr(O)–Cu(O) systems. Only rather specialized compositions were studied for the RE(O)–Ca(O)–Sr(O)–Cu(O) systems, the most interesting perhaps being Sr-substituted $La_2CaCu_2O_{6-w}$, where the hole doping of the pyramidal cuprate sheets induces superconductivity.[353] The superconductivity ($T_c \approx 60$ K) is reached for $(La_{0.8}Sr_{0.2})_2CaCu_2O_{5.94(2)}$ [*I4/mmm*; 382.08(1), 1959.93(7)] which has a slight oxygen deficiency at the apical sites. A variant with Nd instead of La is also described.[354]

7.6. RE(O)–Ba(O)–Cu(O)–M(O) systems. The diversion brought into the RE(O)–AE(O)–Cu(O) systems through the introduction of a fourth kind of metal is much more drastic than in the previous cases when similar AEs or REs are involved. However, the problem is that not even the RE(O)–AE(O)–M(O) systems are known well. For some specific cases concerning superconducting phases, there is an abundance of information about solid solubility for various metals M. Occasionally, the phases in equilibrium at the solubility limits are also stated.

7.6.1. Solid solubilities of M(O) in RE(O)–Ba(O)–Cu(O). *Solid solubility at the RE site* is not common for other elements than REs and AEs. Of alkaline metals, sodium may apparently be present at the Y site up to a few atom percent provided a matching amount is allotted to the Ba site.[31] Cadmium is reported[355] to enter the Y site in $YBa_2Cu_3O_{6+w}$ up to some $x = 0.5$, with a rather surprising negligible effect on T_c, despite a structural conversion from orthorhombic to tetragonal at $x = 0.4$. However, the presence of $BaCuO_2$ impurities suggests that Cd may also be present at the Ba site, although this possibility is not considered in Ref. 355. Curium forms a non-superconducting $CmBa_2Cu_3O_7$ phase.[356] Also an equiatomic Th,Ca mixture is reported partially to enter the Y site of $YBa_2Cu_3O_{6+w}$, $x \leq 0.1$.[357]

The La site in La_2CuO_4 can also be substituted partially, using alkali metals of related size, viz. Na and K[358,359] up to some $x = 0.25$. The $(La_{1-x}M_x)_2CuO_4$ phase becomes superconducting above $x \approx 0.1$ for M = Na, and above $x \approx 0.15$ for M = K. Syntheses of homogeneous, single-phase oxides which contain the alkali metals are difficult owing to the high volatility of the alkali metal peroxides and superoxides. Usually, a deficit in alkali metal is found in the subsequent analyses of the products, despite the precautions taken.

Solid solubility at the Ba site is rarely found for other than REs or AEs. Alkali metals again are practically the only candidates, and minute amounts of K, Rb and Cs are reported either at the Ba site[360] or at both the Y and Ba sites in $YBa_2Cu_3O_{6+w}$.[31,361] No incorporation of Pb at the Ba site was found, and other structures are in fact formed when PbO is introduced into the RE(O)–AE(O)–Cu(O) system. Since these cuprates are often superconducting, section 7.6.3 is devoted to them.

Solid solubilities at the Cu sites are optimal for chemically related metals of similar ionic size. For the $YBa_2(Cu_{1-z}M_z)_3O_{6+w}$-type substitution, an overview of candidates for substituents is presented in Table 5, together with the phases involved in equilibrium at the solid-solution limits. Despite the comprehensive literature on these substitution phases, such key data are not frequently reported,

Table 5. Equilibrium phase composition at the limit of solid solubility for M in $YBa_2(Cu_{1-z}M_z)_3O_{6+w}$ for samples fired at 910 °C and oxidized at 340 °C.

M	Y_2BaCuO_5	$BaCuO_{2+w}$	Other observed phases	z_{lim}	Ref.
Li	+	+	$BaCO_3$(·Li_2CO_3 ?)	0.04(1)	362
Mg	+	+	MgO	0.04(1)	362
Sc	+	–	$BaSc_2O_4$[a]	0.01(1)	362
Ti	+	–	Ba_2TiO_3, $BaTi_2O_5$, $BaTi_4O_9$, TiO_2	0.00(2)	362
V	+	–	$Ba_3V_2O_8$[a]	0.00(4)	362
Cr	+	–	$BaCrO_4$[a]	0.02(1)	362
Mn	+	–	$Ba_3Mn_2O_8$[a]	0.00(3)	362
Fe	–	+[b]	$YBa(Cu_{1-z}Fe_z)_2O_5$[c]	0.22(1)	362
Co	–	–	$YBa(Cu_{1-z}Co_z)_2O_5$,[d] $Ba(Co_{1-z}Cu_z)O_w$[e]	0.30(5)	362
Ni	+[f]	+[f]	NiO	0.08(1)	362
Zn	+[f]	+[f]	[a]	0.09(1)	362
Al				~0.04	363–365
Ga				~0.05	366

[a]A small amount of an additional phase is expected to occur. [b][$Ba(Cu_{0.70(5)}Fe_{0.30(5)}O_{2+w}$; *Im*$\bar{3}$*m*; 1842.4(4)]. [c][$YBa(Cu_{0.6}Fe_{0.4})_2O_5$; *P4mm*; 387.0(1), 767.1(1)]. [d][$YBa(Cu_{>0.5}Co_{<0.5})_2O_5$; *P4mm*; 387.2(1), 756.2(2)]. [e][$BaCoO_{2.80(3)}$; H; 571.65(2), 444.00(2)]. [f]Substitution by M occurs.

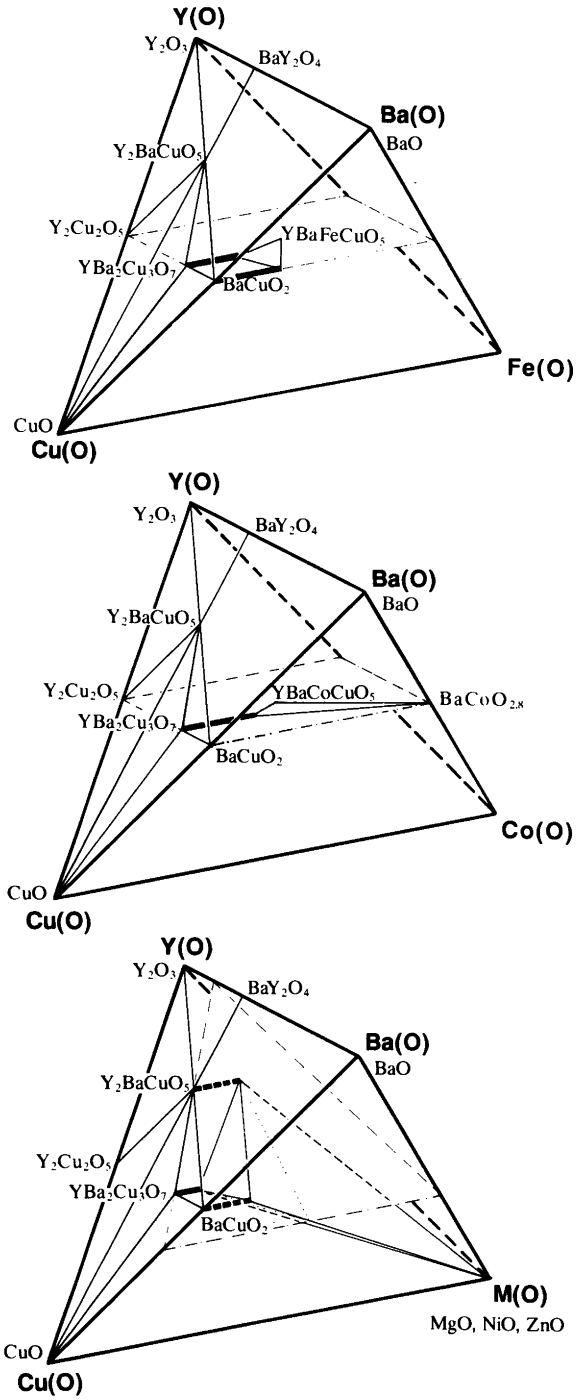

Fig. 33. Four-phase tetrahedral envelopes adjacent to the M-saturated $YBa_2(Cu_{1-z}M_z)_3O_{6+w}$ solid solutions for M = Fe, Co and Ni/Zn/Mg, in subsolidus (pseudoquaternary) tetrahedral phase diagrams, as seen by room-temperature PXD after firing at 900 °C in oxygen.

simply because the extra labour has not been undertaken to perform the tedious experimental work on poly-phase materials to ensure equilibrium. This statement is particularly valid for the investigations on substituents with very low limits of solid solubility,[362] where the detection threshold for the adopted analytical method should also be taken into consideration. For a high sensitivity PXD instrumentation,[362] the detection limit is 0.5 and 1 wt. % for the nearest neighbour phases Y_2BaCuO_5 and $BaCuO_{2+w}$, respectively. Therefore, substitution limits with $z < 0.01$ cannot be ascertained. The solubility limits from Ref. 362 agree reasonably well with the sparse data explicitly stated in the literature, e.g. Fe ($z = 0.18$)[367] Co ($z = 0.25$)[368] Ni ($z = 0.04$,[369] 0.09,[370] 0.10–0.17[371]) and Zn ($z = 0.10$,[364] 0.12[372]). The reported[373,374] substitution limit of $z = 0.10$ for Au is questioned in Ref. 375. Substitution by Pd into the square-planar Cu site is indicated up to $z = 0.17$ (a half occupancy of the Cu site in question), but phase-purity could not be maintained owing to low termal stability.[376] The three- or four-phase neigbourhoods at the solid-solubility limits are included in the tetrahedral diagrams for typical groups of substituents in Fig. 33.

For oxygen saturated $YBa_2(Cu_{1-z}M_z)_3O_{6+w}$, the formal Cu valence remains virtually constant according to iodometry, and when the valence of the substituent exceeds the valence of Cu e.g. Fe^{III}, Co^{III}, $Ni^{>II}$, Al^{III} or Ga^{III}, the oxygen content may hence exceed seven.[362,377] A crossover from orthorhombic to tetragonal symmetry, as seen by PXD at 295 K, occurs at a rather low substitution level, usually below $z = 0.05$.[362,364,366] This behaviour coincides with the fact that Fe, Co, Al and Ga introduce a tendency for non-planar coordination at the Cu square-planar site, where they predominantly reside when the substituent concentration is low and the oxygen fugacity is high.[378–380] This coordination incompatibility is best taken care of at the twin-domain boundaries of the orthorhombic structure, where these elements tend to concentrate. With increasing z, the amount of such boundaries must increase at the expense of the bulk material, and the domain size is reduced to the nanometre scale, observable by HREM.[381,382] However, the orthorhombic structure persists at quite high substitution levels of iron (and cobalt) if a reducing atmosphere is applied during the firing and the samples are reoxidized at low temperatures.[383,384] Under reducing conditions, these higher-valent substituents tend to be located primarily at the square-pyramidal Cu(2) sites where, owing to the site symmetry, they are not coupled via twinning. The critical concentration for the orthorhombic to tetragonal transition is increased to some $z_{O,T} = 0.15$, which is about the same as found for the La for Ba substitution and attributed to the linkage of the copper–oxygen chains where the additional oxygens enter.[317]

Also other phases of the RE(O)–AE(O)–Cu(O) systems are liable to a similar substitution. For example, $YBa_2(Cu_{1-z}Fe_z)_4O_8$ is prepared up to $z = 0.1$ and found tetragonal and non-superconducting above $z = 0.04$, in direct contrast to the relatively benign effect of Fe towards superconductivity in the 123 phase.[385] A second example is the La_2CuO_4-type phase, where Cu can be substituted by Li up to $z = 0.5$,[386] by Co in the $(La,Sr)_2CuO_4$ variant,[387] or by Zn up to $z = 0.45$ in $(La_{0.925}Sr_{0.075})_2CuO_4$, reverting the K_2NiF_4-type structure into the distorted [*Bmab*] structure of the Sr free La_2CuO_4.[388]

7.6.2. Derivative and ordered solid solutions with M(O) in RE(O)–Ba(O)–Cu(O) systems. A special kind of M for Cu substitution occurs within the $REBa_2Cu_3O_{6+w}$-type family for large REs. The introduction of M = Nb or Ta here leads to a complete replacement of the Cu–O coordination square chains by sheets of M-centred octahedra.[389] An oxygen content of 8 per formula is thus obtained for the non-superconducting $La(Ba_{0.95}La_{0.05})_2(Cu_{0.1}Ta_{0.9})Cu_2O_8$ [*P4/mmm*; 396.58(1), 1203.04(3)]. A zig-zag folding of the octahedra occupied by the transition metal is deduced from weak superstructure reflections [*I4/mcm*] observed by neutron diffraction.[390] This indicates that an analogous tilt to that proposed[208,209] for $YBa_2Cu_3O_7$ may be indeed feasible.

Small REs such as Y do not allow such a location of transition metals in the 123 structure, and when this is attempted, a different perovskite arrangement is obtained, despite an analogy in stoichiometry, e.g. $YBa_2Cu_2WO_{9-w}$ [$Fm\bar{3}m$; 833.2].[391] Other substituents may introduce a completely different coordination at one of the Cu sites in $YBa_2Cu_3O_7$, leaving the other untouched. For example, non-superconducting $YBa_2TlCu_2O_7$ [*P4/mmm*; 386.87(1), 1247.3(1)] has a Tl–O monolayer sheet instead of the square chains[392] and is hence not isotypic with $YBa_2Cu_3O_7$. This compound can be made superconducting (T_c = 94 K) by hole doping substitutions.[393]

A complete replacement of Cu in the $YBa_2Cu_3O_7$-type structure is nevertheless possible for M = Co and Fe. The replacement by Co is reported under the condition[394] that some barium is simultaneously substituted by potassium [$Y(Ba_{0.75}K_{0.25})_2Co_3O_8$; *P4/mmm*; 386.8(2), 1123.7(9)]. The formation of the Fe-containing sample requires[395] long-term heat treatments which facilitate the appropriate ordering [$YBa_2Fe_3O_8$; *P4/mmm*; 391.67(3), 1181.8(1)].[266] However, the structural difference between $YBa_2Fe_3O_8$ and $YBa_2Cu_3O_7$ does not allow for the substitution of more than 7 % Fe by Cu in the former and 22 % Cu by Fe in the latter.

7.6.3. A special system: Pb(O)–RE(O)–AE(O)–Cu(O). Substitution of Ba by Pb in $YBa_2Cu_3O_7$ is surprisingly negligible, considering the similarity of these two elements, different phases being formed instead. For example, attempts to use PbO_2 as a source of oxygen pressure in closed systems with $YBa_2Cu_3O_7$ cause a vapour-phase transfer of lead into the cuprate, and upon completion of this process new phases, not found in the Y(O)–Ba(O)–Cu(O) system, are observed. The first such Pb cuprate to be discovered[396] was $YSr_2Cu_3Pb_2O_8$, which is indeed closely related to $YBa_2Cu_3O_7$. Its crystal structure[397] contains the same square-pyramidal Cu–O sheets separated by Y. The pyramidal sheets are, however, connected not by square chains as in the parent structure, but via an assembly of (two) plumbate pyramids (with twice the base of the cuprate) interconnected by a linear cuprite arrangement [$YSr_2Cu_3Pb_2O_8$; *Cmmm*; 538.9, 542.8, 1571.7]. The Ba variant also exists, and here a slight inequality of the Pb–O bonds is detected[398] which excludes the *C* centering of the unit cell reported for the Sr variant [$YBa_2Cu_3Pb_2O_{8+w}$; $P22_12$; 537.5(1), 540.7(1), 1571.3(2)]. In accordance with the formula and the structural arrangement, one Cu^+ and two Cu^{2+} are present in these phases, if Pb is supposed to be divalent. This also explains the need for mildly reducing conditions in the syntheses in order to avoid formation of an $AEPbO_3$ (perovskite). Nevertheless, at a lower temperature of some 450 °C, which is insufficient for the diffusion of the metal atoms and nucleation, but high enough for diffusion of oxygen, the oxygen content in $YSr_2Cu_3Pb_2O_{8+w}$ can be enhanced from $w = 0.0$ and varied within the limits $1.0 < w < 1.9$.[397] The crystal structure[399] turns tetragonal upon oxidation [$YSr_2Cu_3Pb_2O_{9.4}$; T; 544.2(4), 1582.2(8)]. According to refinements in terms of space group *Pmmm*, the additional oxygen atoms are accommodated in much the same way as in $YBa_2Cu_3O_{6+w}$, i.e. forming (disordered) square-planar cuprate chains for $w = 1$, which are converted into octahedral sheets for $w = 2$. The variants with $w = 0$ and $w = 1$ are formed in large domains and thus the low oxidized products really consist of two phases in variable amounts while the unit cell parameters of the two phases remain the same. With continued oxidation to $w > 1$ the oxygen uptake gives rise to a continuous increase in unit cell parameters. Surprisingly, even the fully oxidized phase with $w \approx 1.9$ was not found[399] superconducting, and this is explained as a change in oxidation behaviour when Cu^{2+} is reached for $w = 1$, whereafter Pb^{2+} is subject to oxidation. However, this can be circumvented by 'localizing the oxidation' (hole doping) close to the square-pyramidal cuprate sheets via a Ca for Y substitution, and superconductivity up to 70 K is indeed obtained.[400,401] Based on comparisons with the $YSr_2Cu_3Pb_2O_{8+w}$ model structure, various related structures follow:

(i) If one of the two Pb square-pyramidal sheets in the previous structure is deleted and the linear cuprite arrangement is attached directly to the apex of the square-pyramid in the cuprate sheet, the framework being supported by the presence of Ba as in 123, the crystal structure[402,403] of $YBaSrPbCu_3O_{7+w}$ is obtained [$w = 0.0$; *P4/mmm*; 384.7 (1), 2748(1)]. Also in this structure, the oxygen content can be varied, $0.0 < w < 1.4$, but the oxygen release to $w = 0.0$ takes place rather abruptly at 580 °C.[405]

When the imagined elimination of structural elements from $YSr_2Cu_3Pb_2O_{8+w}$ is continued and the linear copper coordination together with its Ba support (previously mentioned) is removed and half of the Pb atoms are interchanged with Ca, the structure[404] of $YSr(Pb_{0.5}Ca_{0.5})Cu_2O_7$ *P4/mmm*; 382.37(7), 1186.7(3)] is obtained. Also this phase becomes superconducting only when doped by Ca at the Y site ($x \approx < 0.5$).[404] Various solid solutions may be formed. For example, the Pb site can accommodate Sr or Cu instead of Ca, and a variety of REs may replace Y, which in turn partially can be substituted by Ca.[286,405,406]

(ii) Another way of modifying the $YSr_2Cu_3Pb_2O_{8+w}$ structure involves elimination of the Y layer and merging the two cuprate square-pyramidal sheets into one octahedral (imagined as removal of one CuO_2 layer). Such a structure[407] is formed for $(Sr_{1-y}La_y)_2Cu_2Pb_2O_{6+w}$, $0.45 < y <$

0.55 and $w \approx 0$ or $w \approx 1.4$,[408] where a portion of Sr is replaced by La [$SrLaCu_2Pb_2O_{6.1}$; *Cmmm*; 530.3(2), 540.9 (2), 1262.0(2)], the oxidized form being apparently tetragonal, [$SrLaCu_2Pb_2O_{7.4}$; T?; 542.1(2), 1265.2(3)],[409] and non-superconducting.

(iii) Introduction of Ce and oxygen between the square-pyramidal cuprate sheets has already been considered (section 7.1). The Ce atom brings about a tendency to arrange the oxygens into fluorite-type layers as in CeO_2. From the $YSr_2Cu_3Pb_2O_{8+w}$ structure, a cuprate oxide plumbate may be derived, by replacing the Y layer by a $(Ce,Nd)_2O_2$ fluorite interlayer, forming the non-superconducting $CeNdSr_2Cu_3Pb_2O_{8+w}(O)_2$. Since the cuprate plumbate coordination is preserved, the structure of the latter phase[410] is also orthorhombic when reduced and tetragonal when oxidized [$CeNdSr_2Cu_3Pb_2O_8(O)_2$; *Immm*; 547.28(4), 544.81(4), 3703.3(3)].[410]

The cuprate plumbate polyanions in the fluorite-interleaved structure can be further modified as described under (i) and (ii). For example, $CeEu(Sr_{0.65}Ba_{0.35})_2Cu_3PbO_7(O)_2$[411] [T; 385.4(1), 1637.4(2)] may be derived by an imagined elimination of one of the two plumbate square-pyramidal sheets.

8. Concluding remarks

Although chemical information is effectively communicated in the form of phase diagrams, it is clearly seen that only superficial understanding of phase relations and interactions with the atmosphere would be accomplished without the accompanying structural information. In systems like the cuprates, where the directional character of the chemical bond is limited to the anionic network and therefore relatively predictable, the composition and stability of the oxides formed depend largely on the size of the cations and requirements for an efficient filling of space. Each site in such a structure thus represents a void of a certain size and shape which can be filled by a chemically compatible atom which obeys a certain tolerance with respect to size. The more the actual size of the cation in question departs from the optimal size of the void, the more unstable the structure becomes. The span in the size tolerances differs very much, as is nicely demonstrated by the solid-solution properties of the REs, which are chemically closely related but different in size.

For the cuprates, the structural information is indispensable for yet another reason. It has become evident that the superconducting property of these materials is closely related to certain structural features, involving the presence of infinite sheets of the octahedral or square-pyramidal cuprate polyanion for a potential hole superconductor and infinite sheets of the square-planar cuprate polyanion for a potential electron superconductor. Behind these structural features, there seems to be another, more primary common denominator. All these cuprates, when superconducting, possess a copper–oxygen coordination which allows us to imagine the occurrence of a non-bonding, partially filled Cu 3d-orbital, energetically split from the other d-orbitals by the crystal (ligand) field interaction. In this picture, hole superconductivity of a cuprate then occurs when the orbital in question is almost empty, and electron superconductivity when the orbital is almost filled. Remarkably, such an energetically separated, partially filled orbital may also be imagined in the superconducting bismuthates, vanadates or titanates. Finally, other superconductors also show features which comply with the picture of the statistical (partial) presence of non-bonding electron pairs in an 'infinite' bond framework. This may involve, for example, the frustrated sp^2-hybridization in fullerene, C_{60}, where the deformation from the ideal planar 120° graphite bond angle creates a potential, fractional population in an sp^3-orbital per carbon. The potential is put into reality through the formation of a superconducting alkali metal salt of C_{60}, where three noduli of such an sp^3-orbital participate in σ-bonds between the carbons and the fourth is occupied by the electrons from the alkali metal. The latter could be responsible for the superconductivity. Analogous examples of frustrated, non-bonding orbitals can be found in organic superconductors, metallic phosphorus etc.

In this situation, the chemical information provided by a compilation of phase diagrams, which elucidate trends in stability for various structure types, may represent an important link in the quest for new high-T_c superconductors.

Acknowledgement. This work has received financial support from the Norwegian Council for Science and the Humanities (NAVF).

9. References

1. Beyers, R. and Ahn, B. T. *IBM Rep. RJ 7797 (71914)* May 11 (1990).
2. Fjellvåg, H., Karen, P., Kjekshus, A., Kofstad, P. and Norby, T. *Acta Chem. Scand., Ser. A 42* (1988) 178.
3. Cava, R. J., Batlogg, B., Chen, C. H., Rietman, E. A., Zahurak, S. M. and Werder, D. *Nature (London) 329* (1987) 423.
4. Shaked, H. Jorgensen, J. D., Faber, J., Jr., Hinks, D. G. and Dąbrowski, B. *Phys. Rev. B 39* (1989) 7363.
5. Cava, R. J., Hewat, A. W., Hewat, E. A., Batlogg, B., Marezio, M., Rabe, K. M., Krajewski, J. J., Peck, W. F., Jr. and Rupp, L. W., Jr. *Physica C (Amsterdam) 165* (1990) 419.
6. Andersen, N. H., Lebech, B. and Poulsen, H. F. *Physica C (Amsterdam) 172* (1990) 31.
7. Asta, M., DeFontaine, D., Ceder, G., Salomons, E. and Kraitchman, M. *J. Less-Common Met. 168* (1991) 39.
8. Strobel, P., Capponi, J. J., Marezio, M. and Monod, P. *Solid State Commun. 64* (1987) 513.
9. Liang, R. and Nakamura, T. *Jpn. J. Appl. Phys., Part 2, 27* (1988) L1277.
10. Meuffels, P., Naeven, R. and Wenzl, H. *Physica C (Amsterdam) 161* (1989) 539.
11. Schwitzgebel, G. and Junk, S. *Ber. Bunsenges. Phys. Chem. 93* (1989) 1356.
12. Nowotny, J. and Rekas, M. *J. Am. Ceram. Soc. 73* (1990) 1048.
13. Nowotny, J. and Rekas, M. *J. Am. Ceram. Soc. 73* (1990) 1054.

14. Nowotny, J., Rekas, M. and Weppner, W. *J. Am. Ceram. Soc. 73* (1990) 1040.
15. Graf, T., Triscone, G. and Muller, J. *J. Less-Common Met. 159* (1990) 349.
16. Laborde, O., Potel, M., Gougeon, P., Padiou, J., Levet, J. C. and Noel, H. *Phys. Lett. A 147* (1990) 525.
17. Perrin, C., Peña, O., Sergent, M., Christensen, P., Fonteneau, G. and Lucas, J. *Supercond. Sci. Technol. 2* (1989) 35.
18. Johnson, J. R., Suenaga, M., Thompson, P. and Reilly, J. J. *Z. Phys. Chem. 163* (1989) 721.
19. Niedermayer, C., Glückler, H., Simon, R., Golnik, A., Rauer, M., Recknagel, E., Weidinger, A., Budnick, J. I., Paulus, W. and Schöllhorn, R. *Phys. Rev. B 40* (1989) 11386.
20. Ikuma, Y., Yoshimura, M., Kabe, S. *J. Mater. Res. 5* (1990) 17.
21. Pavlyukhin, Y. T., Nemudry, A. P., Khainovsky, N. G. and Boldyrev, V. V. *Solid State Commun. 72* (1989) 107.
22. Khan, N. A., Iqbal, M. Z., Baber, N., Afzal, S., Qurashi, U. S., Afshan, G. and Mazhar, M. *Phys. Rev. B 43* (1991) 13622.
23. Fjellvåg, H., Karen, P. and Kjekshus, A. *Acta Chem. Scand., Ser. A 41* (1987) 283.
24. Smith, D. W. *J. Chem. Educ. 64* (1987) 480.
25. Bratsch, S. G. *J. Chem. Educ. 65* (1988) 877.
26. Komatsu, T., Tanaka, O., Matusita, K., Takata, M. and Yamashita, T. *Jpn. J. Appl. Phys., Part 2, 27* (1988) L1025.
27. Cima, M. J., Schneider, J. S., Peterson, S. C. and Coblenz, W. *Appl. Phys. Lett. 53* (1988) 710.
28. Raeder, C. H. and Knorr, D. B. *J. Am. Ceram. Soc. 73* (1990) 2407.
29. Montzka, S. A., Hybertson, B. M., Barkley, R. M. and Sievers, R. E. *J. Mater. Res. 6* (1991) 891.
30. Yokota, K., Kura, T., Ochi, M. and Katayama, S. *J. Mater. Res. 5* (1990) 2790.
31. Karen, P., Braaten, O., Fjellvåg, H. and Kjekshus, A. *AMSAHTS '90* (NASA Conf. Publ. 3100, 1990) p.117.
32. Karen, P. and Kjekshus, A. *J. Solid State Chem. 94* (1991) 298.
33. Gao, Y., Merkle, K. L., Zhang, C., Balachandran, U. and Poeppel, R. B. *J. Mater. Res. 5* (1990) 1363.
34. Barin, I. and Knacke, O. *Thermochemical Properties of Inorganic Substances,* Springer Verlag, Berlin 1973, pp. 77, 79, 163, 174, 181, 711.
35. Barin, I., Knacke, O. and Kubashevski, O. *Thermochemical Properties of Inorganic Substances, Supplement,* Springer Verlag, Berlin 1977, p. 679.
36. de Leeuw, D. M., Mutsaers, C. A. H. A., Langereis, C., Smoorenburg, H. C. A. and Rommers, P. J. *Physica C (Amsterdam) 152* (1988) 39.
37. Roth, R. S., Rawn, C. J., Beech, F., Whitler, J. D. and Anderson, J. O. In: Yan, M. F., Ed. *Ceram. Supercond. 2, Res. Update,* American Ceramics Society, Washington DC 1988, p. 13.
38. Fjellvåg, H., Karen, P., Kjekshus, A. and Grepstad, J. K. *Acta Chem. Scand., Ser. A 42* (1988) 171.
39. Shaw, T. M., Dimos, D., Batson, P. E., Schrott, A. G., Clarke, D. R. and Duncombe, P. R. *J. Mater. Res. 5* (1990) 1176.
40. Lindemer, T. B., Hubbard, C. R. and Brynestad, J. *Physica C (Amsterdam) 167* (1990) 312.
41. Dąbkovska, M. *Ann. Univ. Mariae Curie-Sklodowska, Sect. AA Phys. Chem. 1976–1977* (published 1980), pp. 31 and 111.
42. Ivanov-Emin, B. N. and Medvedev, J. N. *Zh. Neorg. Khim. 35* (1990) 300.
43. Yazawa, I., Sugise, R., Terada, N., Jo, M., Oka, K., Hayakawa, H. and Ihara, H. *Jpn. J. Appl. Phys., Part 2, 29* (1990) L1480.
44. Schumacher, E. E. *J. Am. Chem. Soc. 48* (1926) 396.
45. Lamoreaux, R. H., Hildenbrand, D. L. and Brewer, L. *J. Phys. Chem. Ref. Data 16* (1987) 419.
46. Guillatt, I. F. and Brett, N. H. J. *Mater. Sci. Lett. 5* (1970) 615.
47. Burgers, W. G. *Z. Phys. 80* (1933) 352.
48. Satterfield, C. N. and Stein, T. W. *Ind. Eng. Chem. 46* (1954) 1734.
49. Holtermann, C. and Laffitte, P. *C. R. Acad. Sci. (Paris) 208* (1939) 517.
50. Kedrovskii, O. V., Kovtunenko, I. V., Kiseleva, E. V. and Bundel, A. A. *Russ. J. Phys. Chem. 41* (1967) 205.
51. Brosset, C. and Vannerberg, N.-G. *Nature (London) 177* (1956) 238.
52. Bernal, J. D., Diatlowa, E., Kasarnowsky, J., Reichstein, S. and Ward, A. G. *Z. Kristallogr. A 92* (1935) 344.
53. Abrahams, S. C. and Kalnajs, J. *Acta Crystallogr. 7* (1954) 838.
54. Gleixner, R. A. and Chang, Y. A. *Metall. Trans. B 16* (1985) 743.
55. Tamaru, S. and Siomi, K. *Z. Phys. Chem. Stoechiom. Verwandschaftsl. A 159* (1932) 227.
56. Chessin, H. and Hamilton, W. C. *Acta Crystallogr. 18* (1965) 689.
57. de Villiers, J. P. R. *Am. Miner. 56* (1971) 758.
58. Foëx, M. and Traverse, J.-P. *Bull. Soc. Fr. Miner. Cristallogr. 89* (1966) 184.
59. Müller-Buschbaum, H. and von Schnering, H. G. *Z. Anorg. Allg. Chem. 340* (1965) 232.
60. Roth, R. S., Schneider, S. J. *J. Res. Natl. Bur. Stand., Sect. A 64* (1960) 309.
61. O'Connor, B. H. and Valentine, T. M. *Acta Crystallogr., Sect. B 25* (1969) 2140.
62. Cromer, D. T. *J. Phys. Chem. 61* (1957) 753.
63. Sawyer, J. O., Hyde, B. G. and Eyring, L. *Proc. Chim. Soc. Fr., Ser. 5* (1965) 1190.
64. Brauer, G. and Gingerich, K. A. *J. Inorg. Nucl. Chem. 16* (1960) 87.
65. Bevan, D. J. M. and Kordis, J. *J. Inorg. Nucl. Chem. 26* (1964) 1509.
66. Bevan, D. J. M. *J. Inorg. Nucl. Chem. 1* (1955) 49.
67. Hyde, B. G., Bevan, D. J. M. and Eyring, L. *Philos. Trans. R. Soc. London, Ser. A 259* (1966) 583.
68. Sieglaff, C. L. and Eyring, L. *J. Am. Chem. Soc. 79* (1957) 3024.
69. Wilbert, Y., Duquesnoy, A. and Marion, F. *C. R. Acad. Sci. (Paris) 264* (1967) 316.
70. Brauer, G. and Pfeiffer, B. *J. Less-Common Met. 5* (1963) 171.
71. Sastry, R. L. N., Mehrotra, P. N. and Rao, C. N. R. *J. Inorg. Nucl. Chem. 28* (1966) 2167.
72. Gruen, D. M., Koehler, W. C. and Katz, J. J. *J. Am. Chem. Soc. 73* (1951) 1475.
73. Burnham, D. A., Eyring, L. and Kordis, J. *J. Phys. Chem. 72* (1968) 4424.
74. Prandtl, W. and Rieder, G. *Z. Anorg. Allg. Chem. 238* (1938) 225.
75. Ramdas, S., Patil, K. C. and Rao, C. N. R. *J. Chem. Soc. A* (1970) 64.
76. Rudenko, V. S. and Boganov, A. G. *Izvest. Akad. Nauk S.S.S.R., Neorg. Mater. 7* (1971) 108.
77. Baenziger, N. C., Eick, H. A., Schuldt, H. S. and Eyring, L. *J. Am. Chem. Soc. 83* (1961) 2219.
78. Kordis, J. and Eyring, L. *J. Phys. Chem. 72* (1968) 2030.
79. Ozin, G. A., Mitchell, S. A. and Garćia-Prieto, J. *J. Am. Chem. Soc. 105* (1983) 6399.
80. O'Keeffe, M. and Bovin, J.-O. *Am. Miner. 63* (1978) 180.
81. Roberts, H. S. and Smyth, F. H. *J. Am. Chem. Soc. 43* (1921) 1061.

82. Collins, B. T., Desisto, W., Kershaw, R., Dwight, K. and Wold, A. *J. Less-Common Met. 156* (1989) 341.
83. Gundermann, J. and Wagner, C. *Z. Phys. Chem. B37* (1937) 155.
84. Massalski, T. B., Ed., *Binary Alloy Phase Diagrams*, American Society for Metals, Metals Park, OH 1986, Vol. 1, p. 943.
85. Schmid, R. *Metall. Trans. B*14 (1983) 473.
86. Åsbrink, S. and Norrby, L.-J. *Acta Crystallogr., Sect. B26* (1970) 8.
87. Wrigge, F. W. and Meisel, K. *Z. Anorg. Allg. Chem. 203* (1932) 312.
88. Niggli, P. *Z. Kristallogr. 57* (1922) 253.
89. Grebenyuk, V. D., Kavich, I. V., Mikolaichuk, A. G. and Romanchuk, I. T. *Ukr. Fiz. Zh. 12* (1967) 876.
90. Abalduev, B. V. and Bolchakov, A. F. *Elektron. Tekh. 4* (1972) 7.
91. Ostapchenko, E. P. *Izvest. Akad. Nauk S.S.S.R., Ser. Fiz. 20* (1956) 1105.
92. Kwestroo, W., van Hal, H. A. M. and Langereis, C. *Mater. Res. Bull. 9* (1974) 1631.
93. Lopato, L. M. *Ceramurgia Int. 2* (1976) 18.
94. Rian, G., Julsrud, S., Karen, P. and Fjellvåg, H. *In preparation.*
95. Costa, G. A., Ferretti, M., Franceschi, E. A. and Olcese, G. L. *Thermochim. Acta 133* (1988) 17.
96. Lopato, L. M., Lugin, L. I. and Shevchenko, A. V. *Dopov. Akad. Nauk Ukr. S.S.R., Ser. B Ukr. Khim. Zh. 32* (1970) 535.
97. Lopato, L. M., Maister, I. M. and Shevchenko, A. V. *Izvest. Akad. Nauk S.S.S.R., Ser. Neorg. Mater. 8* (1972) 861.
98. Müller-Buschbaum, H. and Scheikowski, M. *Z. Anorg. Allg. Chem. 591* (1990) 181.
99. Antipov, E. V., Lykova, L. I. and Kovba, L. M. *Zh. Neorg. Khim. 29* (1984) 1624.
100. Kovba, L. M., Lykova, L. I. and Antipov, E. V. *Zh. Neorg. Khim. 28* (1983) 724.
101. Kale, G. M. and Jacob, K. T. *Solid State Ionics 34* (1989) 247.
102. Guha, J. P. and Kolar, D. *J. Mater. Sci. 6* (1971) 1174.
103. Jacobsen, A. J., Tofield, B. C. and Fender, B. E. F. *Acta Crystallogr., Sect. B28* (1972) 956.
104. Banks, E., La Placa, S. J., Kunnmann, W., Corliss, L. M. and Hastings, J. M. *Acta Crystallogr., Sect. B28* (1972) 3429.
105. Hodorowicz, S. A., Czerwonka, J. and Eick, H. A. *J. Solid State Chem. 88* (1990) 391.
106. Müller-Buschbaum, H. *Z. Anorg. Allg. Chem. 358* (1968) 138.
107. Lopato, L. M., Lugin, L. I. and Shevchenko, A. V. *Ukr. Khim. Zh. 39* (1973) 142.
108. Schulze, A.-R. and Müller-Buschbaum, H. *Z. Anorg. Allg. Chem. 471* (1980) 59.
109. Müller-Buschbaum, H. and Boehlke, A. *Z. Anorg. Allg. Chem. 553* (1987) 212.
110. Schulze, A.-R. and Müller-Buschbaum, H. *Z. Anorg. Allg. Chem. 461* (1980) 48.
111. Longo, V., Minichelli, D. and Ricciadiello, F. *Science of Ceramics 11* (1981) 171.
112. Smith, A. J. and Welch, A. J. E. *Acta Crystallogr. 13* (1960) 653.
113. Mastromonaco, M. D., Barbariol, I. and Cocco, A. *Ann. Chim. (Rome) 59* (1969) 465.
114. Paletta, E. and Müller-Buschbaum, H. *J. Inorg. Nucl. Chem. 30* (1968) 1425.
115. Foëx, M. *Bull. Soc. Chim. Fr.* (1961) 109.
116. Trzebiatowski, W. and Horyń, R. *Bull. Acad. Pol. Sci. 13* (1965) 315.
117. Carter, J. R. and Feigelson, R. S. *J. Am. Ceram. Soc. 47* (1964) 141.
118. Schneider, S. J. and Roth, R. S. *J. Res. Natl. Bur. Stand., Ser. A 64* (1960) 317.
119. Jørgensen, C. K., Pappalardo, R. and Rittershaus, E. *Z. Naturforsch., Teil A 20* (1965) 54.
120. Müller-Buschbaum, H. and Teske, C. *Z. Anorg. Allg. Chem. 369* (1969) 255.
121. Müller-Buschbaum, H. and Graebner, P.-H. *Z. Anorg. Allg. Chem. 386* (1971) 158.
122. Moreau, J. M. *Mater. Res. Bull. 3* (1968) 427.
123. Schneider, S. J., Roth, R. S. and Waring, J. L. *J. Res. Natl. Bur. Stand., Ser. A 65* (1961) 345.
124. Brauer, G. and Gradinger, H. *Z. Anorg. Allg. Chem. 276* (1954) 209.
125. Barker, W. W. and Wilson, A. F. *J. Inorg. Nucl. Chem. 30* (1968) 1415.
126. Bevan, D. J. M., Barker, W. W., Martin, R. L. and Parks, T. C. *Proc. 4th Conf. Rare Earth Res.*, Phoenix, AZ 1964, p. 441.
127. McGullough, J. D. and Britton, J. D. *J. Am. Chem. Soc. 74* (1952) 5225.
128. McGullough, J. D. *J. Am. Chem. Soc. 72* (1950) 1386.
129. Wolf, L. and Schwab, H. *J. Prakt. Chem. [4] 24* (1964) 293.
130. Abbattista, F., Vallino, M., Brisi, C., and Lucco-Borlera, M. *Mater. Res. Bull. 23* (1988) 1509.
131. Wong-Ng, W. K., Davis, K. L. and Roth, R. S. *J. Am. Ceram. Soc. 71* (1988) C64.
132. Gutau, W. and Müller-Buschbaum, H. *J. Less-Common Met. 152* (1989) L11.
133. Teske, C. L. and Müller-Buschbaum, H. *Z. Naturforsch., Teil B27* (1972) 296.
134. Teske, C. L. and Müller-Buschbaum, H. *Z. Anorg. Allg. Chem. 371* (1969) 325.
135. Teske, C. L. and Müller-Buschbaum, H. *Z. Anorg. Allg. Chem. 379* (1970) 234.
136. Takano, M., Takeda, Y., Okada, H., Miyamoto, M. and Kusaka, T. *Physica C (Amsterdam) 159* (1989) 375.
137. McCarron, E. M., Subramanian, M. A., Calabrese, J. C. and Harlow, R. L. *Mater. Res. Bull. 23* (1988) 1355.
138. Teske, C. L. and Müller-Buschbaum, H. *Z. Anorg. Allg. Chem. 379* (1970) 113.
139. Siegrist, T., Roth, R. S., Rawn, C. J. and Ritter, J. J. *Chem. Mater. 2* (1990) 192.
140. Teske, C. L. and Müller-Buschbaum, H. *Z. Anorg. Allg. Chem. 370* (1969) 134.
141. Roth, R. S., Davis, K. L. and Dennis, J. R. *Adv. Ceram. Mater. 2* (1987) 303.
142. Zhang, W., Osamura, K. and Ochiai, S. *J. Am. Ceram. Soc. 73* (1990) 1958.
143. Migeon, H. N., Jeannot, F., Zanne, M. and Aubry, J. *Rev. Chim. Miner. 13* (1976) 440.
144. Paulus, E. E., Miehe, G., Fuess, H., Yehia, I. and Löchner, U. *J. Solid State Chem. 90* (1991) 17.
145. Mazza, D., Vallino, M., Abbattista, F. and Delmastro, S. *Mater. Chem. Phys. 25* (1990) 385.
146. Eriksson, S., Johansson, L.-G., Börjesson, L. and Kakihana, M. *Physica C (Amsterdam) 162–164* (1989) 59.
147. Machida, M., Yasuoka, K., Eguchi, K. and Arai, H. *J. Solid State Chem. 91* (1991) 176.
148. Klinkova, L. A., Soikina, I. V. and Romanenko, I. M. *Zh. Neorg. Khim. 35* (1990) 446.
149. Bazuev, G. V. and Krasilnikov, V. N. *Zh. Neorg. Khim. 36* (1991) 2195.
150. Bertinotti, A., Hamman, J., Luzet, D. and Vincent, E. *Physica C (Amsterdam) 160* (1989) 227.
151. Graf, T., Jorda, J. L. and Muller, J. *J. Less-Common Met. 146* (1989) 49.
152. Chandrachood, M. R., Morris, D. E. and Sinha, A. P. B. *Physica C (Amsterdam) 171* (1990) 187.

153. Graf, T., Triscone, G., Junod, A. and Muller, J. *J. Less-Common Met. 170* (1991) 359.
154. Arjomand, M. and Machin, D. J. *J. Chem. Soc., Dalton Trans. 11* (1975) 1061.
155. Graf, T., Triscone, G. and Muller, J. *J. Less-Common Met. 159* (1990) 349.
156. Roth, R. S., Rawn, C. J., Burton, B. P. and Beech, F. *J. Res. Natl. Bur. Stand. 95* (1990) 291.
157. Alcock, C. B. and Li, B. *J. Am. Ceram. Soc. 73* (1990) 1176.
158. de Leeuw, D. M., Mutsaers, C. A. H. A., Geelen, G. P. J., Smoorenburg, H. C. A. and Langereis, C. *Physica C (Amsterdam) 152* (1988) 508.
159. Roth, R. S., Rawn, C. J., Whitler, J. D., Chiang, C. K. and Wong-Ng, W. K. *J. Am. Ceram. Soc. 72* (1989) 395.
160. Zhou, W., Jones, R., Tang, D., Jefferson, D. A. and Edwards, P. P. *J. Solid State Chem. 86* (1990) 255.
161. Roth, R. S., Rawn, C. J., Ritter, J. J. and Burton, B. P. *J. Am. Ceram. Soc. 72* (1989) 1545.
162. Roth, R. S., Hwang, N. M., Rawn, C. J., Burton, B. P. and Ritter, J. J. *J. Am. Ceram. Soc. 74* (1991) 2148.
163. Brese, N. E., O'Keeffe, M., van Dreele, R. B. and Young, V. G., Jr. *J. Solid State Chem. 83* (1989) 1.
164. Freund, H.-R. and Müller-Buschbaum, H. *Z. Naturforsch., Teil B 32*(1977) 609.
165. Freund, H.-R. and Müller-Buschbaum, H. *Z. Naturforsch., Teil B 32*(1977) 1123.
166. Foëx, M., Mancheron, A. and Liné, M. *C. R. Acad. Sci., Ser. 2, 250* (1960) 3027.
167. Fjellvåg, H., Karen, P. and Kjekshus, A. *Acta Chem. Scand., Ser. A 42* (1988) 144.
168. García-Muñoz, J. L. and Rodríguez-Carvajal, J. *Phys. Lett. A 149* (1990) 319.
169. Kale, G. M. and Jacob, K. T. *Chem. Mater. 1* (1989) 515.
170. Gadalla, A. M. and Kongkachuichay, P. *J. Mater. Res. 6* (1991) 450.
171. Müller-Buschbaum, H. and Wollschläger, W. *Z. Anorg. Allg. Chem. 414* (1975) 76.
172. Grande, B., Müller-Buschbaum, H. and Schweizer, M. *Z. Anorg. Allg. Chem. 428* (1977) 120.
173. Cox, D. E., Goldman, A. I., Subramanian, M. A., Gopalakrishnan, J. and Sleight, A. W. *Phys. Rev. B 40* (1989) 6998.
174. James, A. C. W. P., Zahurak, S. M. and Murphy, D. W. *Nature (London) 338* (1989) 240.
175. Tokura, T., Takagi, H. and Uchida, S. *Nature (London) 337* (1989) 345.
176. Jorda, J. L. and Cohen-Adad, M. T. S. *J. Less-Common Met. 171* (1991) 127.
177. Fotiev, A. A., Shter, G. E., Kosmynin, A. S., Garkuchin, I. K., Balachov, V. L. and Trunin, A. S. *Sverkhprovodimost Fiz. Khim. Tekh. 3* (1990) 1071.
178. Longo, J. M. and Raccah, P. M. *J. Solid State Chem. 6* (1973) 526.
179. Dąbrowski, B., Hinks, D. G., Jorgensen, J. D. and Richards, D. R. *Mater. Res. Soc. Symp. Proc.* (1989) 69.
180. Jorgensen, J. D., Schüttler, H.-B., Hinks, D. G., Capone, D. W., Zhang, H. K., Brodsky, M. B. and Scalapino, D. J. *Phys. Rev. Lett. 58* (1987) 1024.
181. Bednorz, J. G. and Müller, K. A. *Z. Phys. B 64* (1986) 189.
182. Cheong, S. W., Thompson, J. D. and Fisk, Z. *Physica C (Amsterdam) 158* (1989) 109.
183. Webb, A. W., Skelton, E. F., Qadri, S. B., Carpenter, E. R., Jr., Osofsky, M. S., Soulen, R. J. and LeTourneau, V. *Physica C (Amsterdam) 162–164* (1989) 899.
184. Hundley, M. F., Thompson, J. D., Cheong, S. W., Fisk, Z. and Schirber, J. E. *Phys. Rev. B 41* (1990) 4062.
185. Chaillout, C., Chenavas, J., Cheong, S. W., Fisk, Z., Marezio, M., Morosin, B. and Schirber, J. E. *Physica C (Amsterdam) 170* (1990) 87.
186. Zolliker, P., Cox, D. E., Parise, J. B., McCarron, E. M., III and Farneth, W. E. *Phys. Rev. B 42* (1990) 6332.
187. McCarty, K. F., Schirber, J. E., Cheong, S. W. and Fisk, Z. *Phys. Rev. B 43* (1991) 7883.
188. Caneiro, A., Serafini, D., Abriata, J. P. and Andrade Gamboa, J. *Solid State Commun. 75* (1990) 915.
189. Haas, H. and Kordes, E. *Z. Kristallogr. 129* (1969) 259.
190. Köhler, B. U. and Jansen, M. *Z. Anorg. Allg. Chem. 543* (1986) 73.
191. Kubat-Martin, K. A., Garcia, E. and Peterson, D. E. *Physica C (Amsterdam) 172* (1990) 75.
192. Schulze, K., Majewski, P., Hettich, B. and Petzow, G. *Z. Metallk. 81* (1990) 836.
193. Siegrist, T., Zahurak, S. M., Murphy, D. W. and Roth, R. S. *Nature (London) 334* (1988) 231.
194. Smith, M. G., Manthiram, A., Zhou, J., Goodenough, J. B. and Markert, J. T. *Nature (London) 351* (1991) 549.
195. Abbattista, F., Vallino, M. and Mazza, D. *Mater. Chem. Phys. 21* (1989) 521.
196. Sato, S. and Nakada, I. *Acta Crystallogr., Sect. C 45* (1989) 523.
197. Pei, S., Paulikas, A. P., Veal, B. W. and Jorgensen, J. D. *Acta Crystallogr., Sect. C 46* (1990) 1986.
198. Michel, C. and Raveau, B. *J. Solid State Chem. 43* (1982) 73.
199. Aselage, T. and Keefer, K. *J. Mater. Res. 3* (1988) 1279.
200. Nakahigashi, K., Yoshiara, K., Kogachi, M., Nakanishi, S., Sasakura, H., Minamigawa, S., Fukuoka, N. and Yanase, A. *Jpn. J. Appl. Phys., Part 2, 27* (1988) L747.
201. Izakovich, E. N., Zheltova, N. A., Korolev, Y. M., Sokolovskaya, Z. D., Spector, V. N. and Khidekel, M. L. *Phys. Status Solidi 116* (1989) K13.
202. de Leeuw, D. M., Mutsaers, C. A. H. A., Steeman, R. A., Frikkee, E. and Zandbergen, H. W. *Physica C (Amsterdam) 158* (1989) 391.
203. Greaves, C. and Slater, P. R. *Solid State Commun. 73* (1990) 629.
204. Abbattista, F., Vallino, M., Lucco Bolera, M. and Brisi, C. *Mater. Chem. Phys. 20* (1988) 191.
205. Karen, P., Fjellvåg, H., Braaten, O., Kjekshus, A. and Bratsberg, H. *Acta Chem. Scand. 44* (1990) 994.
206. Beno, M. A., Soderholm, L., Capone II, D. W., Hinks, D. G., Jorgensen, J. D., Grace, J. D., Schuller, I. K., Segre, C. U. and Zhang, K. *Appl. Phys. Lett. 51* (1987) 57.
207. Rusiecki, S., Bucher, B., Kaldis, E., Jilek, E., Karpinski, J., Rossel, C., Pümpin, B., Keller, H., Kündig, W., Krekels, T. and van Tendeloo, G. *J. Less-Common Met. 164–165* (1990) 31.
208. Wong-Ng, W., Gayle, F. W., Kaiser, D. L., Watkins, S. F. and Fronczek, F. R. *Phys. Rev. B 41* (1990) 4220.
209. François, M., Junod, A., Yvon, K., Hewat, A. W., Capponi, J. J., Strobel, P., Marezio, M. and Fischer, P. *Solid State Commun. 66* (1988) 1117.
210. Ahn, B. T., Gür, T. M., Huggins, R., Beyers, R. and Engler, E. M. *Mater. Res. Soc. Symp. Proc. 99* (1988) 171.
211. Hewat, A. W., Capponi, J. J., Chaillout, C., Marezio, M. and Hewat, E. A. *Solid State Commun. 64* (1987) 301.
212. Garbauskas, M. F., Green, R. W., Arendt, R. H. and Kasper, J. S. *Inorg. Chem. 27* (1988) 871.
213. Jorgensen, J. D., Veal, B. W., Paulikas, A. P., Nowicki, L. J., Crabtree, G. W., Claus, H. and Kwok, W. K. *Phys. Rev. B 41* (1990) 1863.
214. Verweij, H. *Solid State Commun. 67* (1988) 109.
215. Alario-Franco, M. A., Chaillout, C., Capponi, J. J., Chenavas, J. and Marezio, M. *J. Less-Common Met. 150* (1989) 117.
216. Lin, Y. P., Greedan, J. E., O'Reilly, A. H., Reimers, J. N., Stager, C. V. and Post, M. L. *J. Solid State Chem. 84* (1990) 226.

217. Hou, C. J., Manthiram, A., Rabenberg, L. and Goodenough, J. B. *J. Mater. Res. 5* (1990) 9.
218. Sonntag, R., Hohlwein, D., Brückel, T. and Collin, G. *Phys. Rev. Lett. 66* (1991) 1497.
219. Jorgensen, J. D., Pei, S., Lightfoot, P., Shi, H., Paulikas, A. P. and Veal, B. W. *Physica C (Amsterdam) 167* (1990) 571.
220. Cava, R. J., Batlogg, B., Chen, C. H., Rietman, E. A., Zahurak, S. M. and Werder, D. *Phys. Rev. B 36* (1987) 5719.
221. Ichihashi, T., Iijima, S., Kubo, Y. and Tabuchi, J. *Jpn. J. Appl. Phys., Part 2, 27* (1988) L1187.
222. Ceder, G., Asta, M., Carter, W. C., Kraitchman, M., de Fontaine, D., Mann, M. E. and Sluiter, M. *Phys. Rev. B 41* (1990) 8698.
223. Vettier, C., Burlet, P., Henry, J. Y., Jurgens, M. J., Lapertot, G., Regnault, L. P. and Rossat-Mignod, J. *Phys. Scr. T29* (1989) 110.
224. Andersen, N. H., Lebech, B. and Poulsen, H. F. *J. Less-Common Met. 164–165* (1990) 124.
225. Steinfink, H., Swinnea, J. S., Sui, Z. T., Hsu, H. M. and Goodenough, J. B. *J. Am. Chem. Soc. 109* (1987) 3348.
226. Frase, K. G., Liniger, E. G. and Clarke, D. R. *J. Am. Ceram. Soc. 70* (1987) C204.
227. Wang, G., Hwu, S.-J., Song, S. N., Ketterson, J. B., Marks, L. D., Poeppelmeier, K. R. and Mason, T. O. *Adv. Ceram. Mat. 2* (1987) 313.
228. Frase, K. G. and Clarke, D. R. *Adv. Ceram. Mat. 2* (1987) 295.
229. Yang, K. Y., Homma, H., Lee, R., Bhadra, R., Grimsditch, M., Bader, S. D., Locquet, J. P., Bruynseraede, Y. and Schuller, I. K. *Appl. Phys. Lett. 53* (1988) 808.
230. Saltykova, I. A., Baranova, N. N., Barchatov, V. P., Dubrovina, I. N. and Balakirev, V. F. *Sverkhprovodimost Fiz. Khim. Tekh. 3* (1990) 1250.
231. Koscheeva, S. N., Fotiev, V. A., Fotiev, A. A. and Zubkov, V. G. *Izv. Akad. Nauk. S.S.S.R., Neorg. Mater. 26* (1990) 1491.
232. Iqbal, Z., Reidinger, F., Bose, A., Cipollini, N., Taylor, T. J., Eckhardt, H., Ramakrishna, B. L. and Ong, E. W. *Nature (London) 331* (1988) 326.
233. Umarji, A. M., Somasundaram, P., Ganapathi, L. and Rao, C. N. R. *Solid State Commun. 66* (1988) 177.
234. Karen, P., Kjekshus, A. and Andresen, A. F. *Acta Chem. Scand. 46* (1992). *In press.*
235. Cava, R. J., Krajewski, J. J., Peck, W. F., Jr., Batlogg, B. and Rupp, L. W., Jr. *Physica C (Amsterdam) 159* (1989) 372.
236. Jin, S., O'Bryan, H. M., Gallagher, P. K., Tiefel, T. H., Cava, R. J., Fastnacht, R. A. and Kammlott, G. W. *Physica C (Amsterdam) 165* (1990) 415.
237. Bordet, P., Hodeau, J. L., Argoud, R., Muller, J., Marezio, M., Martinez, J. C., Prejean, J. J., Karpinski, J., Kaldis, E., Rusiecki, S. and Bucher, B. *Physica C (Amsterdam) 162–164* (1989) 524.
238. Kaldis, E., Fischer, P., Hewat, A. W., Hewat, E. A., Karpinski, J. and Rusiecki, S. *Physica C (Amsterdam) 159* (1989) 668.
239. Señaris-Rodriguez, M. A., Chippindale, A. M., Várez, A., Morán, E. and Alario-Franco, M. A. *Physica C (Amsterdam) 172* (1991) 477.
240. Karpinski, J., Kaldis, E., Rusiecki, S., Jilek, E., Fischer, P., Bordet, P., Chaillout, C., Chenavas, J., Hodeau, J. L. and Marezio, M. *J. Less-Common. Met. 150* (1989) 129.
241. Karpinski, J., Kaldis, E., Jilek, E., Rusiecki, S. and Bucher, B. *Nature (London) 336* (1988) 660.
242. Bordet, P., Chaillout, C., Chenavas, J., Hodeau, J. L., Marezio, M., Karpinski, J. and Kaldis, E. *Nature (London) 334* (1988) 596.
243. Tallon, J. L., Pooke, D. M., Buckley, R. G., Presland, M. R. and Blunt, F. J. *Phys. Rev. B 41* (1990) 7220.
244. Karpinski, J., Rusiecki, S., Kaldis, E. and Jilek, E. *J. Less-Common. Met. 164–165* (1990) 3.
245. Karpinski, J., Rusiecki, S., Bucher, B., Kaldis, E. and Jilek, E. *Physica C (Amsterdam) 161* (1989) 618.
246. Karpinski, J., Rusiecki, S., Kaldis, E., Bucher, B. and Jilek, E. *Physica C (Amsterdam) 160* (1989) 449.
247. Voronin, G. F. and Degterov, S. A. *Physica C (Amsterdam) 176* (1991) 387.
248. Yamada, Y., Yata, M., Kaieda, Y., Irie, H. and Matsumoto, T. *Jpn. J. Appl. Phys., Part 2, 28* (1989) L797.
249. Dlyachkova, T. V., Kadyrova, N. I., Talashmanova, N. V., Alyamovskii, S. I., Zainulin, Yu. G. *Zh. Neorg. Khim. 36* (1991) 1091.
250. Ahn, B. T., Lee, V. Y., Beyers, R., Gür, T. M. and Huggins, R. A. *Physica C (Amsterdam) 167* (1990) 529.
251. Nevřiva, M., Pollert, E., Šesták, J. and Tříska, A. *Thermochim. Acta 127* (1988) 395.
252. Idemoto, Y. and Fueki, K. *Jpn. J. Appl. Phys., Part 1, 29* (1989) 2729.
253. Clarke, A. P., Schwarz, R. B. and Thompson, J. D. *J. Less-Common Met. 168* (1991) 1.
254. Wahlbeck, P. G., Myers, D. L. and Ho, J. C. *Physica C (Amsterdam) 161* (1989) 175.
255. Kawabata, S., Hoshizaki, H., Kawahara, N., Enami, H., Shinohara, T. and Imura, T. *Jpn. J. Appl. Phys., Part 2, 29* (1990) L1490.
256. Mikirticheva, G. A., Schitova, V. I., Grabovenko, L. Yu., Romanov, D. I. and Grebenschikov, R. G. *Zh. Neorg. Khim. 36* (1991) 562.
257. Šesták, J., Kamarád, J., Holba, P., Tříska, A., Pollert, E. and Nevřiva, M. *Thermochim. Acta 174* (1991) 99.
258. Licci, F., Tissot, P. and Scheel, H. J. *J. Less-Common Met. 150* (1989) 201.
259. Kosmynin, A. C., Shter, G. E., Garkushin, I. K., Trunin, A. S., Balashov, V. A. and Fotiev, A. A. *Sverkhprovodimost Fiz. Khim. Tekh. 3* (1990) 1870.
260. Hodorowicz, E., Hodorowicz, S. A. and Eick, H. A. *Physica C (Amsterdam) 158* (1989) 127.
261. Hodorowicz, S. A., Lasocha, A., Lasocha, W. and Eick, H. A. *J. Solid State Chem. 75* (1988) 270.
262. Vallino, M., Mazza, D. and Abbattista, F. *J. Less-Common Met. 170* (1991) 83.
263. Zhang, K., Dąbrowski, B., Segre, C. U., Hinks, D. G., Schuller, I. K., Jorgensen, J. D. and Slaski, M. *J. Phys. C 20* (1987) L935.
264. Pieczulewski, C. N., McAdams, J. E. and Mason, T. O. *J. Am. Ceram. Soc. 73* (1990) 3088.
265. Morris, D. E., Asmar, N. G., Wei, J. Y. T., Nickel, J. H., Sid, R. L. and Scott, J. S. *Phys. Rev. B 40* (1989) 11406.
266. Karen, P. *Unpublished results.*
267. Abbattista, F., Vallino, M. and Mazza, D. *Mater. Chem. Phys. 24* (1990) 363.
268. Michel, C., Er-Rakho, L. and Raveau, B. *J. Solid State Chem. 39* (1981) 161.
269. Mizuno, F., Masuda, H., Hirabayashi, I., Tanaka, S., Hasegawa, M. and Mizutani, U. *Nature (London) 345* (1990) 788.
270. Schiffler, S. and Müller-Buschbaum, H. *Z. Anorg. Allg. Chem. 523* (1985) 63.
271. de Leeuw, D. M. *J. Less-Common Met. 150* (1989) 95.
272. Abbattista, F., Brisi, C., Delmastro, S., Lucco-Bolera, M., Mazza, D. and Vallino, M. *Mater. Chem. Phys. 24* (1989) 147.
273. Michel, C., Er-Rakho, L., Hervieu, M., Pannetier, J. and Raveau, B. *J. Solid State Chem. 68* (1987) 143.
274. Davies, P. K. and Katzan, C. M. *J. Solid State Chem. 88* (1990) 368.
275. Okai, B. *Jpn. J. Appl. Phys., Part 2, 29* (1990) L2180.
276. Stavola, M., Krol, D. M., Schneemeyer, L. F., Sunshine, S. A.,

Waszczak, J. V. and Kosinski, S. G. *Phys. Rev. B 39* (1989) 287.
277. de Leeuw, D. M., Mutsaers, C. A. H. A., Geelen, G. P. J. and Langereis, C. *J. Solid State Chem. 80* (1989) 276.
278. Huang, T. C., Torrance, J. B., Nazzal, A. I. and Tokura, Y. *Powder Diffr. 4* (1989) 152.
279. Nguyen, N., Studer, F. and Raveau, B. *J. Phys. Chem. Solids 44* (1983) 389.
280. Moret, R., Pouget, J. P. and Collin, G. *Europhys. Lett. 4* (1987) 365.
281. Gai, P. L. and McCarron, E. M., III, *Science 247* (1990) 553.
282. Birgenau, R. J. and Shirane, G. In: Ginsberg, D. M., Ed., *Physical Properties of High Temperature Superconductors I,* World Scientific, Singapore 1989, p. 155.
283. Scheel, H. J. and Licci, F. *Thermochim. Acta 174* (1991) 115.
284. Er-Rakho, L., Michel, C. and Raveau, B. *J. Solid State Chem. 73* (1988) 514.
285. Tokura, Y., Torrance, J. B., Nazzal, A. I., Huang, T. C. and Ortiz, C. *J. Am. Chem. Soc. 109* (1987) 7555.
286. Lee, J. Y., Kim, J. S., Swinnea, J. S. and Steinfink, H. *J. Solid State Chem. 84* (1990) 335.
287. Nguyen, N., Er-Rakho, L., Michel, C., Choisnet, J. and Raveau, B. *Mater. Res. Bull. 15* (1980) 891.
288. Lightfoot, P., Pei, S., Jorgensen, J. D., Tang, X.-X., Manthiram, A. and Goodenough, J. B. *Physica C (Amsterdam) 169* (1990) 464.
289. Michel, C. and Raveau, B. *Rev. Chim. Miner. 21* (1984) 407.
290. Caignaert, V., Nguyen, N. and Raveau, B. *Mater. Res. Bull. 25* (1990) 199.
291. Doverspike, K., Liu, J.-H., Dwight, K. and Wold, A. *J. Solid State Chem. 82* (1989) 30.
292. Hayri, E. A. and Larese, J. Z. *Physica C (Amsterdam) 170* (1990) 239.
293. Grasmeder, J. R. and Weller, M. T. *J. Solid State Chem. 85* (1990) 88.
294. Nguyen, N., Choisnet, J. and Raveau, B. *Mater. Res. Bull. 17* (1982) 567.
295. Hervieu, M., Caignaert, V., Michel, C., Retoux, R. and Raveau, B. *Microsc. Microanal. Microstruct. 1* (1990) 109.
296. Davies, P. K., Caignol, E. and King, T. *J. Am. Ceram. Soc. 74* (1991) 569.
297. Fuertes, A., Obradors, X., Navarro, J. M., Gomez-Romero, P., Casañ-Pastor, N., Pérez, F., Fontcuberta, J., Miravitlles, C., Rodríguez-Carvajal, J. and Martínez, B. *Physica C (Amsterdam) 170* (1990) 153.
298. Hiratani, M., Saito, S., Suga, M. and Sowa, T. *Solid State Commun. 75* (1990) 425.
299. Cava, R. J., Batlogg, B., Van Dover, R. B., Krajewski, J. J., Waszczak, J. V., Fleming, R. M., Peck, W. F., Jr., Rupp, L. W., Jr., Marsh, P., James, A. C. W. P. and Schneemeyer, L. F. *Nature (London) 345* (1990) 602.
300. Bringley, J. F., Trail, S. S. and Scott, B. A. *J. Solid State Chem. 86* (1990) 310.
301. Lightfoot, P., Pei, S., Jorgensen, J. D., Tang, X.-X., Manthiram, A. and Goodenough, J. B. *Physica C (Amsterdam) 169* (1990) 15.
302. Hundley, M. F., Thompson, J. D., Cheong, S.-W., Fisk, Z., Schwarz, R. B. and Schirber, J. E. *Phys. Rev. B 40* (1989) 5251.
303. Sawa, K., Suzuki, S., Watanabe, M., Akimitsu, J., Matsubara, H., Watabe, H., Uchida, S., Kokusho, K., Asano, H., Izumi, F. and Takayama-Muromachi, E. *Nature (London) 337* (1989) 347.
304. Fisk, Z., Thompson, J. D., Hundley, M. F., Schwarz, R. B., Kwei, G. H., Schirber, J. E., Cheong, S.-W., Cooper, A. S., Bordet, P. and Marezio, M. *J. Less-Common Met. 168* (1991) 31.
305. Tokura, Y., Takagi, H. and Uchida, S. *Nature (London) 337* (1989) 345.
306. Hiratani, M., Takeda, Y., Saitoh, S. and Miyauchi, K. *Jpn. J. Appl. Phys., Part 2, 28* (1989) L769.
307. Kajitani, T., Hiraga, K., Hosoya, S., Fukuda, T., Oh-ishi, K., Kikuchi, M., Syono, Y., Tomiyoshi, S., Takahashi, M. and Muto, Y. *Physica C (Amsterdam) 169* (1990) 227.
308. Takayama-Muromachi, E., Izumi, F., Uchida, Y., Kato, K. and Asano, H. *Physica C (Amsterdam) 159* (1989) 634.
309. Ayoub, N. Y., Almasan, C. C., Early, E. A., Markert, J. T., Seaman, C. L. and Maple, M. B. *Physica C (Amsterdam) 170* (1990) 211.
310. Oka, K. and Unoki, H. *Jpn. J. Appl. Phys., Part 2, 29* (1990) L909.
311. Raychandhuri, A. K., Sreedhar, K., Rajeev, K. P., Mohan Ram, R. A., Ganguly, P. A. and Rao, C. N. R. *Philos. Mag. Lett. 56* (1987) 29.
312. Neukirch, V., Simmons, C. T., Sladeczek, P., Laubschat, C., Strebel, O., Kaindl, G. and Sarma, D. D. *Europhys. Lett. 5* (1988) 567.
313. Thomsen, C., Liu, R., Wittlin, A., Genzel, L., Cardona, M., König, W., Cabañas, M. V. and García, E. *Solid State Commun. 65* (1988) 219.
314. Noto, K., Morita, H., Watanabe, K., Murakami, T., Koyanagi, Y., Yoshi, I., Sato, I., Sugawara, H., Kobyashi, N., Fujimori, H. and Muto, Y. *Physica B (Amsterdam) 148* (1987) 239.
315. Oota, A., Sasaki, Y., Kiyoshima, Y., Ohkubo, M. and Hioki, T. *Jpn. J. Appl. Phys., Part 2, 26* (1987) L2091.
316. Millet, P., Enjalbert, R., Galy, J., Faulmann, C., Cassoux, P., Rakoto, H. and Askénazy, S. *C. R. Acad. Sci., Ser. 2, 306* (1988) 407.
317. Karen, P., Fjellvåg, H., Kjekshus, A. and Andresen, A. F. *J. Solid State Chem. 93* (1991) 163.
318. Segre, C. U., Dąbrowski, B., Hinks, D. G., Zhang, K., Jorgensen, J. D., Beno, M. A. and Schuller, I. K. *Nature (London) 329* (1987) 227.
319. Takita, K., Katoh, H., Akinaga, H., Nishino, M., Ishigaki, T. and Asano, H. *Jpn. J. Appl. Phys., Part 2, 27* (1988) L57.
320. Newsam, J. M., Jacobson, A. J., Goshorn, D. P., Lewandowski, J. T., Mitzi, D. B., Kapitulnik, A., Xie, D. and Yelon, W. B. *Solid State Ionics 32/33* (1989) 1064.
321. Karen, P., Fjellvåg, H. and Kjekshus, A. *J. Solid State Chem. 97* (1992) 257.
322. Morris, D. E., Narwankar, P. K., Sinha, A. P. B., Takano, K. and Shum, V. *Appl. Phys. Lett. (USA) 57* (1990) 715.
323. Sakurai, T., Wada, T., Suziki, N., Koriyama, S., Miyatake, T., Yamauchi, H., Koshizuka, N. and Tanaka, S. *Phys. Rev. B 42* (1990) 8030.
324. Sawa, H., Obara, K., Akimitsu, J., Matsui, Y. and Horiuchi, S. *J. Phys. Soc. Jpn. 58* (1989) 2252.
325. Tsuda, K., Tanaka, M. and Akimitsu, J. *Jpn. J. Appl. Phys., Part 2, 28* (1989) L1552.
326. Nobumasa, H., Shimizu, K., Kitano, Y., Tanaka, M. and Kawai, T. *Jpn. J. Appl. Phys., Part 2, 28* (1989) L1948.
327. Wada, T., Ichinose, A., Yaegashi, Y., Yamauchi, H. and Tanaka, S. *Phys. Rev. B 41* (1990) 1984.
328. Ichinose, A., Wada, T., Yaegashi, Y., Yamauchi, H. and Tanaka, S. *Jpn. J. Appl. Phys., Part 2, 29* (1990) L426.
329. Wada, T., Kaneko, T., Ichinose, A., Yaegashi, Y., Ikegawa, S., Yamauchi, H. and Tanaka, S. *Jpn. J. Appl. Phys., Part 2, 29* (1990) L43.
330. Watanabe, T., Kinoshita, K., Shibata, H., Matsuda, A., Asano, Y. and Yamada, T. *Jpn. J. Appl. Phys., Part 2, 27* (1988) L1245.
331. Takayama-Muromachi, E., Uchida, Y., Kobayashi, M. and Kato, K. *Physica C (Amsterdam) 158* (1989) 449.
332. Akimitsu, J., Suzuki, S., Watanabe, M. and Sawa, H. *Jpn. J. Appl. Phys., Part 2, 27* (1988) L1859.

333. Izumi, F., Takayama-Muromachi, E., Fujimori, A., Kamiyama, T., Asano, H., Akimitsu, J. and Sawa, H. *Physica C (Amsterdam) 158* (1989) 440.
334. Tan, Z., Budnick, J. I., Chen, W. Q., Brewe, D. L., Cheong, S.-W., Cooper, A. S. and Rupp, L. W., Jr. *Phys. Rev. B 42* (1990) 4808.
335. Karen, P., Fjellvåg, H., Kjekshus, A. and Andresen, A. F. *J. Solid State Chem. 92* (1991) 57.
336. Manthiram, A., Lee, S.-J. and Goodenough, J. B. *J. Solid State Chem. 73* (1988) 278.
337. Gledel, C., Marucco, J.-F. and Touzelin, B. *Physica C (Amsterdam) 165* (1990) 437.
338. Morris, D. E., Narwankar, P. K. and Sinha, A. P. B. *Physica C (Amsterdam) 169* (1990) 7.
339. Parise, J. B. and McCarrron, E. M., III *J. Solid State Chem. 83* (1989) 188.
340. McCarron, E. M., III, Crawford, M. K. and Parise, J. B. *J. Solid State Chem. 78* (1989) 192.
341. Liu, R. S., Cooper, J. R., Loram, J. W., Zhou, W., Lo, W., Edwards, P. P., Liang, W. Y. and Chen, L. S. *Solid State Commun. 76* (1990) 679.
342. Miyatake, T., Gotoh, S., Koshizuka, N. and Tanaka, S. *Nature (London) 341* (1989) 41.
343. Wada, T., Suzuki, N., Ichinose, A., Yaegashi, Y., Yamauchi, H. and Tanaka, S. *Jpn. J. Appl. Phys., Part 2, 29* (1990) L915.
344. Mangelschots, I., Mali, M., Roos, J., Zimmermann, H., Brinkmann, D., Rusiecki, S., Karpinski, J., Kaldis, E. and Jilek, E. *Physica C (Amsterdam) 172* (1990) 57.
345. Mangelschots, I., Mali, M., Roos, J., Zimmermann, H., Brinkmann, D., Karpinski, J., Kaldis, E. and Rusiecki, S. *J. Less-Common Met. 164–165* (1990) 78.
346. Murphy, D. W., Sunshine, S., van Dover, R. B., Cava, R. J., Batlogg, B., Zahurak, S. M. and Schneemeyer, L. F. *Phys. Rev. Lett. 58* (1987) 1888.
347. de Leeuw, D. M., Mutsaers, C. A. H. A., van Hal, H. A. M., Verweij, H., Carim, A. H. and Smoorenburg, H. C. A. *Physica C (Amsterdam) 156* (1988) 126.
348. Fu, W. T., Zandbergen, H. W., van der Beek, C. J. and de Jongh, L. J. *Physica C (Amsterdam) 156* (1988) 133.
349. Carim, A. H., de Jong, A. F. and de Leeuw, D. M. *Phys. Rev. B 38* (1988) 7009.
350. Zandbergen, H. W., Fu, W. T. and de Jongh, L. J. *Physica C (Amsterdam) 156* (1988) 307.
351. Bjørnholm, T., Schuller, I. K., Early, E. A., Maple, M. B., Wuyts, B., Vanacken, J. and Bruynseraede, Y. *Phys. Rev. B 41* (1990) 11154.
352. Keller-Berest, F., Metgert, S., Collin, G., Monod, P. and Ribault, M. *Physica C (Amsterdam) 161* (1989) 150.
353. Cava, R. J., Santoro, A., Krajewski, J. J., Fleming, R. M., Waszczak, J. V., Peck, W. F., Jr. and Marsh, P. *Physica C (Amsterdam) 172* (1990) 138.
354. Huang, J. and Sleight, A. W. *Physica C (Amsterdam) 169* (1990) 169.
355. Chen, J. W., Chen, C. F., Chang, T. C. and Yao, Y. D. *Physica C (Amsterdam) 165* (1990) 287.
356. Soderholm, L., Goodman, G. L., Welp, U., Williams, C. W. and Bolender, J. *Physica C (Amsterdam) 161* (1989) 252.
357. Andersson, M., Hegedüs, Z., Nygren, M. and Rapp, Ö. *Physica C (Amsterdam) 160* (1989) 65.
358. Markert, J. T., Seaman, C. L., Zhou, H. and Maple, M. B. *Solid State Commun. 66* (1988) 387.
359. Shibata, H., Kinoshita, K. and Yamada, T. *Physica C (Amsterdam) 170* (1990) 411.
360. Ausloos, M., Laurent, C., Vanderschueren, H. W., Rulmont, A. and Tarte, P. *Solid State Commun. 68* (1988) 539.
361. Tallon, J. L., Pooke, D. M., Staines, M. P., Bowden, M. E., Flower, N. E., Buckley, R. G., Presland, M. R. and Davis, R. L. *Physica C (Amsterdam) 171* (1990) 61.
362. Andresen, P. H., Fjellvåg, H., Karen, P. and Kjekshus, A. *Acta Chem. Scand. 45* (1991) 698.
363. Kirby, P. B., Harrison, M. R., Freeman, W. G., Samuel, I. and Haines, M. J. *Phys. Rev. B 36* (1987) 8315.
364. Takabatake, T. and Ishikawa, M. *Solid State Commun. 66* (1988) 413.
365. Siegrist, T., Schneemeyer, L. F., Waszczak, J. V., Singh, N. P., Opila, R. L., Batlogg, B., Rupp, L. W. and Murphy, D. W. *Phys. Rev. B 36* (1987) 8365.
366. Xu, Y., Sabatini, R. L., Moodenbaugh, A. R. and Suenaga, M. *Phys. Rev. B 38* (1988) 7084.
367. Ullmann, B., Heinemann, K., Krebs, H. U., Freyhardt, H. C. and Schwarzmann, E. *Physica C (Amsterdam) 153–155 (Pt. 1)* (1988) 872.
368. Kiemel, R., Schäfer, W., Kemmler-Sack, S., Kruschel, G. and Elschner, B. *J. Less-Common Met. 143* (1988) L11.
369. Qian, M., Stern, E. A., Ma, Y., Ingalls, R., Sarikaya, M., Thiel, B., Kurosky, R., Han, C., Hutter, L. and Aksay, I. *Phys. Rev. B 39* (1989) 9192.
370. Maeno, Y., Nojima, T., Aoki, Y., Kato, M., Hoshino, K., Minami, A. and Fujita, T. *Jpn. J. Appl. Phys., Part 2, 26* (1987) L774.
371. Tarascon, J. M., Greene, L. H., Barrboux, P., McKinnon, W. R., Hull, G. W., Orlando, T. P., Delin, K. A., Foner, S. and McNiff, E. J., Jr. *Phys. Rev. B 36* (1987) 8393.
372. Xiao, G., Cieplak, M. Z., Gavrin, A., Streitz, F. H., Bakhshai, A. and Chien, C. L. *Phys. Rev. Lett. 60* (1988) 1446.
373. Cieplak, M. Z., Xiao, G., Chien, C. L., Bakshai, A., Artymovicz, D., Bryden, W., Stalick, J. K. and Rhyne, J. J. *Phys. Rev. B 42* (1990) 6200.
374. Hepp, A. F., Gaier, J. R., Pouch, J. J. and Hambourger, P. D. *J. Solid State Chem. 74* (1988) 433.
375. Tallon, J. *Phys. Rev. B 43* (1991). *In press.*
376. Ferey, G., Le Bail, A., Lalignant, Y., Hervieu, M., Raveau, B., Sulpice, A. and Tournier, R. *J. Solid State Chem. 73* (1988) 610.
377. Hiratani, M., Ito, Y., Miyauchi, K. and Kudo, T. *Jpn. J. Appl. Phys., Part 2, 26* (1987) L1997.
378. Bordet, P., Hodeau, J. L., Strobel, P., Marezio, M. and Santoro, A. *Solid State Commun. 66* (1988) 435.
379. Kajitani, T., Kusaba, K., Kikuchi, M., Syono, Y. and Hirabyashi, M. *Jpn. J. Appl. Phys., Part 2, 27* (1988) L354.
380. Miceli, P. F., Tarascon, J. M., Greene, L. H., Barboux, P., Rotella, F. J. and Jorgensen, J. D. *Phys. Rev. B 37* (1988) 5932.
381. Renevier, H., Hodeau, J. L., Bordet, P., Capponi, J. J., Marezio, M., Baudelet, F., Tolentino, H., Tourillon, G., Dartige, E., Fontaine, A., Martinez, J. C. and Prejean, J. J. *Physica C (Amsterdam) 162–164* (1989) 51.
382. Hiroi, Z., Takano, M., Takeda, Y., Kanno, R. and Bando, Y. *Jpn. J. Appl. Phys., Part 2, 27* (1988) L580.
383. Katsuyama, S., Ueda, Y. and Kosuge, K. *Mater. Res. Bull. 24* (1989) 603.
384. Katsuyama, S., Ueda, Y. and Kosuge, K. *Physica C (Amsterdam) 165* (1990) 404.
385. Felner, I., Nowik, I., Brosh, B., Hechel, D. and Bauminger, E. R. *Phys. Rev. B 43* (1991) 8737.
386. Goodenough, J. B., Demazeau, G., Pouchard, M. and Hagenmuller, P. *J. Solid State Chem. 8* (1973) 325.
387. Hohlwein, D., Hoser, A., Ihringer, J., Küster, A., Maichle, J. K., Prandl, W., Ritter, H., Kemmler-Sack, S., Kiemel, R., Schäfer, W., Hewat, A. and Wroblewski, T. *Z. Phys. B 75* (1989) 439.

388. Hilscher, G., Pillmayr, N., Eibler, R., Bauer, E., Remschnig, K. and Rogl, P. *Z. Phys. B 72* (1988) 461.
389. Greaves, C. and Slater, P. R. *Physica C (Amsterdam) 161* (1989) 245.
390. Rey, M.-J., Dehaudt, P., Joubert, J. and Hewat, A. W. *Physica C (Amsterdam) 167* (1990) 162.
391. Yaron, U., Kowal, D., Felner, J. and Einav, M. *Physica C (Amsterdam) 168* (1990) 546.
392. Manako, T., Shimakawa, Y., Kubo, Y., Satoh, T. and Igarashi, H. *Physica C (Amsterdam) 156* (1988) 315.
393. Gopalakrishnan, I. K., Yakhmi, J. V. and Iyer, R. M. *Physica C (Amsterdam) 172* (1991) 450.
394. Geremia, S., Nardin, G., Mosca, R., Randaccio, L. and Zangrando, E. *Solid State Commun. 72* (1989) 333.
395. Huang, Q., Karen, P., Karen, V. L., Kjekshus, A., Lynn, J. W., Mighell, A. D., Rosov, N. and Santoro, A. *Phys. Rev. B 45* (1992). 9611.
396. Cava, R. J., Batlogg, B., Krajewski, J. J., Rupp, L. W., Schneemeyer, L. F., Siegrist, T., van Dover, R. B., Marsh, P., Peck, W. F., Gallagher, P. K., Jr., Glarum, S. H., Marshall, J. H., Farrow, R. C., Waszczak, J. V., Hull, R. and Trevor, P. *Nature (London) 336* (1988) 211.
397. Capponi, J. J., Bordet, P., Chaillout, C., Chenavas, J., Chmaissem, O., Hewat, E. A., Hodeau, J. L., Korczak, W. and Marezio, M. *Physica C (Amsterdam) 162–164* (1989) 53.
398. Fu, W. T., Zandbergen, H. W., Haije, W. G. and de Jongh, L. J. *Physica C (Amsterdam) 159* (1989) 210.
399. Marezio, M., Santoro, A., Capponi, J. J., Hewat, E. A., Cava, R. J. and Beech, F. *Physica C (Amsterdam) 169* (1990) 401.
400. Marezio, M., Bordet, P., Capponi, J. J., Cava, R. J., Chaillout, C., Chenavas, J., Hewat, A. W., Hewat, E. A., Hodeau, J. L. and Strobel, P. *Physica C (Amsterdam) 162–164* (1989) 281.
401. Masuzawa, M., Noji, T., Koike, Y. and Saito, Y. *Jpn. J. Appl. Phys., Part 2, 28* (1989) L1524.
402. Rouillon, T., Retoux, R., Groult, D., Michel, C., Hervieu, M., Provost, J. and Raveau, B. *J. Solid State Chem. 78* (1989) 322.
403. Tokiwa, A., Oku, T., Nagoshi, M., Kikuchi, M., Hiraga, K. and Syono, Y. *Physica C (Amsterdam) 161* (1989) 459.
404. Rouillon, T., Maignan, A., Hervieu, M., Michel, C., Groult, D. and Raveau, B. *Physica C (Amsterdam) 171* (1990) 7.
405. Rouillon, T., Provost, J., Hervieu, M., Groult, D., Michel, C. and Raveau, B. *J. Solid State Chem. 84* (1990) 375.
406. Maeda, T., Sakuyama, K., Koriyama, S., Yamauchi, H. and Tanaka, S. *Phys. Rev. B 43* (1991) 7866.
407. Nakahigashi, K., Sasakura, H., Minamigawa, S. and Kogachi, M. *Jpn. J. Appl. Phys., Part 2, 29* (1990) L1422.
408. Zandbergen, H. W., van Tendeloo, G. and Amelinckx, S. *Solid State Commun. 72* (1989) 445.
409. Zandbergen, H. W., Fu, W. T. and Van Ruitenbeek, J. M. *Physica C (Amsterdam) 166* (1990) 502.
410. Mochiku, T., Osawa, M. and Asano, H. *Jpn. J. Appl. Phys., Part 2, 29* (1990) L1406.
411. Tokiwa, A., Oku, T., Nagoshi, M., Shindo, D., Kikuchi, M., Oikawa, T., Hiraga, K. and Syono, Y. *Physica C (Amsterdam) 172* (1990) 155.

Received November 5, 1991.